Characterizing thermal properties of tapered nanofibers

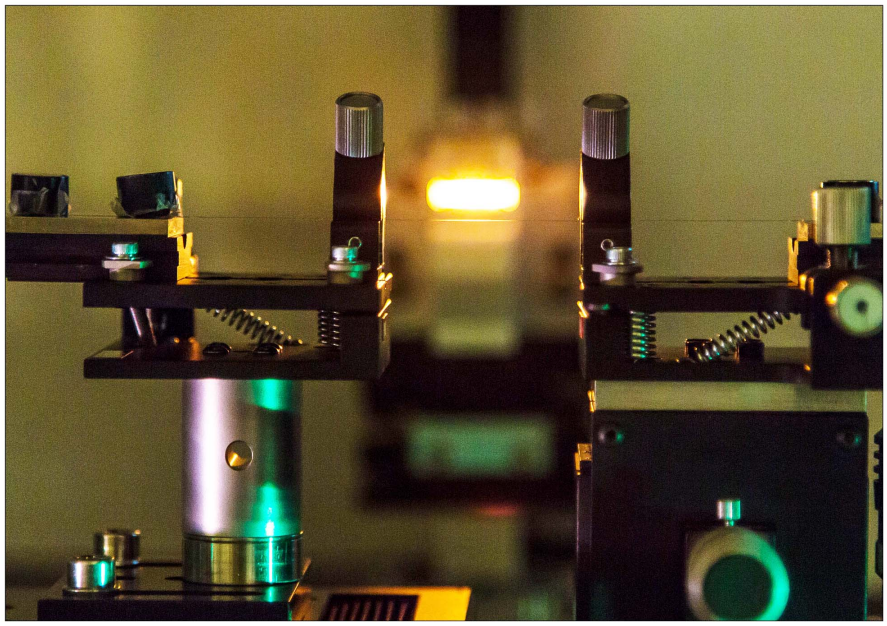

Master Thesis

Christine Pepke Pedersen

Niels Bohr Institute
University of Copenhagen
30. June 2015

Supervisers: Jörg Helge Müller & Jürgen Appel

Contents

Acknowledgments

I would like to thank my family and friends for the support and inspiration for this thesis. Especially thanks to Andri Gunnarsson for helping out in the lab, bringing our dinner to the lab, etc. The experiment was much easier to run with the extra help in the late evenings.

Thanks to my supervisors Jörg Helge Müller & Jürgen Appel for the supervision, and thanks to all the people in QUANTOP, I am thankful for the opportunity to work in the group. In particular thanks to Jörg for showing up in the lab during the Easter holidays to discuss my experiment.

Finally I would like to thanks Ola Joensen for the nice pictures of my setup.

Abstract

The purpose of the project was to produce and investigate the breaking due to high laser power of tapered nanofibers, with a diameter of 500 nm, placed in vacuum. Furthermore to look for characteristics of the fiber breaking, i.e. to investigate if it is possible to tell in advance, on the optical path length change that the fiber is going to break. An experimental setup was build for this purpose using an interferometric method. Several experimental problems were solved and resulted in an improved and more stable setup.

During the experiment the purpose was extended to also investigate the thermal properties of the nanofibers, i.e. the heating and cooling of the nanofibers and their thermodynamics.

The heating and cooling of the fibers is investigated experimentally and analytical expressions for the rate of optical path length change as a function of the optical path length change is found.

The results also showed indications that the radiation from the fibers obeys Plancks law of radiation.

It was found that it was not possible to predict at what power a fiber would break, since the power needed to break a fiber seemed to be individual for each fiber. It was found, however, that careful treatment and cleaning of the fiber and keeping it free from contaminations before inserting in the vacuum chamber was essential for producing a good tapered fiber.

Chapter 1

Introduction

My master thesis was done at QUANTOP in 2014-2015. The thesis is written with the future students in mind who are going to work with the experiment. I have tried to pass on the knowledge that was gained in the laboratory and therefore also explained how the tapered nanofibers are prepared, how the setup was build, how to use the fiberburning setup, and especially my experiences with the working setup. I have also included an overview of the literature and theory that I have studied on during the project time. I therefore hope that the thesis will be used and can give inspiration to new exciting experiments.

Investigating the thermal properties of tapered nanofibers is relevant for several applications of nanofibers among them atom trap experiments.

A nanofiber with a diameter d smaller than the wavelength λ of the light guided in the nanofiber is an efficient quantum interface as it can couple atoms and light strongly. As $d < \lambda$, a significant part of the light propagates outside of the fiber and this intense evanescent field of light surrounding the nanofiber can be used for atom trapping along the fiber [1].

The purpose of the interface is to create entangled states of the atoms and use it for quantum information experiments, e.g. working towards creating quantum memories and optical fiber quantum networks [2].

A solid understanding of the thermal behaviour of nanofibers is important if the nanofibers are going to be used in quantum information experiments, as understanding how the fiber heats and cools together with the heating and cooling time constants, (and the concerns of the nanofiber melting or breaking) are important fiber properties that needs to be investigated.

In this experiment tapered 500 nm diameter nanofibers are produced by a heat and pull procedure and transferred to vacuum. The nanofiber is placed in one arm of a Mach-Zehnder interferometer using a laser of 852 nm wavelength and heated with another laser of 789.6 nm wavelength. The interference fringes are counted as the fiber is heated and cooled and by looking at the change in optical path length of the light through the fiber it is possible to examine when the fiber is heated and when it is cooled.

The heating and cooling transients are investigated to describe how the fiber heats and cools and to see if it is possible to describe the thermodynamics governing the heating and cooling.

The fibers are heated till they break, the breaking power is measured and it is examined if the fibers show any characteristic signatures around the point of breaking.

Chapter 2

Theory

In this section I will explain the relevant theory I have studied about optical fibers and tapered nanofibers. I will start with optical fibers and then introduce the tapered nanofibers. Then I will discuss the thermal properties of tapered nanofibers inspired by the theory and experiment investigated in [3]. Finally I will discuss an important application of tapered nanofibers as an atomic trap.

2.1 Optical fibers

An optical fiber is a fiber used to guide light. An optical fiber is usually made of glass (silica) but it can also be made of plastic. The optical fiber consists of a core, a cladding and a protective coating called buffer, see figure 2.1.

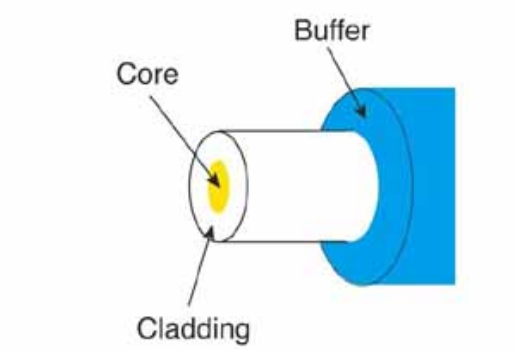

Figure 2.1: The figure shows an optical fiber with core, cladding and buffer. From [4].

Optical fibers are used for communication; to send signals over long distances at a high bandwidth (data rate). The optical fibers are flexible as they can be bended and be bundled into cables. Compared to copper wires, used for communication with electrical signals, fibers are more efficient, as there is less loss in the transmitted signal, there is no electromagnetic interference (electrical disturbances), and the data bandwidth is larger. Besides fiber optic communication, optical fibers are used for fiberscopes, fiber optic sensors, fiber amplifiers and fiber lasers.

The index of refraction, which determines the speed of the guided light in the fiber, is typical 1.44-1.5 for glass fibers. The core has a little higher index of refraction than the cladding because then the light in the fiber can be guided by total internal reflection (as explained below). The core of the silica glass fiber is often doped with GeO_2 or Al_2O_3 to increase its refractive index. The difference in refractive index between the core and the cladding is usually less than 1%.

The power of the light propagating in an optical fiber decays exponentially with distance. This loss of power, or attenuation, is given in dB/m. E.g. a single mode fiber, has a loss of 0.2 dB/km for a wavelength of 1550 nm (this wavelength is used for telecommunication) [5].

There is loss in fibers because of scattering and absorption. The guided light can scatter on defects or irregularities in the fiber. These irregularities can e.g. be rough surfaces and different crystalline sections in the fiber. Glass is amorphous silica so there exist no long range crystalline order but each SiO_4 tetrahedras exhibits a local (short range) order. The scattering is an energy loss because it couples energy from the guided modes into the radiation modes. There can also be Rayleigh scattering in the fiber, which is scattering on particles which are small compared to the lights wavelength. The scattering intensity I depends on wavelength as $I \propto \frac{1}{\lambda^4}$, so increasing the wavelength can reduce the Rayleigh scattering loss.

Absorption of the guided light, can occur if the atoms or molecules in the fiber can absorb the wavelength of the guided light. That is, if the frequency of the light matches either the electronically allowed transitions, or the vibration frequency of the atoms or molecules e.g. the vibrational mode of the Si-O chemical bonds in silica glass fibers. The absorbed light can be converted to heat in the fiber. Often the impurities or the dopants, added to change the fibers refractive index, absorbs most of the light.

Silica fibers have a high transmission of optical wavelengths. At wavelengths of 1550 nm (near infrared), silica has, as mentioned earlier, a very low loss of around 0.2 dB, because of the ultra pure silica has a low concentration of absorption molecules [6]. The low loss in silica fibers is what makes silica an attractive material for optical fibers.

Optical glass fibers typical have diameters in the range 100-125 µm (without the coating). The diameter of the total fiber (with the coating) is around 250-500 µm, whereas the diameter of the core is around 8-62.5 µm [7]. Optical plastic fibers have much larger dimensions; here the core diameter is often 0.5 mm or higher.

We distinguish between single mode and multimode optical fibers. The single mode fibers guide only one mode of light whereas the multimode fibers can guide several modes. In a single mode fiber most of the light will be in the core mode but some light in other modes might also propagate through the fiber, although this will only be a small procent of all the light. Light in the core mode can couple to cladding modes or radiative modes, which will then decrease the amount of transmitted light through the fiber. The modes that can pass through the fiber are the modes that share the symmetries of the guided mode e.g. they spatially look like the guided mode. The effective size of the core, the mode field diameter, is small for single mode fibers, around 8-10 µm and larger for multimode fibers usually 50 or 62.5 µm [4].

2.1.1 Description of the fiber

I use an optical fiber (Fibercore SM750) which is (125±1) µm in diameter. The mode field diameter, which is a measure of the size of the field, is 4.6 µm. The fiber is tapered[1] to a diameter of 400-500 nm. The nanofiber section, the fiber waist, is known from a simulation to be approximately 1-2 mm long while the tapered fiber part (the length the fiber is pulled) is around 35-37 mm. The nanofiber region is the interesting part because here a significant part of the light propagates outside the fiber as the fiber has a diameter smaller than the wavelength

[1] A tapered fiber is an optical fiber which over some length is stretched out to a very small diameter

of light. This is the evanescent field and it is here that atoms can be trapped as explained in section 2.4.

Before the fiber is tapered the coating is removed by stripping the fiber. The fiber is then tapered by a heat and pull method where the fiber is pulled at both ends while it is heated by an oven. The silica melts and the fiber is elongated so its diameter gradually decreases. The nanofiber is then transferred to vacuum to be heated, as will be explained later.

The optical fiber we consider here is a single mode step index fiber, with the refractive index of the core n_{co}=1.4536 and refractive index of the cladding n_{cl}=1.4468.

The complex refractive index consists of a real and an imaginary part $n = n_{real} + i \cdot n_{imag}$. The real part, the refractive index, determines the phase shift of the light and is around 1.45 and the imaginary part (the extinction coefficient) determines the absorption of the light and is around 10^{-7} for a wavelength $\lambda = 789.6$ nm in Silica, as inferred from figure 2.2. So for our purposes the optical fiber is not absorbing the light (the light is actually absorbed by eventual particles on the fiber) and it is transparent at $\lambda = 789.6$ nm. It is also the transparency of Silica in the infrared range of wavelengths which makes it attractive for transmitting optical signals.

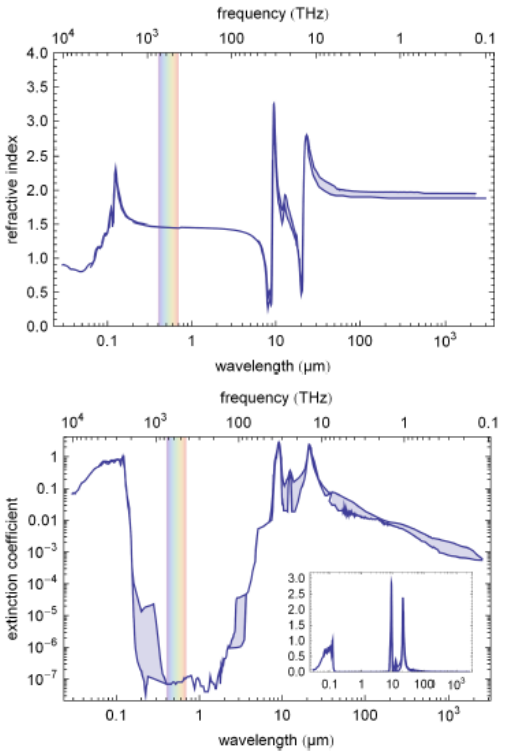

Figure 2.2: Index of refraction and extinction coefficient for fused silica as a function of wavelength. From [3].

2.1.2 Total internal reflection

The optical fiber can confine and guide light by the principle of total internal reflection (TIR). TIR can be explained by considering the light fields in the ray optics representation where the light beam is described by a ray with a height and an angle with respect to the propagation axis.

At the interface between two different optical dense materials light is refracted according to

Snells law:

$$n_1 \cdot \sin(\theta_1) = n_2 \cdot \sin(\theta_2) \tag{2.1}$$

where n_1 is the refractive index of the first material, n_2 is the refractive index of the second material, θ_1 is the angle of incidence of the incoming light and θ_2 is the angle of the refracted light, see figure 2.3.

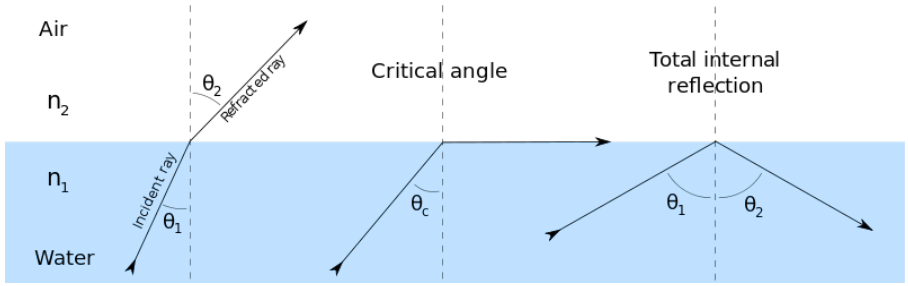

Figure 2.3: TIR at an interface. Light incident on the interface with $\theta < \theta_c$ is refracted. Light with $\theta > \theta_c$ is reflected back.

We consider $n_1 = n_{co}$ and $n_2 = n_{cl}$. For $n_{co} > n_{cl}$ it is possible that the light from the core incident on the core-cladding interface is reflected back into the core instead of being refracted into the cladding. This is called total internal reflection. If $\theta_2 = 90°$, the maximum value of θ_2, the light is neither reflected nor refracted, so the light moves along the interface. From equation (2.1) with $\theta_2 = 90°$ we have $\theta_1 = \sin^{-1}(\frac{n_2}{n_1})$, which we define as the critical angle θ_c. To achieve TIR the angle of incidence θ must be greater than the critical angle θ_c. For $\theta < \theta_c$ the light will split; some light will be reflected and some will be refracted through the interface. The closer θ is to θ_c the more light will be reflected and for $\theta > \theta_c$ all light will be reflected back into the core. As $\sin^{-1}(x)$ is defined for $-1 < x < 1$ we see that to achieve TIR we must have $n_1 > n_2$, i.e. we will only have TIR in a high index material surrounded by a low index material.

TIR can be used to confine light in the core. This is the principle of transport of signals in optical fibers where TIR is used to guide light in the fiber. Only light with incident angle $\theta > \theta_c$ is guided in the fiber, as seen in figure 2.3.

We can lose light from a fiber if it leaks from the core to the cladding. E.g. if the fiber is bent, the light incident on the interface of core and cladding may have an angle of incidence less than the critial angle in the bend. So the light that gets into the fiber (with $\theta > \theta_c$) may have $\theta < \theta_c$ inside the fiber, because the fiber bends. The power losses due to bending are exponentially decaying with attenuation coefficient α, where α depends on the radius of curvature of the bend. After a propagation length l the power of the light in the fiber will thus be reduced by a factor of $e^{-\alpha l}$.

2.1.3 Evanescent wave

In total internal reflection a small part of the light will escape the core and propagate to the cladding. This is the evanescent field. The evanescent wave is exponentially attenuated, so it decays exponentially with distance from the core. The evanescent field appears because Snells law for $\theta_i > \theta_c$ has no real solutions but only imaginary solutions that allow transmission of some light.

We consider a plane wave $E_I = E_i e^{i(\vec{k_i} \cdot \vec{r} - \omega t)}$ incident on the core-cladddding interface, where part of it will be reflected and a little transmitted see figure 2.4.

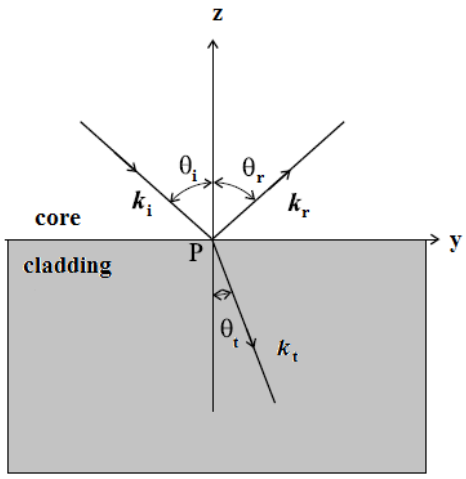

Figure 2.4: The incident field k_i is partly reflected k_r and transmitted k_t.

The transmitted field is, $E_T = E_t e^{i(\vec{k_t}\cdot\vec{r}-\omega t)}$, where $\vec{r} = (x, y, z)$. Using Snells law we find $\vec{k_t}\cdot\vec{r} = k_t \cdot \sin(\theta_t)\cdot y + k_t \cdot \cos(\theta_t)\cdot z = k_t \cdot y \cdot \frac{n_1}{n_2}\cdot\sin(\theta_i) + k_t \cdot z \cdot \sqrt{1-(\frac{n_1}{n_2})^2\cdot\sin^2(\theta_i)}$. The square root is imaginary for $\theta_i > \theta_c = \sin^{-1}(\frac{n_2}{n_1})$ i.e. for total internal reflection. We have $E_T = E_t e^{-i\omega t}e^{i\alpha y}e^{-\beta z}$ where $\alpha = k_t \cdot \frac{n_1}{n_2}\cdot\sin(\theta_i)$ and $\beta = k_t \cdot \sqrt{(\frac{n_1}{n_2})^2\cdot\sin^2(\theta_i)-1}$. The transmitted field is thus a plane wave with an exponentially decaying term $e^{-\beta z}$. The intensity $I = E_T^* E_T = E_t^2 e^{-2\beta z}$ of the transmitted field - the evanescent field - is seen to be exponentially decaying with distance z into the cladding.

In the untapered fiber the evanescent field leaks into the vacuum around the fiber. The penetration depth of the evanescent field is small and is of the order of the wavelength of the light. In the tapered nanofiber the evanescent field that leaks into the vacuum is considerably larger because the fiber diameter is less than the wavelength of light, so a penetration depth of the order of the wavelength is larger than the diameter of the fiber, which means that a significant fraction of the lights energy will propagate outside the fiber.

2.1.4 Propagation of light in optical fibers: fiber modes

An optical fiber mode is a field distribution which is conserved in form while propagating through the fiber and it only experiences a phase shift $e^{i\beta z}$ with propagation constant β due to the propagation (optical path length change). Fiber modes are either core or cladding modes. If the fiber is coated the coating can absorb the cladding modes and the light signal will propagate in the core modes.

The light modes that are allowed to propagate in a fiber can be found by solving Maxwells equations. Here the following discussion applies to fibers with $n_{co} - n_{cl} << 1$, which is called the weak guiding approximation. In this approximation the derivative of the dielectric function $\epsilon = n^2$ is neglected. For my fiber, $\nabla\epsilon = 0$, because the index of refraction is constant within the core and within the cladding. For a more comprehensive review the reader is referred to other literature e.g. [6].

In the weak guidance approximation, the electric field mode $E(\vec{r}, \omega)$, in order to conserve its form while propagating, should satisfy the Helmholtz equation:

$$\nabla^2 E(\vec{r},\omega) + n^2(\omega)\frac{\omega^2}{c^2}E(\vec{r},\omega) = 0 \tag{2.2}$$

where $n(\omega)$ is the refractive index as a function of the lights frequency ω, $\vec{r}$ is the radial direction vector and c the speed of light in vacuum.

For the fiber, with core radius a, we have the boundary conditions:

$n = n_{co}$ for $r < a$ and $n = n_{cl}$ for $r > a$

As the fiber has cylindrical symmetry we will use cylindrical coordinates (r, ϕ, z) so the Helmholtz equation is:

$$\frac{\partial^2 E}{\partial r^2} + \frac{1}{r}\frac{\partial E}{\partial r} + \frac{1}{r^2}\frac{\partial^2 E}{\partial \phi^2} + \frac{\partial^2 E}{\partial z^2} + n^2\frac{\omega^2}{c^2}E = 0 \tag{2.3}$$

Because of the cylindrical symmetry the field will be of the form $E(r,\phi,z) = F(r)e^{im\phi}e^{i\beta z}$ where the factor $e^{im\phi}$, with m an integer, ensures the cylindrical symmetry, so that a 2π rotation around the fiber axis will not change the field. The factor $e^{i\beta z}$ is a phase shift.

In the fiber core, $r < a$, equation (2.3) will be an ordinary differential equation for the radial part $F(r)$:

$$\frac{d^2 F}{dr^2} + \frac{1}{r}\frac{dF}{dr} + (\kappa^2 - \frac{m^2}{r^2})F = 0 \tag{2.4}$$

where

$$\kappa^2 = n_{co}^2\frac{\omega^2}{c^2} - \beta^2 \tag{2.5}$$

This is a Bessel equation which has Bessel functions of the first kind $J_m(\kappa r)$ as solutions. The solutions are physical as they are finite at $r = 0$.

In the fiber cladding, $r > a$, we have:

$$\frac{d^2 F}{dr^2} + \frac{1}{r}\frac{dF}{dr} - (\gamma^2 + \frac{m^2}{r^2})F = 0 \tag{2.6}$$

where

$$\gamma^2 = \beta^2 - n_{cl}^2\frac{\omega^2}{c^2} \tag{2.7}$$

Assuming γ is real, we will have physical solutions that goes towards zero as r goes towards infinity. The solutions are the modified Bessel functions of the second kind $K_m(\gamma r)$. The Bessel functions of the first and second kind are shown in figure 2.5. The Bessel functions of the first kind, the solutions in the core, are oscillating field functions whereas the modified Bessel functions of the second kind, the cladding solutions, are exponentially decaying field functions.

All the components of the electric field $\vec{E} = (E_r, E_\phi, E_z)$ and magnetic field $\vec{H} = (H_r, H_\phi, H_z)$ can thus be found by solving equation (2.3) and will as described be of the form:
$\Psi(r,\phi,z) = F(r)e^{im\phi}e^{i\beta z}$ where Ψ is either E or H and $F(r) = A \cdot J_m(\kappa r)$ for $r < a$, $F(r) = B \cdot K_m(\gamma r)$ for $r > a$ and A and B are constants.

From Maxwells equations the four tangential field components E_ϕ, E_z, H_ϕ and H_z must be

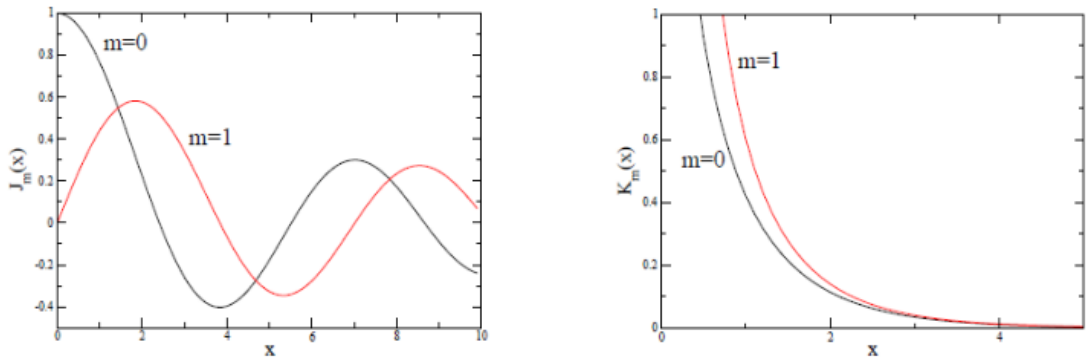

Figure 2.5: Bessel functions of the first kind $J_m(x = \kappa r)$ (left) and of the modified second kind $K_m(x = \gamma r)$ (right). From [6].

continuous at the core to cladding transition $r = a$ which, following [8], leads to four homogeneous linear algebraic equations for the four constants A, B, C, D in $F(r)$. These equations have nonzero solutions when the determinant of the matrix of coefficients vanish. This gives a characteristic equation with the Bessel functions, that can be solved numerically. The solution determines the propagation constant β, which depends on the index m. Also for each m there will be more solutions for β denoted by the integer j, where j=0,1,2,3... Every β_{mj} is specifying one mode.

We see that the guided fiber modes decay with radial distance from the fiber. It can be shown [8] that if γ is real, which we assumed above, i.e. $\gamma^2 > 0$ the mode is guided but if γ is imaginary i.e. $\gamma^2 < 0$ the mode is not guided. So $\gamma^2 = 0$ is the cutoff between a mode being guided or not. According to equation (2.5) and equation (2.7) for $\gamma^2 = 0$ we get $\kappa = k_0 \cdot \sqrt{n_{co}^2 - n_{cl}^2}$, where $k_0 = \frac{\omega}{c}$ is the wavevector.

The effective index of refraction that the mode experiences is $n_{\text{eff}} = \frac{\beta}{k}$ where β is the β-constant of that mode and $k = \frac{2\pi}{\lambda}$ is the wavevector.

In the weak guidance approximation the guided modes of the circular symmetric fiber are called LP_{lm} modes where l is the azimuthal index and m is the radial index which describes the azimuthal and radial dependence of the intensity distribution of the mode. The LP_{lm} modes are shown in figure 2.6. We can see that the number of nodes (the zero planes where the field intensity distribution is zero) is $2l$ (going around in a circle at constant radius) and the number of nodes along the radial direction (outwards) is m-1.

The LP_{lm} modes are linearly polarized along one axis transverse to the fiber, and the polarization along the fiber axis is neglected, because only light rays almost parallel to the fiberaxis are guided, as explained in the next section. As the propagation vector $\vec{k}$ is then parallel to the fiber axis the field is polarized transversely to the axis. The LP_{lm} modes can couple to other LP_{lm} modes with the same azimuthal spatial symmetry i.e. the same l number. E.g. the LP_{01} mode couples to the LP_{02}, and as seen on figure 2.6 their intensity distributions overlap. Coupling to modes with another l number is possible if the fiber does not have azimuthal symmetry, e.g. if the fiber is bended or if there is dust on the fiber. Then it will be most likely that the coupling is to modes with a similar β value.

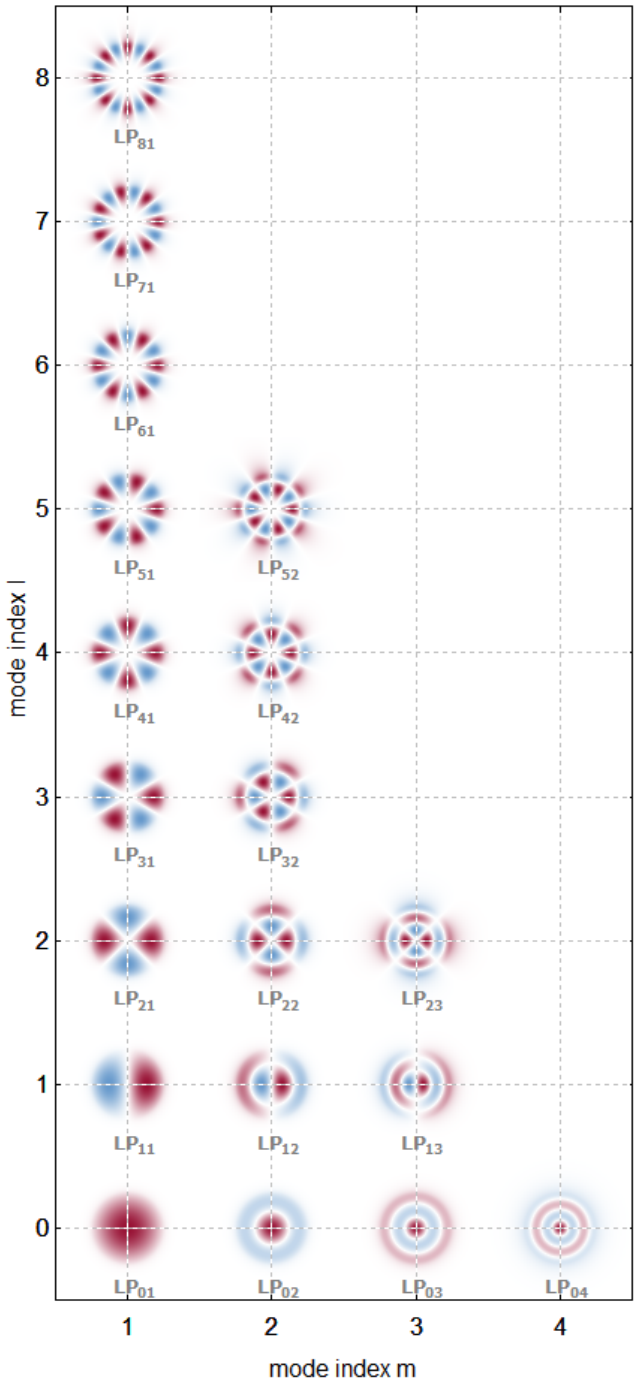

Figure 2.6: The intensity field distributions of the LP_{lm} modes. The colour is the phase, so a colour change is a phase change i.e. a change of the sign of the distribution. From [9].

2.1.5 Numerical aperture and the V-number

The numerical aperture NA of an optical system describes the angles over which the system can either receive or emit light. The numerical aperture of an optical system e.g. a lens is defined as $NA = n \cdot \sin(\theta)$ where n is the refractive index of the medium the lens is placed in, and θ is the half-angle of the maximum cone of light that can either enter or exit through the lens, see figure 2.7. If there is no power lost at the interface, the NA is constant for the beam, as the beam propagates between the two materials. This is seen from Snells law as $NA = n_1 \cdot \sin(\theta_1) = n_2 \cdot \sin(\theta_2)$, also seen on figure 2.7.

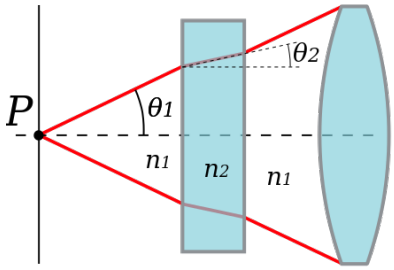

Figure 2.7: Numerical aperture of a lens.

The numerical aperture of a fiber is

$$NA = \sqrt{n_{co}^2 - n_{cl}^2}$$

this is seen from figure 2.8 where n_1 is n_{co} and n_2 is n_{cl}.

Here we have TIR for

$$\theta \geq \theta_c = \sin^{-1}(\tfrac{n_2}{n_1})$$

and if we apply Snells law at the air fiber interface we have

$$n\sin(\phi) = n_1 \sin(\alpha) = n_1 \sin(\tfrac{\pi}{2} - \theta) = n_1 \cos(\theta) = n_1\sqrt{1 - \sin^2(\theta)}$$

for $\theta = \theta_c$ we have

$$n\sin(\phi) = n_1\sqrt{(1 - \sin^2(\sin^{-1}(\tfrac{n_2}{n_1})))} = n_1\sqrt{(1 - (\tfrac{n_2}{n_1})^2)} = \sqrt{n_1^2 - n_2^2}$$

where we used that $\sin^2(\sin^{-1}(x)) = x^2$.

We then define $NA \equiv \sqrt{n_1^2 - n_2^2}$

Since θ is at minimum equal to θ_c for TIR and as we have for a decrease in θ, ϕ increases (figure 2.8) we see that $\phi_{max} = \sin^{-1}(\frac{NA}{n})$ is the maximum acceptance angle of the light for which we have TIR in the core. For a fiber in vacuum $n = 1$ and light will be guided for $\sin(\phi) \leq \sqrt{n_1^2 - n_2^2}$. For a typical optical fiber $n_1 \cong n_2$ so we see that only light rays with small ϕ i.e. nearly parallel to the fiber are guided. We see that the NA describes the different angles of light that the fiber can receive and guide.

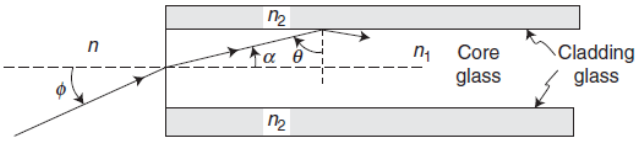

Figure 2.8: Numerical aperture of an optical fiber. From [8].

The number of modes that can propagate in a fiber is described by a dimensionless constant called the V-number or normalized frequency given by:

$$V = \frac{2\pi a}{\lambda} \cdot \sqrt{n_{co}^2 - n_{cl}^2} = \frac{2\pi a}{\lambda} \cdot NA \tag{2.8}$$

where a is the fiber core radius, λ is the vacuum wavelength of the light guided in the fiber, n_{co} is the core index of refraction and n_{cl} is the cladding index of refraction. The number of modes for $V \gg 1$ is approximately $\frac{V^2}{2}$. For a step-index fiber the mode volume is $\frac{4V^2}{\pi^2}$. If V is small, only the fundamental mode ($m = 0$) is guided and the fiber is single mode. It can be shown [8] that a step index fiber supports only the single mode with $m = 0$ for $V < V_c$ where V_c is the smallest value of V that satisfies $J_0(V_c) = 0$. Here $J_m(x)$ is again the Bessel function of the first kind. The smallest x that gives $J_0(x) = 0$ is $x = 2.4048$ which is the first root of the Bessel function, see figure 2.5. That is, for $V = 2.4048$ the fiber is single mode. This value of V is called the single-mode cutoff. Therefore the core radius a of the fiber is chosen such that $V < 2.4048$ for the fiber to be single mode. Then the fiber core should, according to the theory, only guide the fundamental mode and the higher order modes should be guided in the cladding.

To satisfy the single mode condition $V < 2.4048$ the numerical aperture must be small, if we consider infrared wavelengths (few μm) and few μm core radii, which have been used for optical communication. A small NA indicates that the mode is approximately paraxial so the z component is small compared to the x,y components and the modes are transverse, as found earlier. The field for a single mode fiber is often approximated by a Gaussian function $E(r, z) \approx E_0 e^{-\frac{r^2}{w^2}} e^{i\beta z}$ where the spot size w depends on the V-number and $w \simeq a$ for $V = 2$. So the single guided modes are paraxial, transverse and gaussian with a spot size on the order of the core diameter.

The table and figure 2.9 shows at which V-parameters the LP modes, guided in the fiber, are cutoff. We see that only the fundamental mode LP_{01} is guided in the fiber core for $V < 2.4048$. We also see that $n_{cl} < n_{eff} < n_{co}$ and that the modes for high V are mostly guided in the core but for lower V they tend to be guided in the cladding. For $V < 1$ the LP_{01} mode goes from core mode to cladding mode.

LP_{ml}	m=0	m=1	m=2	m=3	m=4	m=5
l=1	0	2.4048	3.8317	5.1356	6.3802	7.5883
l=2	3.8317	5.5201	7.0156	8.4172	9.7610	11.0647
l=3	7.0156	8.6537	10.1735	11.6198	13.0152	14.3725
l=4	10.1735	11.7915	13.3237	14.7960	16.2235	17.6160
l=5	13.3237	14.9309	16.4706	17.9598	19.4094	20.8269

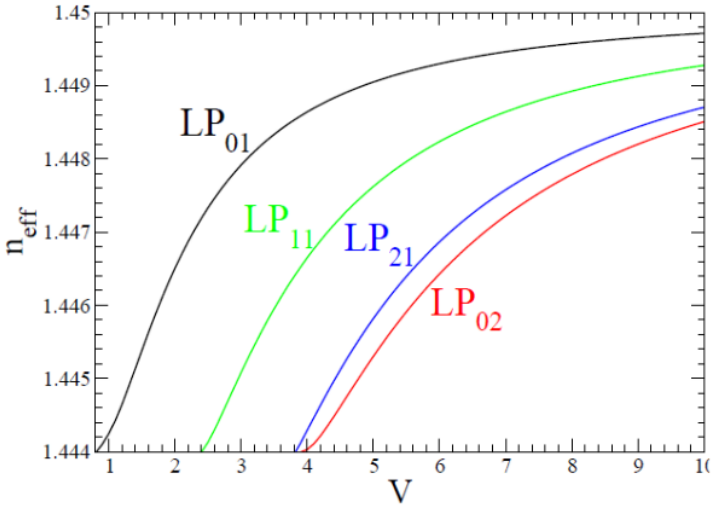

Figure 2.9: Table of cutoff values for the V-parameter for the LP_{lm} modes and plot of the effective index of refraction n_{eff} as function of V for the LP_{lm} modes. The calculations are done for a step index fiber with $n_{cl} = 1.444$ and $n_{co} = 1.45$. Notice that this figure use LP_{ml} instead of LP_{lm}. From [6].

For the fiber used in the experiments, the core diameter, which gives a single mode fiber guiding 852 nm light, can be calculated.

The numerical aperture for my fiber is $NA = \sqrt{n_{co}^2 - n_{cl}^2} = \sqrt{(1.4536)^2 - (1.4468)^2} = 0.14$ For a fiber to be single mode $V < 2.4048$ so we set $V = 2.4048$ and solve for a.
$V = \frac{2\pi a}{\lambda} \cdot NA \Rightarrow a = \frac{V \cdot \lambda}{2 \cdot \pi \cdot NA} = 2.33$ μm. So for a core diameter $d \leq 4.66$ μm the fiber is singlemode.

When we calculate the V-number we neglect the air surrounding the fiber and therefore assume that the cladding is infinite. This approximation is ok as the cladding diameter is much larger than the core diameter and also because the E and H fields of the guided mode outside the core decay exponentially so not much of the light goes to the outer surface of the cladding.

The calculation above is valid for the unpulled optical fiber whereas for the pulled nanofiber we have to consider how the tapering changes the index of refraction. When the fiber is tapered to a nanofiber the core is almost disappearing as it becomes very thin. Therefore at the nanofiber section, the fiber mostly consist of silica, with the index of refraction of the original cladding. That is, when we calculate the single mode diameter, we should consider the light as guided by the cladding-air interface and use n_{cl} as the new index of refraction for the core and n_{air} as the new index of refraction of the cladding.

For the pulled fiber we then have $NA = \sqrt{n_{co}^2 - n_{cl}^2} = \sqrt{(1.4468)^2 - (1.0003)^2} = 1.05$. For $V = 2.4048$ we find $a = \frac{V \cdot \lambda}{2 \cdot \pi \cdot NA} = 310.6$ nm. So for $d \leq 621$ nm the fiber is single mode.

Therefore I want to pull the fiber a length l such that its diameter becomes less than 621 nm in order to have a single mode fiber.

2.1.6 Graded index fibers and step index fibers

There exist two different types of optical fibers: graded index fibers and step index fibers see figure 2.10. In the graded index fiber the index of refraction changes gradually from the center of the fiber to the surface of the fiber. Whereas in the step index fiber the index of refraction is a little different in the two parts of the fiber: the core and the cladding on which interface the index of refraction changes in one step. The graded index fiber reduces intermodal dispersion, which is a pulse broadening effect because incident rays can have different angles of incidence θ when propagating in the fiber, as seen in figure 2.8.

Different angles gives different modes of propagation. Different propagation lengths give a time difference in propagation time through the fiber for the light pulses. So a multimode pulse, which consist of different modes will be temporally broadened because the pulses will arrive at the end of the fiber at different times. For the step index fiber the temporal spread in the arrival of two pulses scales as $(NA)^2$ whereas for a graded index fiber it scales as $(NA)^4$ so for a small (NA) the graded index fiber reduces intermodal dispersion.

There is of course no intermodal dispersion in a single mode fiber as only one mode can propagate in the fiber.

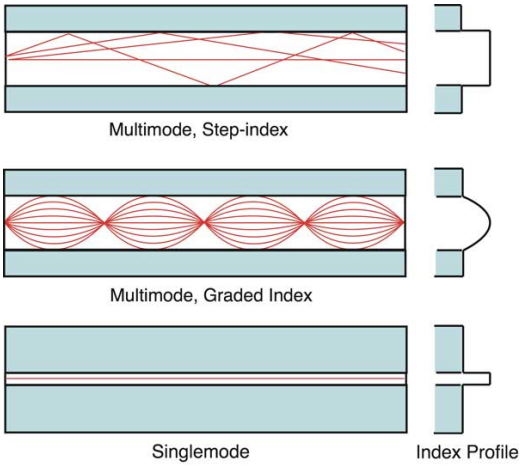

Figure 2.10: The figure shows how the light propagates in the fiber and how the index of refraction profile is. In the single mode fiber the light travels in one ray, one mode.

2.2 Tapered nanofibers

When the fiber is tapered the fiber diameter is gradually decreased, see figure 2.12. This changes the modes that can propagate in the fiber at the tapered section. The decreasing diameter means that for $d < \lambda$ a larger part of the evanescent field propagates outside the fiber. The light in the tapered fiber is guided by the cladding-air interface instead of the core-cladding interface. As the index of refraction of the fiber is very different from the index of refraction of the surrounding air we cannot use the weak guiding approximation. For the nanofiber we will then have to consider the solutions to Maxwells equations, the exact modes of a step index fiber as found in e.g. [6]. The guided modes are found by solving the wave equation in every region of constant refractive index. This gives an eigenvalue problem where the solutions to the resulting eigenvalue equations should be matched at the boundaries, using the boundary conditions. (The eigenmodes are the guided modes and the eigenvalues are the effective indices of the modes).

The exact modes are separated in transverse modes and hybrid modes. The transverse modes have the z or longitudinal component of either the E or H field equal to zero, and are then perpendicular to the propagation direction (z). The modes are called transverse electric (TE-modes) for $E_z = 0$ (and $E_r = H_\phi = 0$) and transverse magnetic (TM-modes) for $H_z = 0$ (and $H_r = E_\phi = 0$). The hybrid modes have no zero components of either E or H fields and are denoted HE (EH) when E_z is smaller (larger) than H_z. The fundamental mode is the HE_{11} hybrid mode.

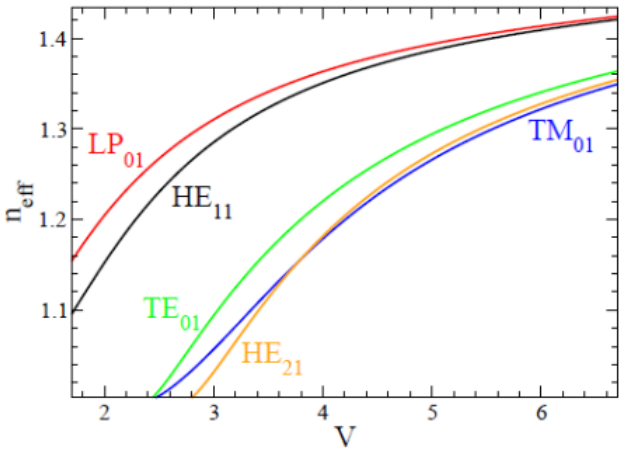

Figure 2.11: Dispersion curves for the exact fiber modes together with the weakly guided LP_{01} mode. From [6].

The TE_{01} mode has the same dispersion (n_{eff},V)-curve as the LP_{11} mode so the single mode cutoff is still $V = 2.4048$ and below this V value only the fundamental mode HE_{11} is guided (as the LP_{01} mode in the weakly guiding approximation).

There is a correspondence between the exact modes and the LP_{lm} modes from the weak guidance approximation. E.g. the fundamental exact HE_{11} mode which is spherically symmetric corresponds to the fundamental weak guidance LP_{01} mode. It can be shown [6] that within the weak guiding approximation the LP_{lm} modes can be seen as linear combinations of the exact modes.

We can think of it as the LP_{lm} modes split into the exact modes when the light propagates from the optical fiber to the tapered nanofiber.

As the light propagates through the fiber the guided modes thus changes. In the untapered part the modes sees an effective index $n_{cl} < n_{eff} < n_{co}$, and $n_{co} - n_{cl} \ll 1$ so the guiding is

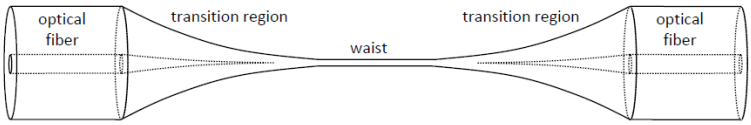

Figure 2.12: In the tapered fiber, the modes change during propagation through the fiber, because of the changing shape. From [11].

weak and $NA \ll 1$. In the tapered part $n_{air} < n_{eff} < n_{cl}$ the guiding is strong, $NA > 1$ and $V \gg 1$. The fiber is multimode and the number of modes is proportional to $\frac{V^2}{2}$. If the diameter decreased enough such that $V < 2.4048$ at the waist the fiber is again single mode here. At the beginning of the tapered section the light in the guided core mode couples into the guided cladding modes and at the end of the tapered section some of the light in the cladding modes couples back into the guided core mode, but some light couples to radiation modes and is lost. Making the fiber shape adiabatic is about preventing this loss. In [10] they use Rayleigh scattering to observe and show that they have control over the propagation of the modes through the nanofiber. As $n_{eff} = \frac{\beta}{k}$ changes along the tapered fiber the phase factor that the field achieves due to propagation through the fiber is now an integral over β along the fiber (z axis) i.e. $E \propto E_0 e^{-i\int_0^z \beta(z')dz'}$.

2.2.1 Adiabatic tapered nanofibers

An adiabatic fiber is a fiber with a certain local core taper angle $\Omega(z)$ along the fiber, see figure 2.13, such that coupling to higher order modes is minimized. The adiabacity means that the fiber shape changes so slowly that the light does not discover the change, so the light travels in the same mode through the fiber. The local core taper angle can be calculated as a function of fiber radius and if the tapered fiber is produced such that its local core taper angle is always below the adiabatic boundary condition curve, then the fiber is adiabatic. Then the fiber is adiabatic all the way through the tapering process and a minimum of light will be lost by coupling to higher order modes as the fiber is tapered, so the fiber will have a high transmission. High transmission fibers are very attractive for applications, especially for strong light matter interactions e.g. when using the nanofiber as an atom trap.

The local taper angle Ω is inferred from figure 2.13 as $\Omega(z) = \tan^{-1}(\frac{r(z)}{z_t})$ where $r(z)$ is the local core radius and z_t is the local taper length. For small angles $\Omega(z) = \tan^{-1}(\frac{r(z)}{z_t}) \simeq \frac{r(z)}{z_t}$. The local cladding taper angle can be found from scaling Ω_{co} as $\Omega_{cl} = \frac{r_{cl}}{r_{co}}\Omega_{co}$.

The beat length $z_b = \frac{2\pi}{\beta_1 - \beta_2}$ is the interference length where the two modes β_1 and β_2 are in phase and can interfere or beat. It is seen that coupling is most likely to occur between modes with similar β value because this will produce a long beat length.

To consider adiabatic behavior we compare the beat length z_b with the local taper length $z_t = \frac{r(z)}{\Omega(z)}$. For $z_t >> z_b$ the fiber is long enough that the propagation is adiabatic for the considered mode and the mode will follow the variations in the taper shape. For $z_t << z_b$ the propagation is not adiabatic, the fundamental mode and the dominant coupling mode are in phase over the whole relevant length z_t so the modes beats; there is a coupling between the modes, and energy is lost from the fundamental mode i.e. the guided mode β_g to excite higher order modes β_{cl} i.e. the cladding modes.

The boundary condition between adiabatic and non adiabatic behavior is $z_t = z_b$. This gives

$$\Omega(z) = \frac{r(z)}{2\pi}(\beta_1 - \beta_2) \tag{2.9}$$

So for $\Omega(z) \leq \frac{r(z)}{2\pi}(\beta_1 - \beta_2)$ the propagation is adiabatic. This condition is called the adiabatic

criteria [12]. Wee see that for similar β values, z_b is long and the adiabatic criterion is more difficult to satisfy. Ω should be slowly warying within beat length.

The maximum Ω curve can be calculated for the fiber as a function of radius using equation 2.9. E.g. [12] finds the curve for Ω as a function of the radius as shown in figure 2.14 for the LP_{01} and LP_{02} modes. When Ω is below the curve the fiber is adiabatic for the considered mode. When Ω is above the curve the fiber is lossy for that mode. It is seen that the fiber shape should be first steep (high Ω) for high radius and the shape then flattens (low Ω) as the radius is decreased until it is steep again for very low radius. In the figure the dashed lines indicate the curves for Ω when the fundamental mode is guided by the core-cladding interface and by the cladding-air interface. It is seen that the minimum Ω for adiabatic propagation is close to the transition from core guidance to cladding guidance.

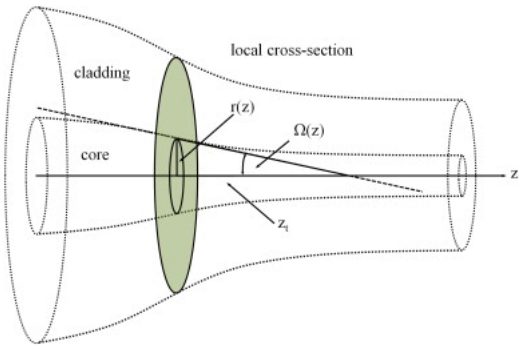

Figure 2.13: The taper transition in an optical fiber. $\Omega(z)$ is the local taper angle, $r(z)$ is the local core radius and z_t is the taper length. From [13].

So the angle Ω should be small enough everywhere such that the mode only sees a straight fiber. But it is not always possible to produce the whole tapered fiber with Ω below the curve because this will result in very long tapered sections which are more sensitive to the environment e.g. dust. Therefore it is often attractive to have short tapers.

Adiabatic fibers can be produced by pulling the fibers asymmetrically There are also other things to consider than adiabacity for the fibers to get an optimal form. For trapping atoms around the nanofiber we want the fiber to be to some extent symmetric around the center of the tapered waist such that the coupling to the atoms is equal on both sides of the fiber. In addition the tapered nanofiber section should be long enough to trap the desired number of atoms around the nanofiber, but not to long because then it can start vibrating.

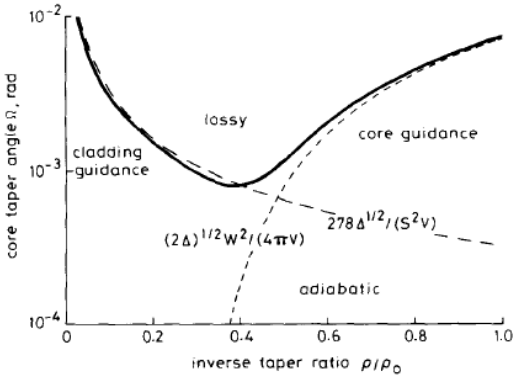

Figure 2.14: The local core taper angle Ω in radians as a function of the normalized taper core radius $\frac{\rho(z)}{\rho(0)}$. $\rho(0)$ is the initial radius. From [12].

Many have developed methods to taper fibers precisely and have succeeded in getting an ultra high transmission through the adiabatic fibers together with showing that the fiber shape

is important for the applications of the fiber. E.g. [14] shows that they are able to produce and control precise shaping of tapered fibers while [15] demonstrated design and fabrication of adiabatic tapered optical fibers with a very high transmission of 99.7%. In [16] and [17] a transmission for the fundamental mode of 99.95% was obtained.

Designing high transmission fibers for higher order modes is also an experimental aim, especially because the interference between the higher order modes can create a distribution of the evanescent field which is attractive for atomic physics experiments, as it breaks the symmetry of the mode propagation axis such that the need of a standing wave for atomic trapping is suppressed. It has be shown [13] that by reducing the cladding to core radius ratio the requirement for adiabatic propagation of the LP_{11} mode can be reached. In [18] 85-95% transmission for higher order modes were obtained. Whereas in [19] a transmission of 97.8% for the first excited LP_{11} group of modes was obtained. Also research in producing fibers for other applications, e.g. for coupling to wispering gallery modes is investigated [20]. (A wispering gallery mode is a mode that can travel around a concave surface). This shows that the shape of the tapered nanofiber is important for its applications.

2.2.2 The shape of the tapered nanofibers

The shape of a tapered fiber which has been produced by symmetrically pulling it i.e. pulling the same distance in each direction (left and right) at the same speed, is expected to be exponential [21] as shown in figure 2.12 and figure 2.15.

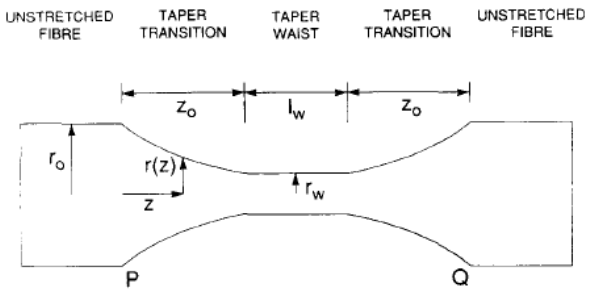

Figure 2.15: The fiber shape after tapering. It consist of the untapered optical fiber outside points P and Q and the tapered fiber inside. The tapered fiber consists of the taper waist of length l_w and on both sides the taper transitions each of length z_0. $r(z)$ is the taper profile function and r_0 is the initial radius. r_w is the waist radius. From [21].

In [21] it is explained how the shape of the fiber can be modelled without using fluid dynamics. To do this it is assumed that the fiber is heated uniformly and that the heated section is cylindrical. This can be satisfied by using a box-shaped temperature distribution and pulling the fiber symmetrically. The box-shaped temperature distribution is a good approximation for small heaters whereas for wider heaters the temperature distribution is better described with a Gaussian distribution, where the maximum temperature is in the center and the temperature is decreasing outwards, as also found in [22]. But the assumption in [21] avoids using fluid dynamics as the viscosity distribution of the fiber resembles the temperature distribution.

At the time t during elongation the hotzone AB of length L is heated, see figure 2.16. It is assumed that in the hotzone the silica glass is soft enough to be stretched but not so soft that it sags under its own weight and that the fiber is cold outside the hotzone. At a later time $t + \delta t$ the hotzone AB has been stretched through δx and now only A'B' is being heated. The model by [21] use conservation of volume of the fiber during elongation and the fact that the local taper profile radius $r(z)$ at point z is equal to the waist radius r_w as that point was

pulled out of the hotzone see figure 2.15. For the pulling setup which I use there the hotzone is constant ($\delta l = 0$ in figure 2.16). With a constant hotzone length L_0 [21] find the taper profile function $r(z)$ to be described by a decaying exponential profile:

$$r(z) = r_0 e^{-\frac{z}{L_0}} \tag{2.10}$$

where r_0 is the initial fiber radius.

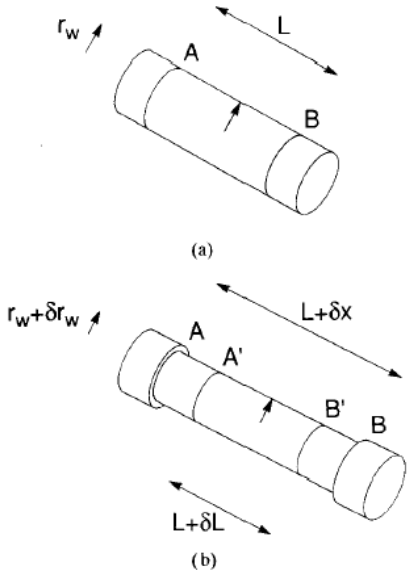

Figure 2.16: a) At time t the cylindrical fiber is heated between points A and B (the length L). b) At time $t + \delta t$ the fiber has been elongated δx. From [21].

I have mostly pulled symmetric fibers to have the same fiber shapes to heat in the vacuum chamber. If the heated fiber burns in the chamber it will usually be at the waist that it burns, because the fiber gets hottest at the waist where it is thinnest. Therefore I do not think it will make a significant difference on the power at which the fiber burns if the fiber shape is adiabatic and the fiber is pulled asymmetrically or if the fiber shape is not adiabatic and the fiber is pulled symmetrically. So I do not expect that the fiber shape will influence the power needed to burn the fiber because the fiber burns at the same place, i.e. the waist, every time. But the length of the waist and diameter might influence the breaking power.

To find the length I have to pull the fibers in order to obtain the wanted waist diameter I use an algorithm developed in [22] and [23]. The algorithm models the fiber shape using the fibers fluid dynamics. The algorithm takes as input the pulling length and the fluidity profile τ(z) of the fiber. The fluidity is the inverse of the viscosity and tells about how willingly fiber mass is to flow in the fiber. The quantity τ(z) can be determined from the cross section area A(z,t) of the fiber. The area is measured, using another algorithm, from a picture taken of a fiber that is pulled only a short distance (1-2 mm). Using the axial velocity profile v(z) of mass flow in the fiber, τ(z) can be determined, and the algorithm then finds the simulated fiber profile (and diameter) for the given pull length.

According to the simulation the fibers produced in this project have a waist of approximately 1 mm (2 mm) when their diameter is 500 nm (400 nm). The longer the fiber is pulled the longer the taper section becomes. There is an uncertainty on the algorithm as it uses the fibers fluidity profile which is much dependent on how the fiber, used for the simulation, is placed in the oven.

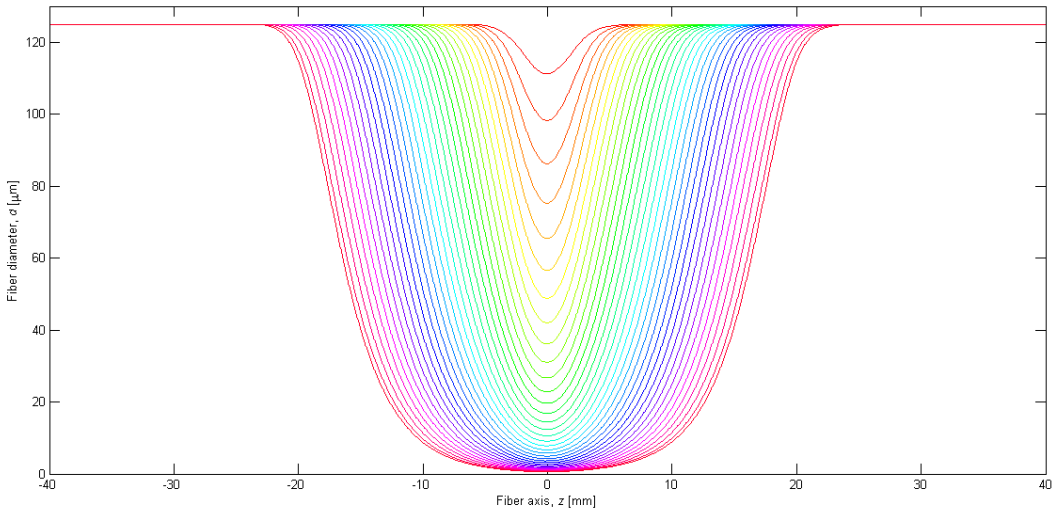

Figure 2.17: The modeled diameter of the fiber after 35 consecutive pulls of 1 mm followed by 1 pull of 0.7 mm. The fiber is simulated to be pulled a total of 35.7 mm which gives a nanofiber diameter at the waist of 500 nm.

2.3 Thermal properties of nanofibers

2.3.1 The violation of Plancks law by a nanofiber

The thermal properties of tapered 500 nm diameter nanofibers are investigated in a paper by Wuttke and Rauschenbeutel [3]. Here it is found that because the diameter d of the fiber is less than the thermal wavelength λ_T, then the thermal radiation of the fiber can not be described classically by Plancks law and instead fluctuational electrodynamics (FED) has to be considered. Because $d < \lambda_T$ the volume of the emitter (i.e. the nanofiber) also has to be considered when the thermal properties are described.

In [3] the tapered 500 nm diameter silica nanofiber was also produced by a heat and pull proces. They also consider the change in optical path length change of the light through the fiber, as they heat the fiber with a laser. In the fiber they have two fiber Bragg gratings which functions as mirrors such that the nanofiber is a Fabry Perot resonator for the light. They then look at the Fabry Perot transmission peaks.

A fiber bragg grating (FBG) is a bragg grating in the fiber that reflects some wavelengths and transmit all other wavelengths. The grating is made by a periodic variation of the refractive index in the fiber core. This means that the when light is sent through the fiber some light will be transmitted through the first FBG_1 to the second FBG_2 where some light is reflected back to FBG_1 and some light is transmitted through FBG_2. The part T_1 that is transmitted through FBG_2 interferes with the part T_2 that first gets reflected from FBG_2 to FBG_1 and then reflected from FBG_1 to FBG_2. When the fiber is heated the optical path length of the light through the fiber changes so the freqency of the transmitted Fabry Perot resonance peaks are changed. They then count the peaks and as they know the difference in optical path length change between the peaks, $\Delta L_{opl} = \lambda_{laser}/2$, they can calculate the optical path length change.

They observe that the optical path length change of the light through the fiber increases linearly with heating power. Classically they calculate, using Plancks law, that the optical path length change should not depend linearly on heating power but follow a more logarithmic function which also seems to saturate for high heating powers.

Classically the heat radiataion of an emitter (black body) is described by Plancks law.

A black body is an ideal perfect absorber and a black body in thermal equilibrium is also an ideal perfect emitter. The emission is called black body radiation and has a spectrum $P(\nu, T)$ given by Plancks law:

$$P(\nu, T) = \frac{2\pi h\nu^3}{c^2} \frac{1}{e^{\frac{h\nu}{k_B T}-1}} \tag{2.11}$$

which shows that the radiation spectrum for a frequency ν only depends on the black bodys temperature and not on the bodys shape or material.

Stefan-Boltzmanns law is Plancks formula integrated over angles and frequencies. This gives the total power H radiated pr unit area A and is for a black body: $\frac{H}{A} = \sigma T^4$ where $\sigma = \frac{\pi^2 k_B^4}{60\hbar^3 c^2}$ is a constant.

A real (gray) object (not a black body) can be related to black body radiation by introducing a correction factor: the spectral emissivity ϵ which is surface property. In this way the surface area of the emitter is taken into account. A black body then has $\epsilon = 1$ whereas a gray body emits radiation less efficient than a black body and has $\epsilon < 1$. The emissivity is the effectiveness in emitting energy (thermal radiation) and it is given as the ratio of the emitted thermal radiation of the gray body to the emitted thermal radiation from a black body. The emissivity can depend on wavelength and angle of the emitted light.

But Plancks law is only correct when the size of the emitting object d is larger than the thermal wavelength λ_T and therefore should not apply for the tapered nanofibers, which is also what [3] concludes although others [24] have observed the opposite.

In [3] they consider a thermodynamic model of the fiber in order to compute the temperature distribution $T(t, z)$ of the fiber, as a function of time t and position z. The heat equation in units of power is:

$$c_p \cdot \rho \cdot \partial_t T dV = -dH_{rad}(T) + dH_{rad}(T_0) + dP_{heating} + \nabla(\lambda \nabla T) dV - \sqrt{\frac{k_B f^2}{8\pi M T_0}} p(T - T_0) dS \tag{2.12}$$

The term on the left hand side is the heat inside the fiber at temperature T. The quantity c_p is the specific heat capacity of silica and ρ is the density of silica. The terms on the right hand side are the radiated heat at temperature T, $-dH_{rad}(T)$, the absorbed heat at room temperature T_0, $dH_{rad}(T_0)$, the power of the heating laser $dP_{heating}$, and the heat conductivity of the fiber λ. The last term $\sqrt{\frac{k_B f^2}{8\pi M T_0}} p(T - T_0)$ describes the heat transport from the fiber to eventual particles in the surrounding and can be neglected since the fiber is in a vacuum chamber. They also show that heat diffusion through the surrounding gas in the vacuum is negligible for the pressures $p < 10^{-4}$ mbar they achieve.

As the fiber at the nanosection is very thin it is assumed that the temperature is constant across the fibers diameter and then the problem can be reduced to only considering the temperature distribution along the fibers length, the z axis.

The equation can then be solved numerically, for a given radius profile of the fiber and by applying the relevant boundary conditions the fibers temperature distribution $T(t, z)$ is obtained. (They assume a boundary condition where the fiber is initially thermalized and where

no heat flow occurs at the boundary).

The equation is first solved using Plancks law to compute the radiated heat $dH_{rad}(T)$ and then using the predictions from FED theory.

The FED theory is inspired by [25], from where it is known that for objects with sizes d smaller than or on the order of the thermal wavelength $\lambda_T = \frac{\hbar c}{k_B T}$ (the thermal wavelength is approximately 7.6 μm at room temperature), then the radiated energy is different from Plancks law because of interference effects of the small emitting object with the emitted radiation. Then the emissivity depends on the size and shape of the object. Also if the emitting object is very small then the volume of the object should be considered rather than the surface area of the object when calculating the emitted power.

In [3] the radiated power per unit length of an infinite cylinder of radius a and at temperature T is calculated. The spectral emissivity $\epsilon(\nu)$ is found by normalizing the total radiated power per surface area with the radiated power from a black body equation(2.11) (Plancks formula). This emissivity is only valid for the cylinder diameter it was calculated for and will give a wrong result for another diameter. Especially for nanofibers (very thin cylinders) the heat radiation scales with volume and not surface area as for bigger objects and because emissivity is a surface property it does not exactly apply to nanofibers. Actually, as the emissivity is defined as a surface property, the emissivity of nanostructures (with $d < \lambda$) can exceed 1 which means that their thermal emission is higher than that of a black body [26].

In figure 2.18 the spectral emissivity, (the fraction of power radiated at a given wavelength), as a function of optical frequency of a nanofiber and a black body is compared. We observe that for 789.6 nm light (380 THz) the emissivity for the nanofiber is low, around 10^{-6} whereas it is high for the black body. For the black body as the temperature is increased it emits more light at higher frequencies and in the visible region. But here the nanofiber has a low emissivity and is transparent.

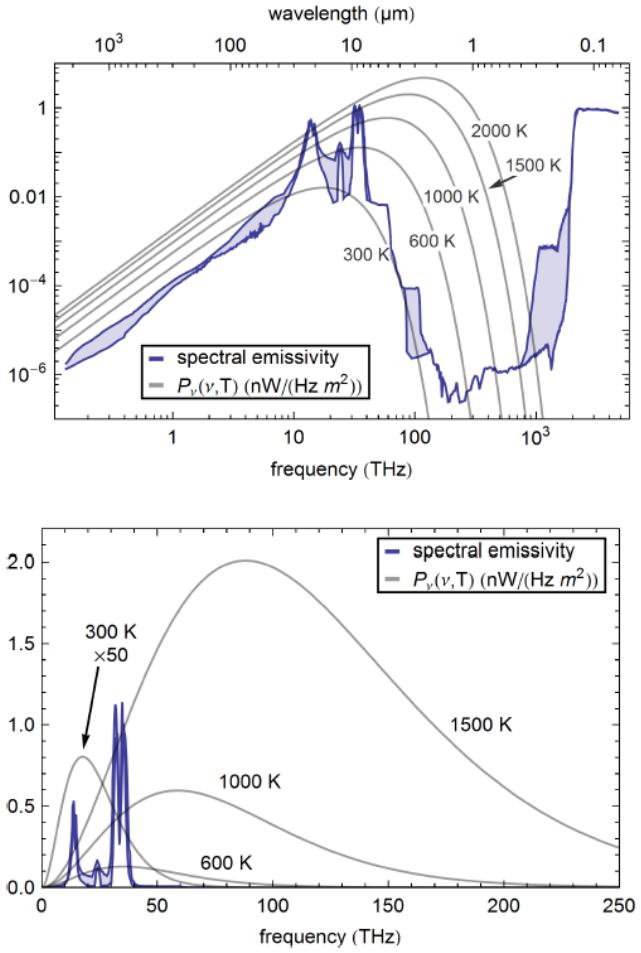

Figure 2.18: The spectral emissivity as a function of optical frequency of a nanofiber and a black body. From [3].

The emissivity of the nanofiber-vacuum interface as a function of temperature can be found from Stefan-Boltzmanns law which for a gray body is $H(T) = \epsilon(T)\sigma T^4 A$. In [3] $\epsilon(T)$ is found from Kirchoffs thermal law $\epsilon_\lambda = \alpha_\lambda$ which states that the emissivity at λ equals the absorptivity at λ. This theory then neglects transmission of light through the object and is therefore actually not valid for the nanofiber because the nanofiber is transparent for visible and IR light. The emissivity is found in [3] to be constant at 0.9 for $T > 1500$K.

As mentioned [3] finds that the FED theory describes the thermal properties of the nanofiber better than the Planck theory. They conclude that this is because Planck law which is valid for macroscopic objects cannot be applied to objects with $d < \lambda_T$, as here the thermal radiation becomes a volumetric effect.

2.3.2 Contributions to the optical path length change of light through a heated tapered nanofiber

The optical path length of the light through the nanofiber changes when the fiber is heated and cooled as it is in the experiment. The optical path length change is given by the integral of the refractive index $n(l)$ along the path length l: $\Delta opl = \int n(l)dl$.

The optical path length changes (according to [3]) because of the thermo optic effect of sil-

ica, the strain optic effect of silica, and the thermal expansion of the fiber radius a.

The thermo optic effect is the dependence of the refractive index n on the temperature: $n(T) = n_0 + \alpha T$ where $\alpha = \frac{\partial n}{\partial T}$ is the thermo optic coefficient.

The strain optic effect is the dependence of the refractive index n on the strain of the fiber.

As the fiber is heated it thermally expands in all three directions; axial (fiber length l) and radial (radius a) but if the fiber is pre-tensioned a length longer than it can elongate axially by thermal expansion, then it will not expand axially but only radially. The linear thermal expansion coefficient of silica is $\alpha_{te} = \frac{\Delta L}{L}\frac{1}{\Delta T} = (4-7)\cdot 10^{-7}/K$ [3].

In [3] the tapered fiber is pre-tensioned after producing it such that the nanofiber waist is elongated by $\frac{\Delta L_{strain}}{L_0} = 5\%$ of its physical length L_0. As this pre-tension elongation is much longer than the axial thermal expansion of the fiber that the fiber can achieve when it is heated, which is around 0.1% of the fiber length, then the axial thermal expansion will not change the physical length of the fiber but will only lower the stress in the pre-tensioned fiber.

As n or a changes this changes the V-parameter $V = \frac{2\pi a}{\lambda}\cdot\sqrt{n_{co}^2 - n_{cl}^2}$ and the effective index of refraction of the guided mode of light is changed $n_{eff} = \frac{\beta(V)}{k}$. Therefore we consider the effective index of refraction in the following.

It can be shown [3] that the fibers effective index of refraction as a function of radius and temperature is given by

$$\frac{dn_{eff}(a,T)}{dT} = \frac{\partial n_{eff}(a)}{\partial n}\left(\frac{\partial n(T)}{\partial T} - n\alpha_{te}(T)\alpha_{so}\right) + \frac{\partial n_{eff}(a)}{\partial a}(1+\mu_p)\alpha_{te}(T)a \tag{2.13}$$

where $\frac{\partial n(T)}{\partial T}$ is the thermo optic coefficient, α_{so} is the strain optic coefficient, α_{te} is the thermal expansion coefficient and μ_p is the Poissons ratio, i.e. the ratio of transverse (radial) strain to axial strain.

Figure 2.19 shows equation 2.13 and we see that the main contribution to the change of the effective index of refraction is due to the thermo optic effect and that there is only a negligible contribution from the strain optic effect and the radial thermal expansion.

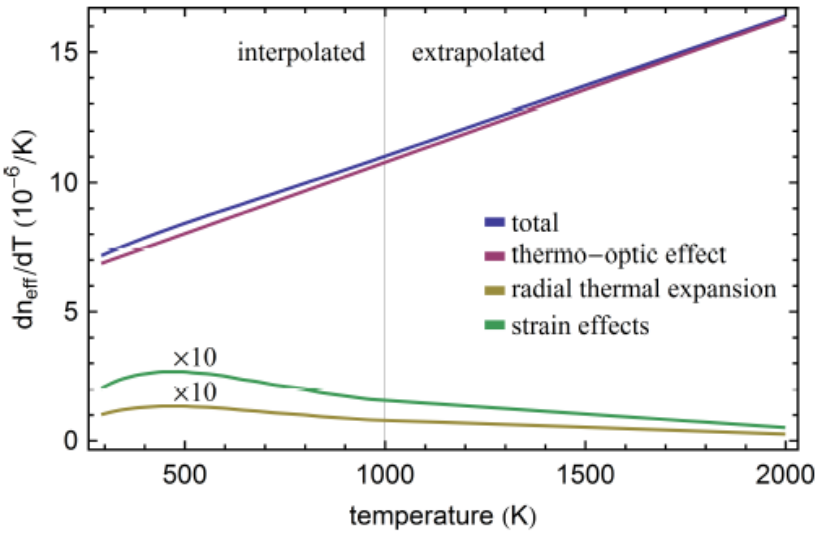

Figure 2.19: The change in n_{eff}, $\frac{dn_{eff}}{dT}$ [10^{-6} /K] as a function of temperature T [K]. From [3].

2.3.3 Pre-tension of the tapered nanofiber

As mentioned, reference [3] pre-tension the fibers after they are produced, before measuring on them. In [27] this is investigated by exposing tapered nanofibers to tensile-stress and analysing the stress-strain behaviour. (We recall that the stress is a measure of the internal forces the particles in the fiber exert on each other. The stress is measured in pressure $\sigma = \frac{F}{A}$, where F is the force and A is the area. The strain is a measure of the deformity of the material. The strain ϵ is given by the deformation Δl divided by the initial length L), $\epsilon = \frac{\Delta l}{L}$. In [27] they stretch the fiber, such that it elongates, while measuring the tensile force with a force sensor. The tensile force is the force required to pull the fiber to the point where it breaks. They plot the elongation versus the force and see that the data is linear for low strain but for higher strain and close to the breaking point of the fiber the data is described by a nonlinear model that includes a quadratic term. They find that most of the fibers can be pre-tensioned on average approximately 7% of the initial waist length before they breaks. For a 500 nm diameter fiber with a waist of 2 mm it has a strain of $7.9 \pm 0.2\%$ so it can be tensioned 7.9 % of the initial length before it breaks. The stress is then 7.0 ± 0.2GPa. They also find that the nanofiber is a brittle material, i.e. they do not break in the same way when exposed to stress.

Based on this discussion I will also pre-tension the fibers before measuring on them. The pre-tension also stretches the fiber and ensures that it lies more straight. Futhermore the pre-tension will make the fiber vibrate less which is convenient for atom trapping around the fiber.

2.3.4 Expected experimental results and comparison with other experimental results

The experimental setup and the way the optical path length change is measured in [3] is different from my experiment but I think it is still interesting to compare the results to see if one can use it to explain some of the measurements.

As the nanofibers investigated in both experiments have a diameter of 500 nm so $d < \lambda_T$, we could expect to observe some of the same behaviour.

As mentioned, [3] observes that the optical path length change increases linearly with power, which they describe being due to the fiber being a nanofiber and $d < \lambda_T$ so the thermodynamic behaviour of the fiber cannot be described by Plancks law.

The investigated fibers in this project have a shorter waist section, i.e. nanofiber section, than the fibers investigated in [3], so this fact might influence the observations. The fibers I have looked at had a waist section of 1-2 mm whereas the fibers inspected by [3] had a waist section of 5-10 mm.

As the fiber is heated it can get rid of the heat by radiation, heat conduction in fiber or heat transfer to eventual particles in vacuum (heat convection).

It could be expected that a fiber with a long waist will be more likely to conduct heat by radiation because of the larger resistance along the thin waist to conduct heat in the fiber. Whereas a fiber with a shorter waist could easier conduct heat in the fiber.

Besides the experiments not being equivalent this could affect the observations and we might observe another behaviour than [3].

Another factor that could influence the observations is that the vacuum in my experiment is not ultrahigh vacuum. Eventual dust particles in the chamber or on the fiber could also be expected to influence the observations. If there are any dust particles on the nanofiber they will be absorbing most of the heat from the heating laser. The dust might evaporate as the fiber is heated and this would be expected to be visible on the measured optical path length

change.

In [3] it is found that for their fibers when they are heated the strain (from the pre-tension) is released and the fibers stays stressed during the measurements (measured up to a temperature of 1800 K which is above the melting temperature of silica).

Therefore, as the fibers in this experiment are also pre-tensioned, it is not expected that the fiber will deform as it is heated. It is expected that the fiber when it is heated will relax from the pre-tensioning and for high power, close to the melting temperature of silica (1450 K), the fiber could be ripped apart. If the fiber for high heating power is deformed we expect to see it in the optical path length change.

The facts discussed here are important to consider when the data is analysed.

2.4 A tapered nanofiber as an optical trap for atoms

A motivation for investigating the thermal properties of tapered nanofibers is the use of nanofibers as atom traps [28], [29], [30], [31], [2], [32], [1].

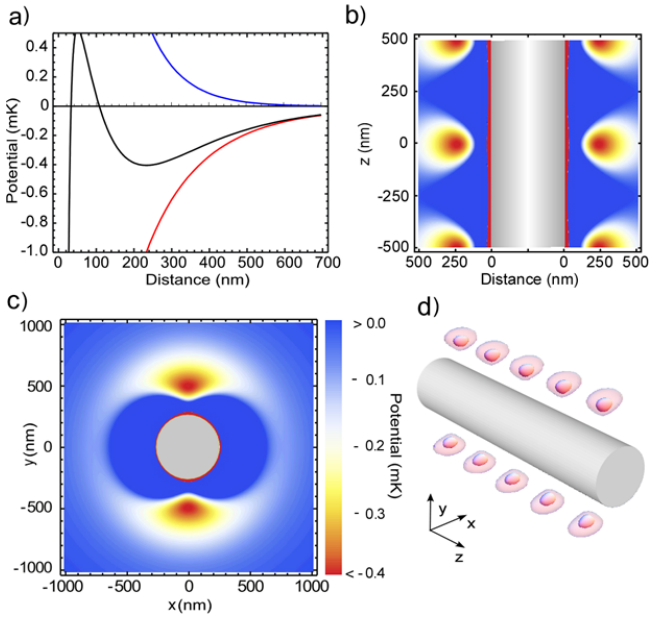

Figure 2.20: a) The potential for atom trapping close to the nanofiber surface. The red detuned beam creates an attractive potential while the blue detuned beam creates a repulsive potential. The total potential is shown in black. The potential minimum is at 200 nm from the fiber surface, here the potential is a trap for atoms. b) The atoms along the nanofiber are separated by $\lambda/2$. c) Cross section of the nanofiber. The atoms are trapped above and below the nanofiber. d) The nanofiber with atoms trapped around it. From [1].

A tapered nanofiber is currently used at QUANTOP in a setup where Cs atoms are trapped around the nanofiber in the evanescent field of the light sent through the nanofiber. As $d < \lambda$ i.e. the wavelength of the light through the fiber is greater than the diameter of the nanofiber (500 nm) the light will propagate with a very intense evanescent field around the tapered nanofiber section and this can be used for creating a potential well for trapping atoms. The atoms can be trapped in the focus of the intense light. The trap uses a red detuned 1064 nm beam and a blue detuned 780 nm beam which are sent through the nanofiber (detuned with respect to the atomic Cs D2 line of 852 nm), see figure 2.21. The red detuned beam creates an attractive potential for the atoms, while the blue detuned beam creates a repulsive potential for the atoms, so the total potential that the atoms feel is a potential well, that they can be trapped in at a distance of 200 nm from fiber surface, see figure 2.20a. This trap is created along the fiber because of the fibers cylindrical symmetry. To trap the atoms at separated positions two counter propagating red detuned beams are used. The two beams create a standing wave, as they propagate against each other and the interference of the two beams creates a periodic potential with minima and maxima of the potential energy. This is then a 1D optical lattice where the atoms are trapped in a row along the fiber (i.e. on the antinodes of the standing wave). The atoms are separated by $\lambda/2$. Two 1D optical lattices are created one above and one below the fiber so atoms are trapped above and below the fiber, figure 2.20d.

The tapered nanofiber is placed in vacuum in a MOT (Magneto Optical Trap) used for collecting and cooling the Cs atoms.

For the nanofiber trap at QUANTOP they need tapered nanofibers that can stand 15 mW of laser power. Therefore in this experiment it will be investigated if the fibers can stand 15 mW of heating power.

The 500 nm diameter of the fiber is chosen as this diameter results in a high power density of the evanescent field around the fiber. (Actually a diameter of 400 nm would give the highest power density [33]). Also at a diameter of 500 nm the nanofiber is single mode and guides only the fundamental mode HE_{11} for the two wavelengths used (780 nm and 852 nm).

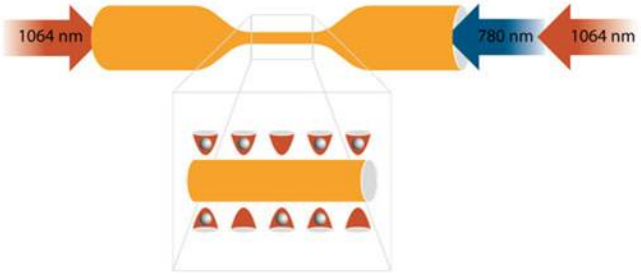

Figure 2.21: The blue detuned and two counter propagating red detuned beams create a trap for the atoms. There can be trapped 0 or 1 atoms in each well separated by $\lambda/2$. Figure from [34].

Two probe beams each achieve a phase shift when they propagate through the atoms. As the two beams have different frequency, the phase shifts are different for the two beams and the difference in phase shift can be used to calculate the number of atoms around the nanofiber. Approximately 2500 Cs atoms are trapped along the nanofiber. The phase shift measurement is non destructive, so this is a QND (quantum non demolition) measurement, as the atoms do not absorb the light (because the light is not on resonance with the atoms) which means that the photons are not scattered and the atoms stay in the trap. The noise on the measurements is the natural quantum noise so the method can be used to measure on entangled states of atoms which interacts with the light through the nanofiber. This is relevant for use in future quantum computers.

Chapter 3

Experimental part

In this section I will describe the experimental setup used for pulling fibers and the setup used for heating and burning the fibers. When I started there was a working setup for pulling fibers; a 852 nm laser, an oven and translation stages which just needed alignment. The oven and the translation stages were placed inside a flowbox with a flow of air downwards to keep the enclosure clean to avoid contamination of the fibers which are produced in there. Then I have built the setup for heating and burning the fibers and I have often changed and improved the setup when new ideas appeared that could make the setup better, less sensitive to laser modejumps and to fluctuations in the interferometer, or more convenient to work with.

3.1 Fiberpulling

In this section it is described how the fibers are pulled. First the experimental setup for fiberpulling is described and then it is described how the fibers are prepared for the fiberpulling including the importance of cleaning the fibers. The heat and pull method for fibermaking is described followed by an analysis of the transmitted light through the fibers. Finally it is explained how the fibers are glued and transferred to the vacuum chamber.

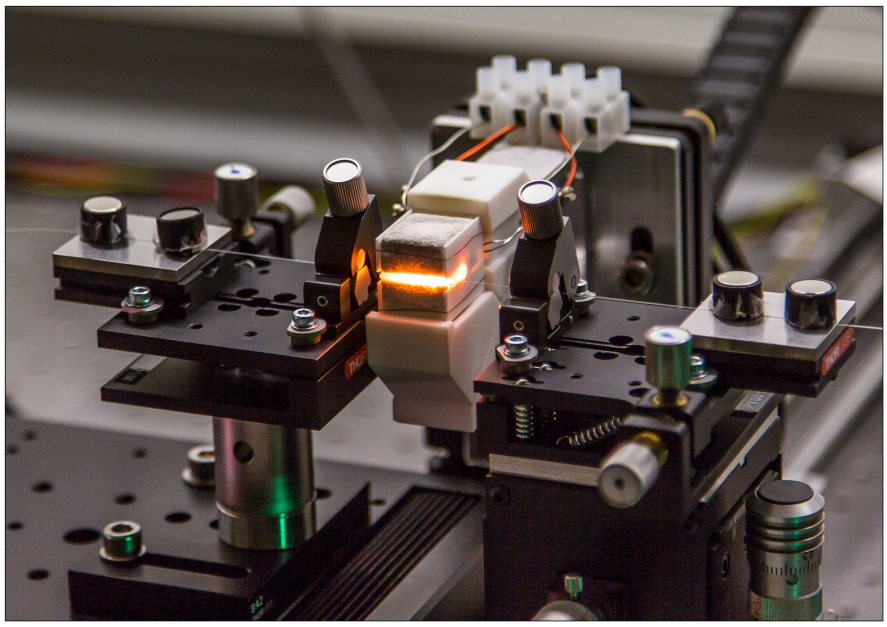

Figure 3.1: The oven heats the fiber, which is placed in the clamps, while the stages pull the fiber.

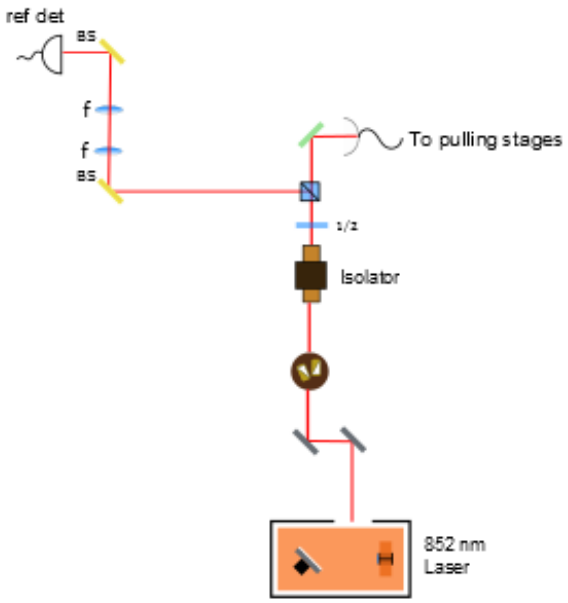

Figure 3.2: The experimental setup for fiberpulling. The beam from the laser (red) is directed with two mirrors through the prism pair into the isolator. After the isolator there is a $\lambda/2$ waveplate followed by a PBS. The transmitted beam from the PBS is reflected at a beamsplitter (green) and coupled into the fiber that goes to the pulling stages. The reflected beam at the PBS is with two beamsamplers (BS) and two lenses (f) directed to a reference detector (ref det).

3.1.1 Experimental setup

The fiber pulling setup is seen on figure 3.2. The 852 nm (Cs D2 line) laser beam is directed with two mirrors though a prism pair, used for changing the shape of the beam from elliptical to circular, into the isolator. The isolator should avoid back reflections into the laser. The beam then passes a $\frac{\lambda}{2}$ waveplate and a polarizing beam splitter (PBS) where the waveplate is used to change the intensity of the light into the two polarization arms (H and V) after the PBS. One arm is reflected at a 50:50 beamsplitter (BSW11) to a fibercoupler which couples the light into the SM750 fiber from Fibercore.

The fiber end, where the laser beam is coupled into is angle-polished. This is done every time the fiberspool is changed. For angle polishing I use the angle polishment from Thorlabs. The fiber end is angle polished by 8 degrees, to prevent backreflections of the light at the end face. There is a 4% coupling loss on the end face. The other end of the fiber is coupled into a detector to measure the transmission of light through the fiber, while the fiber is being pulled, see figure 3.8. This end is not angle polished, as this would take too long time to do if it should be done each time a new fiber was pulled and since it was not important for the experiment to have a maximum throughput. This fiber end is cleaved with a Fujikura cleaver at an angle of 0 degrees. (Since this end is not angle cleaved the light can reflect back through the fiber). When I started, the coupling of light through the fiber to the detector was around 10% but now I have a coupling of around 12%.

I have added a beam sampler (BS) (BSF10_B) after the PBS to be able to measure a reference signal from the laser, while the fiber is being pulled, in order to see if something strange happens with the laser. I use this to check if the laser e.g. was modejumping while the transmission was being recorded. I also use this detector as a reference detector for the 789.6 nm light in the fiberburning experiment, as explained later, see figure 3.16.

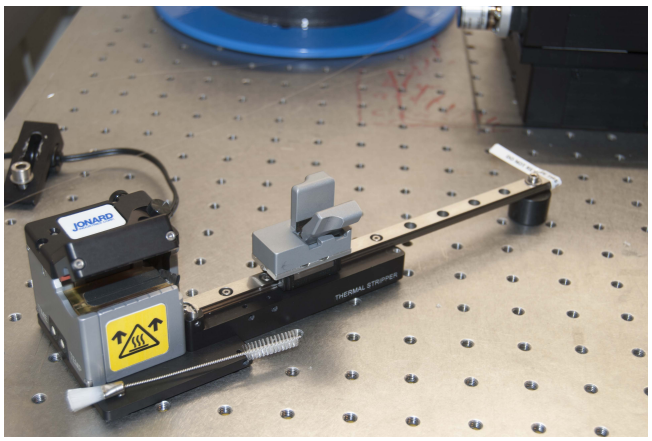

Figure 3.3: The thermal stripper.

3.1.2 Preparing fibers for pulling

The fibers are prepared for pulling by stripping and cleaning them. The glass fibers have a protective layer of plastic buffer around them. This buffer is stripped off the fiber, on the part (approximately 10 cm) of the fiber that I want to put into the fibermounts and oven. In the beginning, I used a mechanical stripper and stripped the fiber by hand. I would strip the fiber a couple of times to remove all the leftovers of the buffer. This mechanical stripping is not ideal, as it can make scratches in the glass which can scatter light and damage the fiber.

In the summer 2014 we got a Jonard thermal stripper. The thermal stripper heats the fiber so the buffer becomes soft and then the buffer is stripped of the fiber by pulling the fiber slowly through the stripper. (The thermal stripper is set to strip fibers of 125 µm diameter. It could in the beginning only strip the fibers 7 cm so the stages were moved closer to each other to fit this length). I found the thermal stripper to be more effective than the mechanical stripper because the mechanical stripper left more buffer material on the fiber, which is probably because the thermal stripper heats the buffer so it is easier to remove. In December I had a specially designed rail made for the thermal stripper. This improved fiber stripping significantly since now the wagon on the rail holding the fiber slides better and do not move in jumps as it did before. It is also now possible to move the wagon at a constant speed which makes the fibers better stripped. I also had the rail made such that I could strip longer fibers (up to 20 cm) if I wanted to make fibers with a longer taper section (this would, however, also require to move the stages sideways when the fiber is inside the oven, to make the oven heat a larger part of the fiber).

3.1.3 Cleaning fibers

The cleaning of the fibers is the most difficult step as everything afterwards depends on it. This is also the part of the preparation that usually takes most time.

In the beginning I cleaned the fibers with Kimwipes lens tissues soaked with ethanol. Then I found that cleaning the fibers with first acetone and then isopropanol, made the fibers more clean. The actone, which is a good solvent for plastic, dissolves the leftovers of plastic buffer on the fiber, whereas the isopropanol, which is a good cleaning alcohol removes the dust. Isopropanol is better than ethanol for cleaning because it evaporates quickly and does not leave as many droplet traces as ethanol. The best cleaning result is obtained by moving the tissue soaked with chemicals from the un-stripped part along the stripped fiber and end at the un-stripped part. Then the tissue will collect and push all the dirt to the un-stripped part. It is important to hold the tissue tight on the fiber so the chemical touches the whole fiber, but not to tight since then the fiber can break.

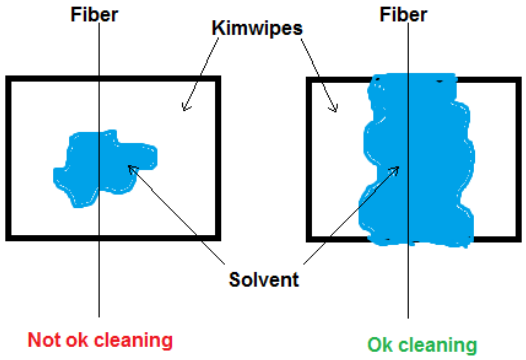

Figure 3.4: The figure shows how to clean the fiber (thin black line). With only a small amount of cleaning chemical not covering the whole Kimwipe tissue and the risk of the fiber touching the dry tissue the fiber will not be as clean as with the tissue wet everywhere the fiber will touch it.

The dirt on the fiber can be dust from the environment, from the Kimwipes, from the leftovers of the plastic buffer, from the droplets of the cleaning chemicals, or from other particles in the cleaning chemicals. Although both the acetone and isopropanol are spectroscopic grade, the top of the container with the chemicals could become contaminated. As the Kimwipes can also pollute the fibers while they are cleaned, it is very important that the Kimwipe is wet everywhere it touches the fiber, see figure 3.4.

It can take a long time to get a clean fiber, and cleaning it too much can also make it more dirty than it was, as more dust is applied than removed with the tissue. Often after a couple of times cleaning the fiber you will end in an equilibrium where you apply as much dirt as you remove, and then my experience is that it is best to take a new fiber and start over.

In [17] they actually used the opposite of what I found most efficient for cleaning: first isopropanol and then acetone, followed by a final clean with methanol. They did comment that they discovered that it was not good to use acetone at all, because acetone can make the cleaning process take longer time, as acetone spreads small buffer particulate along the stripped fiber. Therefore I think it is best first to clean once with acetone (to remove the worst particles) and thereafter only use isopropanol. I did try to clean the fiber with one drop of methanol and slide it across the fiber which was lying in the stages (such that the whole fiber was covered in methanol). The first time it did not clean the fiber so well, but the second time with a methanol drop, the fiber was clean except for one big dust particle. Maybe the cleaning chemical does not make a big difference but the difference is in the method you choose to apply the cleaning chemical: the single drop could be more efficient than the kimwipes tissues.

After the fiber is cleaned it is placed in the stages and inspected with a CCD camera for contaminations, see figure 3.5. If there is dirt on the fiber, the fiber is taken out and cleaned again. It is very important that the fiber is clean because dust on the fiber can melt and burn into the fiber and break the fiber when it is heated in the oven. The dust can also scatter light, change the propagating modes and decrease the transmission.

When the fiber is clean, it is placed in the mounts on the stages and first tensioned 200 µm then relaxed 20 µm (these numbers were inspired by [17]). The fiber is tensioned so that it is lying straight in the stages and it is relaxed a bit, so it is not overtensioned. If the fiber is overtensioned, then when it is heated it will relax and deform a bit. While the fiber is tensioned it is watched with the camera how the fiber moves. Usually it is enough to tension the fiber 200 µm but if the fiber is misplaced in the mounts it should be tensioned more. If the fiber

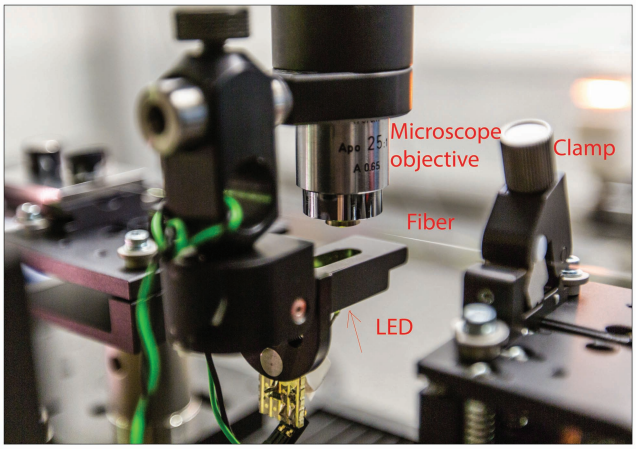

Figure 3.5: The camera is a 768·1024 pixel CCD camera. It has a microscope objective with a magnification of M=25 and an adjustable focus. A green LED illuminates the fiber from below.

moves a lot (transverse to the fiber axis) while it is tensioned, it is very misplaced and should be taken out and repositioned in the stages. The fiber from the last part of a fiber spool is more difficult to place well in the stages as this part of the fiber is a bit more bended from the curvature around the spool. This fiber part memorizes some of the initial stress and needs more tension when it is placed in the stages.

3.1.4 Making tapered fibers: heat and pull method

The tapered nanofibers are produced by a heat and pull method. The stripped and cleaned fiber is placed in the stages which pulls the fiber apart while an oven heats and melts a small section of the fiber as seen in figure 3.1. In this way the fiber radius is gradually decreased to a nanofiber section.

I use a heat and pull setup which was build by Heidi Sørensen. I will give a brief overview of the setup, but more details can be found in her thesis [22] and paper [23]. The fiber pulling setup consists of a pair of translation stages and an oven see figure 3.6. The translations stages are motorized and programmed to move at a constant speed of 50 µm/s. The stages are placed on top of each other and the top stage does the actual pulling whereas the bottom stages only translates the fiber. For a symmetric pull the top stage then moves twice the distance as the bottom stage. On the top stage there is a pitch and yaw translation stage and placed on this is a mount with the fiber clamps. On the bottom stage there is a XYZ translation stage, a pitch and yaw translation stage and a mount with the fiber clamps.

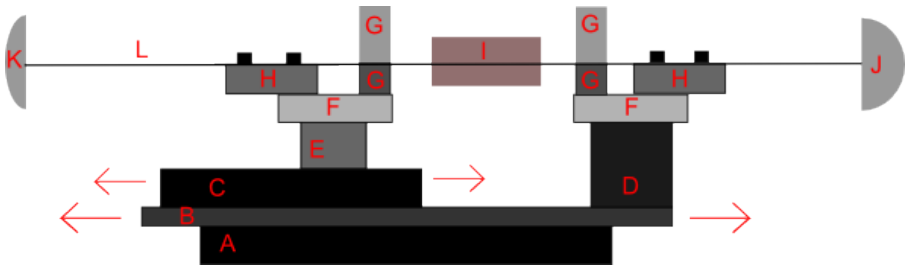

Figure 3.6: The heat and pull setup. A: The bottom stage which is stationary. B: Adaptor plate which can be translated. In the text I refer to this plate as the bottom stage. This stage translates the whole setup. C: The top stage. D: XYZ flexure translation stage. E: A mount to make the two F the same height. F: Pitch and yaw stages. G: Fiber clamps. H: Mounts with magnetic clamps. I: The oven. The camera can also be placed here when the oven is out. J: Transmission detector. K: Fibercoupler, with light from the laser. L: The fiber.

In the original setup the fiber clamps, for holding the fiber on the stages, consisted of only two magnets and the unstripped fiber was then placed in a V-shaped groove. It is more accurate if the fiber is clamped also at the stripped part where it is clean, because the buffer might not have the same diameter everywhere or might be dirty which can cause some tension in the fiber as it is clamped. Therefore we applied some new clamps which holds the fiber at the stripped part. The clamps, see figure 3.7, turned out to be good for holding the stripped fiber but they were difficult to align as they are very sensitive to the alignment. (It should be noted that the clamps are very sensitive to the position of white plastic cylinder on top of the hexagonal metal element holding the fiber. They are also sensitive to the screw that tightens the metal element as too much tightening can lift it up and too little will make it loose. There is another sensitivity in how much to tighten the spring which closes the clamp. All this can change the position of the fiber and therefore the alignment). The magnetic clamps are still important to ensure that the fiber does not slip when it is pulled.

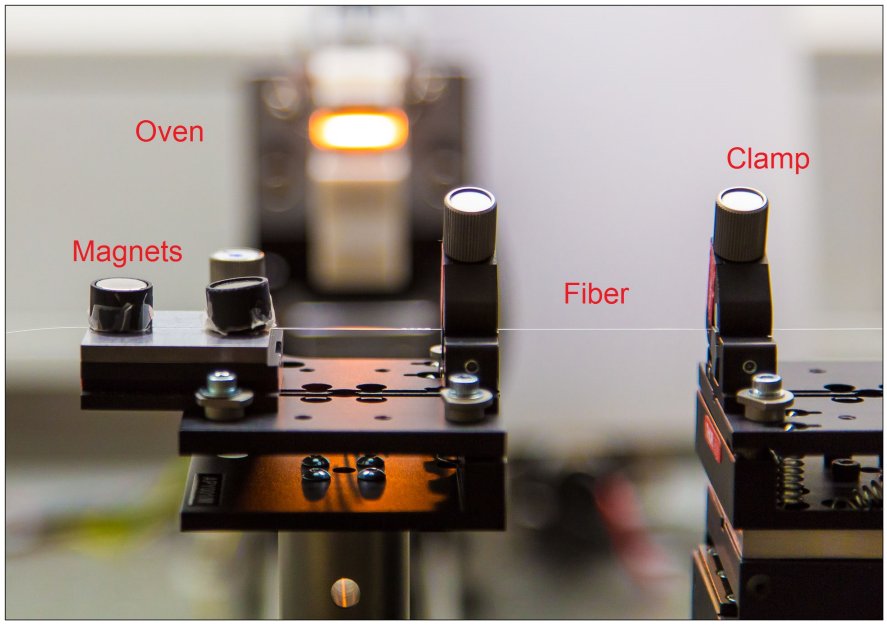

Figure 3.7: The fiber clamps and magnetic clamps. The oven is seen in the background.

The oven is an electric ceramic micro heater and is placed on a motorized rail such that it can drive in between the two mounts to heat the fiber. The oven has a 2 mm wide slit where the fiber goes in and the oven is around 1.6 cm long.

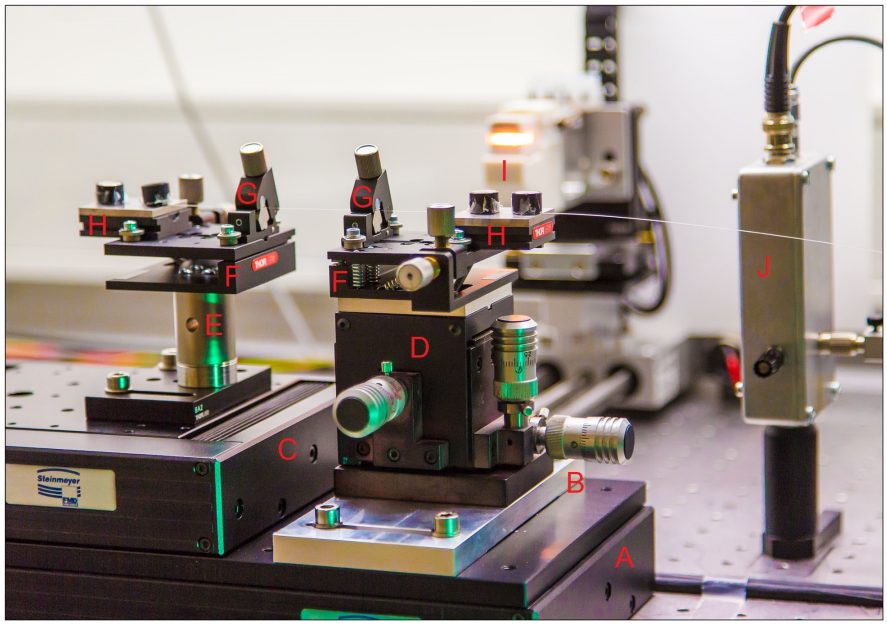

Figure 3.8: Fiber pulling setup. The drawing figure 3.6 shows the layout schematic. The letters also refer to figure 3.6.

That the stages should be moving and the oven standing still was chosen [22] because this would avoid air currents carrying heat away from the oven, which could happen if the oven is moving as the surrounding air will be pushed by the oven. The air currents could also make the oven heat the fiber in an non-uniform way. Even then, as discussed in the theory section, the oven temperature distribution does not allow the fiber to be heated equally everywhere as it is not described by a box-shaped profile but turns out to be described by a Gaussian profile [22]. (It is possible to adjust the position of the oven relative to the stages so the oven can be aligned to them. After aligning the stages the oven should be aligned such that the fiber is in the middel of the oven without touching it).

Each time something on the stages is changed, e.g. the position of the clamps, the stages and oven must be re-aligned. The stages can be aligned using the camera but it is more precise using a laser module. The stages are aligned to the middle position of the top stage because then the misalignement in the two outerpositions of the top stage will be equal. The alignment is first done by eye using the tilt, height and transverse position of the two pitch and yaw stages. Then the XYZ stage is used to align horizontally and vertically (i.e. the focus), by looking at the fibers position with the camera at the two camera limits(the limits where the camera can be placed between the stages). This alignment typically gives a misalignment between the two fiber ends of 5-10 pixels in the middleposition and 30-40 pixels in the outer position. (1 pixel = 0.18µm [22])

When the camera is used for alignment it is not possible to inspect the whole fibers position, because of the camera limits, the camera cannot be positioned very close to the fiber clamps, see figure 3.5. By shining light on the fiber with a laser, it is possible to see the fibers position close to the clamps. This gives a better alignment because close to the clamps the fiber is more affected by the clamping (clamping force and the direction the fiber points in when clamped), so when this part of the fiber can be inspected, the alignment can be optimized.

The green LED laser light is diffracted on the fiber and by watching the diffraction pattern, when the fiber is moved through the laser, the stages can be aligned. The fibers diffraction

pattern looks complicated (probably because the fiber is transparent) but is dominated by a green line with black fringes. The LED laser is focused with a 50 mm lens on the fiber with the diameter of 125 µm. With this lens, the size of the beam is on the same order as the size of the fiber. When the laser is positioned above the fiber the horizontal position of the fiber can be aligned and when the laser is positioned on the side of the fiber, the fibers vertical position can be aligned, see figure 3.9 and figure 3.10. If the fiber is vertically or (horizontally) misaligned the position of the diffraction pattern changes when the fiber is scanned through the laser and the fringes in the pattern moves up/down. (First the vertical (transverse horizontal) screw on the XYZ stage are changed and then the vertical (horizontal) screws on the pitch and yaw stages until neither the position of diffraction pattern or the fringes in the pattern change as the fiber is scanned through the laser). The laser alingment is now so good that the fiber is only misaligned by 5-10 pixels in the outer positions and 0 pixels in the middleposition.

If the alignment is done well, it means that the tension in the fiber will be mostly along the fiber axis.

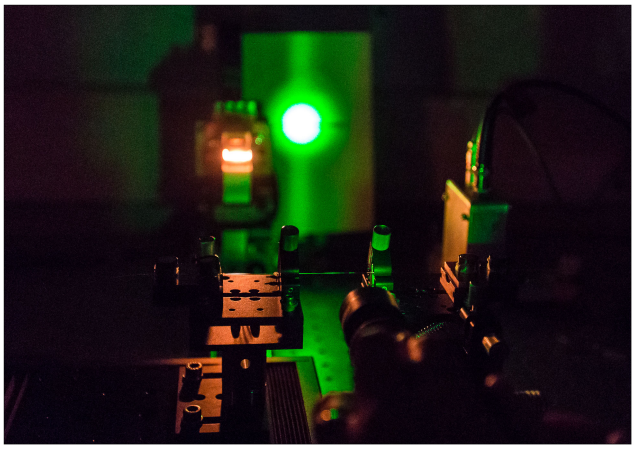

Figure 3.9: Vertical alignment of the stages, as explained in the text.

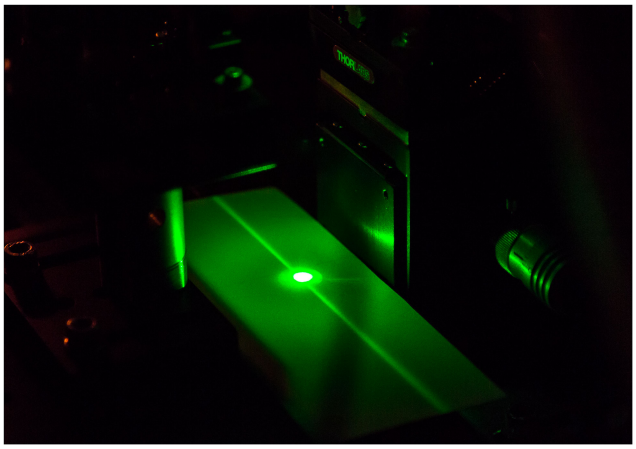

Figure 3.10: Horizontal alignment of the stages, as explained in the text.

The procedure that works best for pulling fibers symmetrically is the following:
- The oven goes in on the left side of the fiber (close to the left clamp) and tension the fiber 200 µm.
- Then the oven goes to the center of the fiber and the pulling starts.
- When the pulling is finished the oven goes straight back.

The fiber is tensioned in the left side, before the pull in the center, because when the oven first meets the fiber, something (e.g. a small wiggle or twist) could happen to the fiber. Therefore it is better if this happens at another point than the center where the nanosection will be. I have experimented with the oven in the right side and in the left side, heating the fiber, while the fiber is tensioned, before the fiber pulling begins in the center. It turned out that the best result was obtained when the oven tensioned the fiber in the left side. Then the fiber was lying more straight i.e. better aligned after being tapered and it was easier to image the whole fiber. I think it could be due to a small difference in the structure of the clamps.

After pulling the fiber it can be inspected with the camera e.g. to see if the fiber is clean and if it is lying straight, see figure 3.11. It is important that the fiber is clean if it should survive high powers in the vacuum chamber. Dust on the tapered part of the fiber scatters light from the evanescent field and this decreases the transmission of light through the fiber. Dust anywhere on the fiber will absorb the heat from the heating laser and can make the fiber break in vacuum. Also dust on the fiber it will not make the potential for atom trapping symmetric

around the tapered section. Figure 3.11 shows a picture of the pulled fiber taken with the camera.

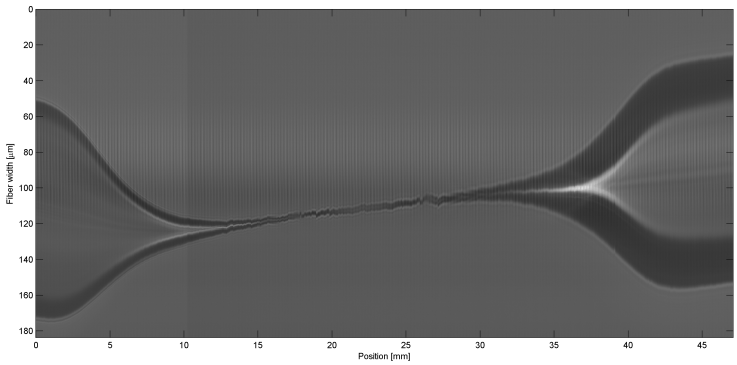

Figure 3.11: Image of the tapered fiber taken with the camera. The camera cannot resolve the nanosection of the fiber. The background light from the LED is subtracted in the picture.

Notice that the x-axis (the position along the fiber axis) is in mm and y-axis (the fiber width/diameter) is in µm so the fiber is actually lying very straight. After the tapering the fiber is often bending a bit. I suspect it is due to the tension in the fiber which is released when the fiber is heated and then if the fiber is not placed correctly in the clamps the released tension will make it bend a bit. Or it is an alignment issue with the clamps, even though much time was spent on aligning the stages and this did reduced the bending of the fiber after tapering it a lot. If the fiber is bend the light through the fiber can couple to other modes and the transmission is decreased. If the fiber is straight the light will mostly only couple to one mode with the same symmetry as the fundamental mode so the coupling to other modes will be lower and the transmission will be higher. The fiber can be imaged by moving the bottom stage in steps of 0.1 mm. For each step the camera takes an image and the images are then stacked to show the whole fiber. It is necessary to turn off the flow in the flowbox when the fiber is imaged because the flow makes the thin part of the fiber vibrate and then the image is blurred. There is thus a risk of the fiber being contaminated while it is imaged. Therefore I do not image all the fibers that I want to transfer to the vacuum chamber. The camera has a limited resolution of 0.18 µm/pixels as found in [22] so it is difficult to image the nanosection of the fiber as this part will only be a few pixels.

3.1.5 Analysis of transmitted light through fiber being tapered

The light transmitted through the fiber is measured and analysed with a Gabor transform.

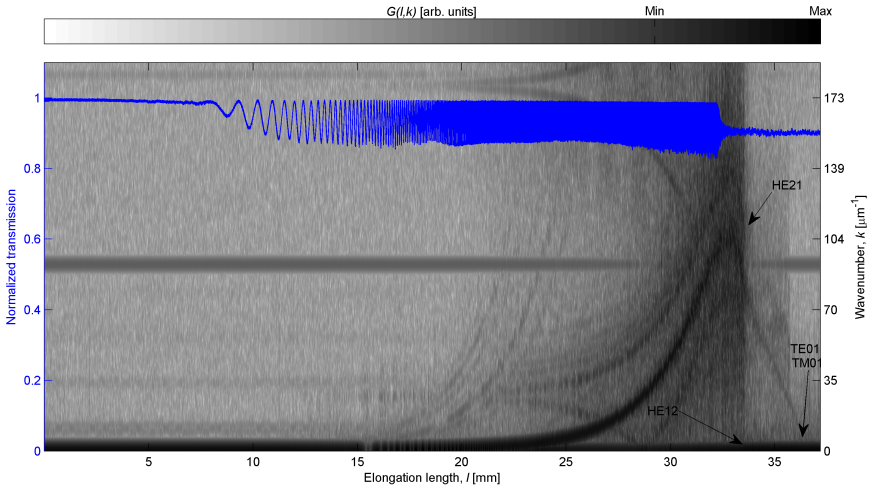

Figure 3.12: The transmission through the fiber during tapering is shown in blue. The transmission oscillates due to the beating of excited higher order modes. The beat modes in the signal are shown in black. The mode drops are indicated with arrows.

Figure 3.12 shows the transmitted light through the fiber as a function of elongation length (i.e. pull length). The final transmission is 90%. The transmission decreases due to excitation of higher order modes, scattering of light and other types of loss in the fiber. The transmission start oscillating at an elongation length of approximately 8 mm and stops again around 33 mm elongation length. With the present pulling procedure the "record" final transmission was 94% for a 500 nm fiber but usually I get a final transmission around 90%. A transmission higher than 94% can be obtained by pulling the fibers adiabatic, as described in section 2.2.1.

The optical fiber is a single mode fiber before it is pulled, but as the fiber waist is tapered higher order modes can propagate in the fiber. The fiber is thus multimode. The fiber becomes single mode again when it reaches a diameter $d \leq 621$ nm as calculated in section 2.1.5. The oscillations in the transmission are the excited higher order modes beating against each other. As the fiber is elongated the excited modes will interfere in and out of phase with each other thereby enhancing or decreasing the transmission. When the oscillations stop, there is no more beating between the modes, so there can only be one mode propagating in the fiber. Thus, by inspecting the transmission, it can be determined when the fiber becomes single mode.

Besides the oscillations, other drops are visible in the transmission. When the transmission drops a guided mode is no longer guided in the fiber. As the fiber diameter is decreased, at a certain diameter a specific mode is no longer guided in the fiber and will therefore disappear. The diameter where the mode disappears is the cut off diameter.

As mentioned in section 2.1.4 each mode is characterized by its β-constant and the mode experiences an effective index of refraction $n_{eff} = \frac{\beta}{k}$, where $k = \frac{2\pi}{\lambda}$ is the wavevector of the mode.

The modes in the fiber, can be seen with a Gabor transform of the transmission signal.

A Gabor transform $G(t, \nu)$ is a short time Fourier transform of the transmission signal, with

a Gaussian window:

$$G(t,\nu) = \int_{-\infty}^{\infty} e^{-\pi(t-\tau)^2} e^{2\pi i\nu\tau} X(\tau) d\tau \tag{3.1}$$

Where $X(\tau)$ is the signal at time τ and ν is the frequency. The Gaussian window is for splitting the signal up in small time parts and analysing a smaller amount of data. It is more interesting to write the Gabor transform in terms of k, l instead of ν, t because we are interested in the signal as a function of pull length l not time. The pull length is $l = v \cdot t$, where v is the pull speed and t is the time, and the beat wavenumber is $k = \frac{2\pi}{\lambda} = \frac{2\pi\nu}{v}$. We can then write:

$$G(l,k) = \int_{-\infty}^{\infty} e^{-\alpha(l-z)^2} e^{ikz} T(z) dz \tag{3.2}$$

where $T(z)$ is the transmission signal and α is a constant.

The Gabor transform of the transmission is shown on figure 3.12. It shows the beating k modes (black) in units of wavenumber present in the fiber during the pull and when they disappear.

The beating modes in the Gabor transform is the result of the interaction between the different modes excited in the fiber. The different modes k_1 and k_2 in the fiber beat at the wavenumber k seen in the transform. E.g. a mode with k_1 and another with k_2 beat at the sum and difference $k_1 \pm k_2$. The beating is due to the phase difference between the modes. The modes propagating in the fiber achieves a phaseshift since $n_{eff} = \frac{\beta}{k}$ changes and the fiber length changes when the fiber is pulled. The phases ϕ_1 and ϕ_2 of the modes k_1 and k_2 can interfere constructively or destructively through the fiber so the transmission oscillates. The constructive interference is almost 100% for elongation lengths up to 33 mm, as seen in the figure. At the end of the tapered section, if the modes interfere constructively, they couple back into the guided core mode whereas if the modes interfere destructively, they couple into the cladding mode and are lost. Here the final transmission is 90%, so 10% of the energy is lost. When all the beating modes have disappeared from the transmission signal there can not be more than one mode so the fiber is now single mode. The transmission oscillates and the higher order modes are excited in the fiber because the pulling is not adiabatic. The adiabatic pulling would have a higher final transmission but could also show oscillations in the transmission.

It is interesting when the beating components disappear because this gives information on the diameter of the fiber and when the nanofiber becomes single mode. The visible modedrops are indicated with arrows in figure 3.12. It is possible to tell which mode disappears at which modedrop, since the cut off diameters of the fibers are known.

From figure 2.11 we know which modes will drop first, as the fiber radius decrease and n_{eff} and V changes. We see that the HE_{21} mode will disappear before the TE_{01} and TM_{01} modes. The mode starting at 26 mm ending at 34.2 mm could be the HE_{21} mode and the mode that disappears at 36.6 mm could be the TE_{01}/TM_{01} modes. The intense mode starting at 25 mm and disappearing at 33.5 mm could be the HE_{12} mode since this mode has a spatial overlap (same l value) as the fundamental HE_{11} mode so it is very likely that this mode will be excited. The HE_{12} mode has a larger cutoff diameter than the HE_{21}, TE_{01} and TM_{01} modes so it disappears before the other modes as the fiber is tapered.

We see that the beat wavenumber increase a lot just before the mode disappears. This is because as the fiber is tapered n_{eff} decreases and the difference between the refractive index of two modes n_{eff1} and n_{eff2} (i.e. the beating mode $n_{eff} = \frac{\beta}{k}$) increases (see figure 2.11). The

amplitude of the signal is determined by the mode coupling. Usually the more adiabatic the fiber is the smaller the amplitude is and the less the number of excited modes in the signal.

The constant lines in the signal is probably noise, because it is also present before we start the pull (i.e. at elongation length equal to zero). It can be electronic noise, noise from the laser or the background light.

3.1.6 Glueing fibers and transferring them to the vacuum chamber

The tapered fiber is glued with UV glue (Norland optical adhesive) to a specially designed device, figure 3.13, and transferred to the vacuum chamber. The fiber is transferred to vacuum to investigate its thermal properties. If there is air around the fiber the fiber can transfer heat to the air molecules, and then it will be difficult to heat the fiber. Before the fiber is glued it is tensioned a bit. E.g. for a 400 nm fiber with a waist of 2 mm a tension of 100 µm corresponds to an elongation of 5% of the waist length, which will not break the fiber according to [27]. Gluing the fibers in order to transfer them to the vacuum chamber has been quite an experiment as many fibers have broken during this step. But I have found a successful method of gluing the fibers, however, it takes some time, so there is a risk of the fiber becoming contaminated, but the method will avoid the fiber from breaking in the vacuum chamber, when the chamber is sealed. Figure 3.13 shows a picture of how and where the fiber is glued and is ready to be transfered into the vacuum chamber.

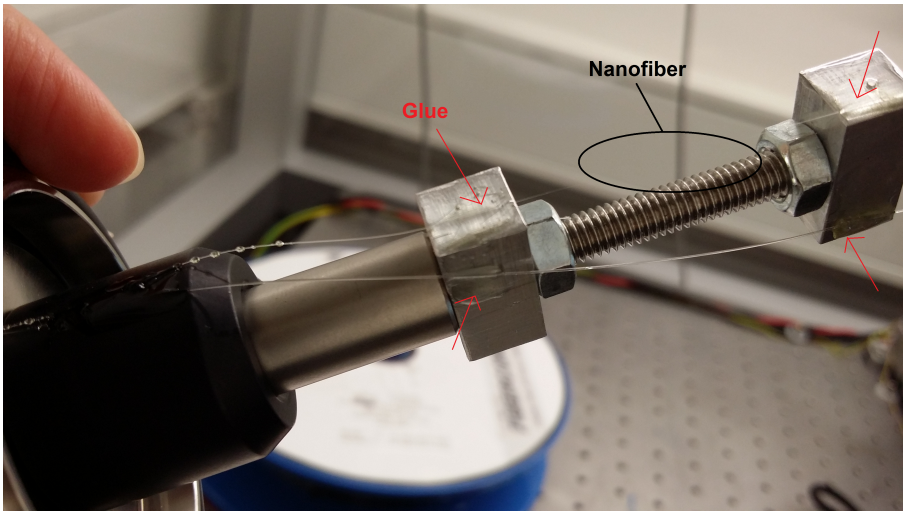

Figure 3.13: The glued fiber. After gluing the fiber to the cubes, the fiber is curved around the bolt and glued at all critical breaking points.

I have experienced that it is most easy to glue the fiber to a pair of aluminium cubes that are separated by an M6 bolt. In the beginning I tried to glue the fibers to wingnuts instead of the cubes but this turned out to be very difficult because it was almost impossible to get the wingnuts exactly across each other and if they are not in front of each other they will not hit the fiber at the same height. The shape and surface of the wingnuts also made it difficult to glue the fiber to as the glue would leak down the wingnut when applied and the wingnut surface was not smooth. The aluminium cubes have a flat, smooth surface and the area (1 cm^2) is much larger than the fiber diameter so it is not a problem to hit the fiber even though the cubes are not exactly across each other.

The glue is applied with a little wooden stick on top of each cube. (I also apply some glue on the edges of the cube because here the fiber can break if it experiences some tension (e.g. when sealing the chamber) that press the fiber end to the sharp edge). The cubes on the M6 bolt are then moved up to the fiber using a mount with two screws where I can change the horizontal and vertical position of the cubes. The glue droplet on the cubes should touch the fiber but the cube should certainly not, as this can break the fiber. I did try to apply the glue after the cubes were moved to the fiber and just touching it, but this is more difficult as the fiber can break from the small force exerted on it when the glue is applied whereas the fiber will not break due to the force from touching the glue. I have measured the transmission of light through the fiber while gluing it and found that the transmission did not change so the gluing does not affect the transmission.

The fiber should be glued at the transition between stripped and un-stripped fiber. The fiber is also glued at the edges of the cube to guide it around the bolt. Finally the two fiberends are glued to the Thorlabs mount so the ends will not twist around each other at any place after the glue.

The vacuum chamber, see figure 3.15, is made of stainless steal KF components from Pink Vacuum. I have designed it such that there are two windows to look through so that one can inspect the fiber with the IR viewer to see if e.g. light is scattered on the fiber as an indication of dust. The reason for using a vacuum chamber is that the nanofiber trap experiments are done in vacuum and therefore the fibers have to be tested under the same conditions. In air heat can be conducted away from the fiber, so in air the fiber will burn at a higher power than in vacuum.

The chamber is sealed by a method described in [35]. We form the vacuum seal around the fiber by tightening a Swagelok nut compressing a teflon ferrule around the fiber. On the vacuum flange there is welded a Swagelok fitting where the fiberends come out. The fiber ends are transferred through the teflon ferrule and the Swagelok nut seals the chamber, see figure 3.14.

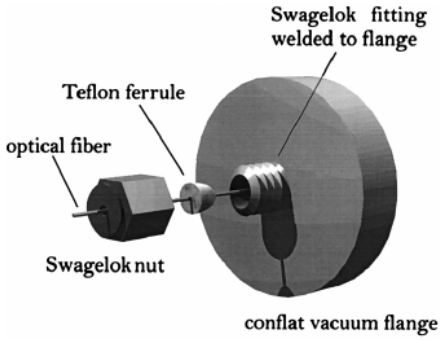

Figure 3.14: Teflon fiber feedthrough. From [35]. We use KF components not CF.

I have experienced several critical points which are important to glue as the fiber can break here when the chamber is being sealed. I think that the fibers did break because when the Swagelok nut is closed the two fiber ends twisted around each other and the tension from this twisting could make the fiber break at these sensitive points.

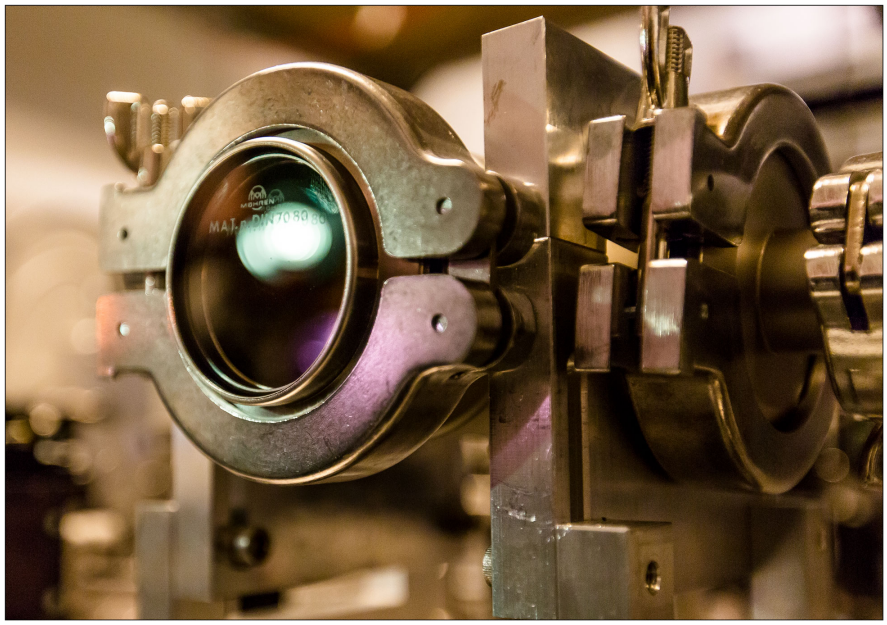

Figure 3.15: The vacuum chamber. Through the window the fiber can be observed.

3.2 Fiberburning

In this section the experimental setup for fiberburning is described. Some of the significant changes in the setup are explained and the experimental procedure is described. Finally the E-field and intensity at the fringes detector is calculated.

3.2.1 Experimental setup

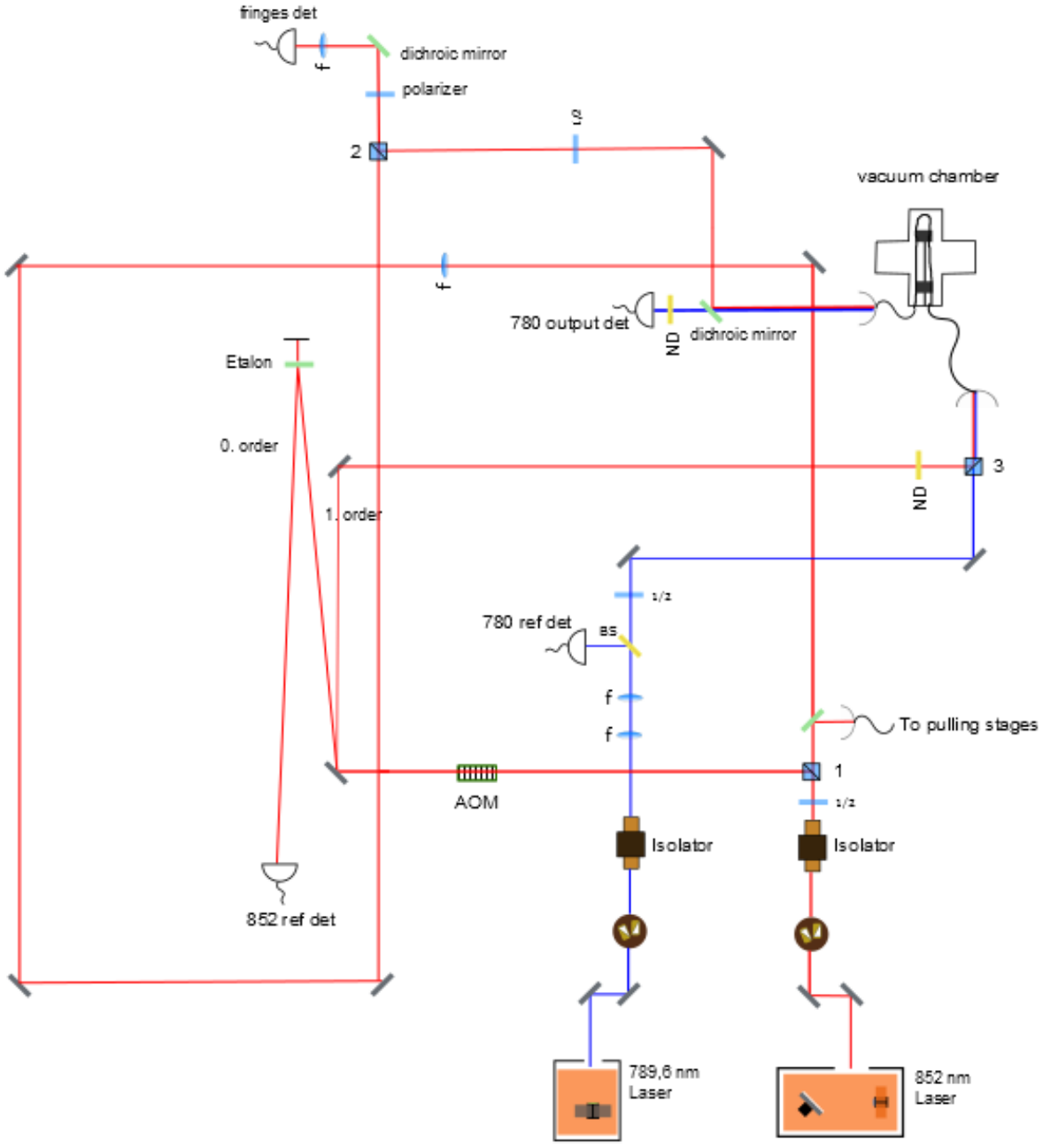

Figure 3.16: The experimental setup. The elements are described in the text.

The experimental setup for fiber heating and burning consists of an interferometer with the fiber in one arm. The current setup is shown in figure 3.16. The laser used in the interferometer is a 852 nm diode laser (red in figure 3.16), denoted the measuring laser. This laser is also

used in the fiberpulling setup, see figure 3.2. A diode laser is a semiconductor p-i-n junction laser which outputs an elliptical beam. The output beam is elliptical because it diverges a lot after being sent out, and the diverging is different in the horizontal and the vertical axes, so the beam size is larger in one of the axes, which makes it elliptical. The laser beam is directed using two mirrors through a prism pair to make the elliptical beam more circular. The prism pair consists of two prisms that are angled with respect to each other in such a way that the beam passing through is transformed from elliptical to circular. This is done by reducing the beam size in the elongated direction.

The beam then passes an isolator, to avoid optical feedback i.e. back reflections into the laser. Back reflections are unwanted as they can cause the laser to mode jump, frequency shift the laser light or make fluctuations in the amplitude of the light. An optical isolator is a device consisting of two polarizers with a Faraday rotator in between, that allows light to travel through but not back. It is based on the Faraday Effect that the lights plane of polarization is rotated as the light is transmitted through glass exposed to a magnetic field. The isolator rotates the polarization of light in such a way that the backreflected light is polarized perpendicular to the incoming light, and will therefore not be able to go back through the first polarizer.

Before the polarizing beam splitter (PBS) a waveplate is inserted. A waveplate is a birefringent material that changes the polarization direction of the beam by introducing a phase shift between the extraordinary and ordinary axes of the crystal. The phaseshift between the two components of the light determines the polarization of the outgoing light. A birefringent crystal has two optical axes with different refractive indices, so light that travels along the two axes has two different velocity components. The different velocities gives rise to a phaseshift between the light components along the two axes. The waveplate can thus be used to change the intensity of the beam in the two arms of the interferometer, as the two arms are differently polarized. PBS 1 splits the beam into the two arms; one arm goes through the fiber while the other arm does not. The PBS is a cube that splits the incoming beam into two beams of different linear polarization orthogonally to each other, ideally totally polarized beams. The two beams meet again at another PBS 2 and interfere at the fringes detector.

The beam in the arm which is reflected from the PBS passes through an acoustic optic modulator (AOM) (ATM-801A2) where the light is shifted in frequency with 80 MHz. The 1. order (+80 MHz) of the beam is sent to a mirror while the 0. order is sent to an etalon and then to a reference detector. This is done to be able to measure on the 852 nm light while the fiber is being heated to be able to monitor if anything unusual happens in the transmitted light. The light is reflected from the surface of the etalon and from the surface inside the etalon so the two beams will interfere on the detector and changes in the interference pattern will be detected.

The AOM diffracts and shifts the frequency of light using the acoustic optic effect. A voltage applied to the AOM crystal provides an RF (radio frequency) signal with a frequency of 80 MHz. This creates strain in the crystal and the refractive index of the crystal changes. The changes in the refractive index are moving periodic planes of expansion and compression i.e. sound waves which propagates in the crystal. The sound waves have the same effect as a diffraction grating for the laser light which is Bragg diffracted on them. The diffracted waves have different frequencies depending on diffraction angle.

The 1. order of the 852 nm beam is then sent through a Neutral Density filter (ND) with ND=1 to attenuate it and through another PBS 3 where it is reflected to the fibercoupler and coupled into the fiber. A dichroic mirror (DMSP805) reflects the beam after the fiber and

sends it through a waveplate, where the polarization is changed, to PBS 2 where it is combined with the beam from the other arm. The dichroic mirror transmits wavelengths < 805 nm and reflects wavelengths > 805 nm.

It is necessary to have an AOM in one arm to shift the frequency of the beam such that the beams have different frequencies and can be mixed at the fringes detector as calculated in section 3.2.5.

The arm which is transmitted through PBS 1 should have the same optical path length as the beam in the fiber arm because the interferometer is more stable to frequency fluctuations when the length of the two arms are equal. An interferometer measures the optical path length change through a phase change of the two arms, and the phase change of each arm is proportional to the length of the arm. If the two arms then have the same length they have the same phase shift and the interferometer is more stable to frequency changes, e.g. laser mode jumps. Therefore this beam moves a long distance before arriving at the detector. First some light is taken out by a beam sampler to measure the transmission through the fiber as it is pulled. Then the beam is reflected from four mirrors, to get the desired optical path length, before it is send to the PBS 2 to combine with the other beam. A lens of f = 1000 mm is used for collimating the beam on the way.

The polarizing filter polarizes the beams to the same polarisation before they hit the fringes detector where they interfere, thereby allowing only one specific polarization to pass determined by the rotation of the filter. This is necessary as there is only interference between waves with the same polarization (or with a small angle between the polarisation directions).

It is easier to hit the detector with a mirror in front of it. I have used a dichroic mirror (DMSP805) in front of the detector that reflects the 852 nm beam and transmits the 789.6 nm beam. In this way the high power 789.6 nm beam will not saturate the detector, and the detector will only measure the interference fringes produced by the two 852 nm arms. The lens in front of the detector has a focal length of f = 60 mm, and is used for focusing the light on the detector. In the experiment it was a problem that the lens was focusing the light to much on the detector such that it was locally saturated, so the lens was moved a bit from the focal length f, to avoid saturation. The fringes detector is a Thorlabs (PDA10A-EC) fast photodetector with a bandwidth of 150 MHz, so it can measure frequencies below 150 MHz. The photoelectric effect converts photons into electrons as each photon knocks off an electron from the photodetector metal. This creates a current and the voltage over the current is measured, although with some electronic noise.

The other detectors used in the experiment, are also photodetectors. They are calibrated by trying different settings of the detector gain together with different ND filters to ensure that the value in voltage on the detector is less than 10 V in the laser current interval used and that the detector noise (for no beam) is low. A linear fit of the measured power to the detector voltage then gives the conversion formula. The noise on the detector is seen to scale approximately linearly with the signal, figure 3.17. The electronic noise (this is from the transmission detector when the heating laser light is blocked) is seen on figure 3.18. It is seen to oscillate with a frequency of 50 MHz, as expected.

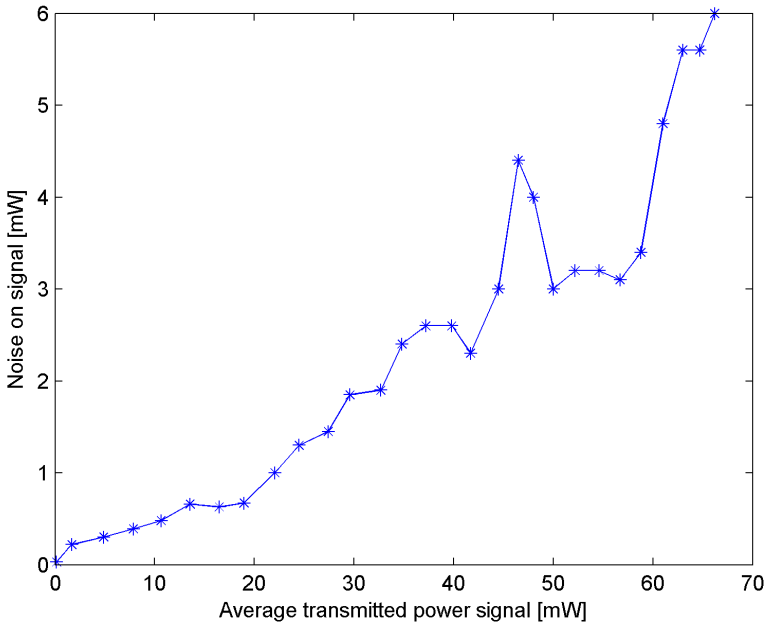

Figure 3.17: The noise on detector signal [mW] increases linearly with detector signal in [mW].

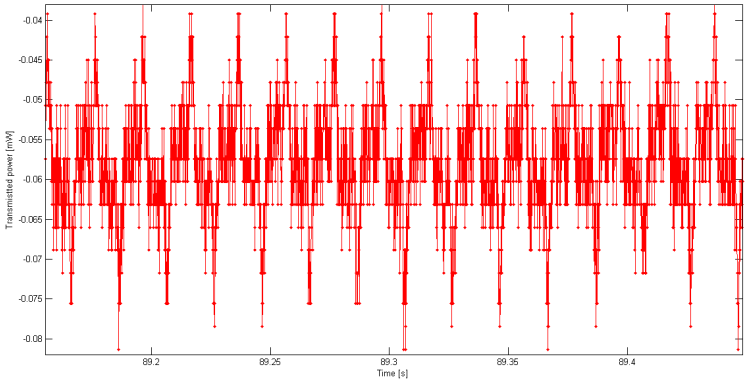

Figure 3.18: The electronic noise in [mW] on the transmission detector when the laser light is blocked as a function of time in [s].

The other laser, the heating laser, (blue in figure 3.16) is a 789.6 nm diode laser that I have constructed for heating the fiber. The laser beam passes a prism pair and an isolator followed by two lenses of f = 50 mm and f = 63.3 mm to collimate the beam and make it fit the beam size on the other side of the fiber. It should be noted for future users that the prism pair was especially difficult to align, as it was broken in several corners which made it difficult to position it. The lenses where chosen by considering the size of the beam waist on both sides of the fibercoupler. I have measured the beam waist of the incoming and outgoing 789.6 nm beams. The beam waist input should look like the output, so the data were plotted in Matlab and fitted to a Gaussian beam function to find the optimal beam waist w_0 and the optimal value of the offset z i.e. the position of the beam waist from $z = 0$. Then a Mathmatica program was used to find the position and focal length of the lens(es). The program takes as input the q parameters of the two beams. We want $q_{in} = q_{out}$ where $q = z + i \cdot z_R$, z is the position of the beam waist, and z_R is the Rayleigh range, both values found with Matlab. Then the program uses the theory of ABCD matrices for a propagating beam and takes as input the focal lengths of the lenses. The program outputs the position of the lenses. The only working combination

was a setup with first a lens of f = 50 mm placed 15 cm from the 789.6 nm isolator and then a lens of f = 63.3 mm placed 11.4 cm from the first lens. The lenses optimized the coupling into the fiber. The lenses where found when the setup was as in figure 3.19 but they where kept when the setup was changed, as they did still improve the coupling into the fiber.

Part of the beam is guided to the reference detector with a beam sampler which transmits 90% of the light. The reference detector measures the heating laser, before it enters the fiber, while the fiber is heated. The beam passes a waveplate that is locked to the degree that sends most light through the fiber. The waveplate is placed after the reference detector because it is a low order waveplate which is a bit wavelength dependent. The beam is then coupled with two mirrors into the fiber. Before the fiber, the beam is transmitted through PBS 3. When the PBS is changed (to couple the measuring laser into the fiber) it should not change the heating laser beam significantly because this beam is transmitted through the PBS.

After the vacuum chamber the beam goes to the output detector, which measures the amount of light going through the fiber. The dichroic mirror separates the two beams going out of the fiber by transmitting $\lambda < 805$ and reflecting $\lambda > 805$. The ND filter in front of the detector is a ND=2 reflective filter, to avoid saturating the detector. The filter is tilted such that the reflection does not go back into the fiber.

It should be noted that I also use the 789.6 nm reference detector as a reference detector for the 852 nm light in the fiberpulling experiment, see figure 3.16. (For this experiment I removed the magnetic beam sampler. The lenses are placed to collimate the 789.6 nm beam, so other focal lengths might be better for the 852 nm beam but I found it convenient to use the same detector, also because of the lack of space for yet another detector).

The fibercoupler used for coupling the beam into the fiber is a free space fibercoupler (A230-TM-B). Several fibercouplers were tried before this was chosen. The problem with the other fibercouplers was usually that the lens in front of the fibercoupler could not be positioned to the correct length for collimating the beam correctly and other lenses in front of the fibercoupler did not help either.

In the experiment the change in the optical path length of the light is measured by looking at the interference signal on the detector. The distance that the interference fringes move corresponds to the optical path length change. When the fiber is heated with the laser the interference signal reveals that the fringes move and that the fiber is elongated. The fringes move in the opposite direction when the fiber is cooled and contracts. In this way the optical path length change of the light through the nanofiber in vacuum can be measured as the nanofiber is heated.

3.2.2 Significant changes in the setup

The building of the setup started in the spring 2014 then during the summer 2014 the setup was moved as it used too much space and it was moved again in the beginning of the autumn 2014 to make it more convenient working with it so for example that the vacuum chamber did not have to be moved so much every time a new fiber was transferred. This meant that there have been many opportunities to change and improve the setup. Many adjustments were small improvements like e.g. the path for coupling the 789.6 nm light into the fiber consisted in the

beginning of two PBS´s but was changed to two mirrors. In October 2014 the setup looked like figure 3.19. In March an etalon was added together with the 852 nm zero order reference detector, figure 3.20. In April the two arms of the interferometer was changed and the setup is now as shown in figure 3.16.

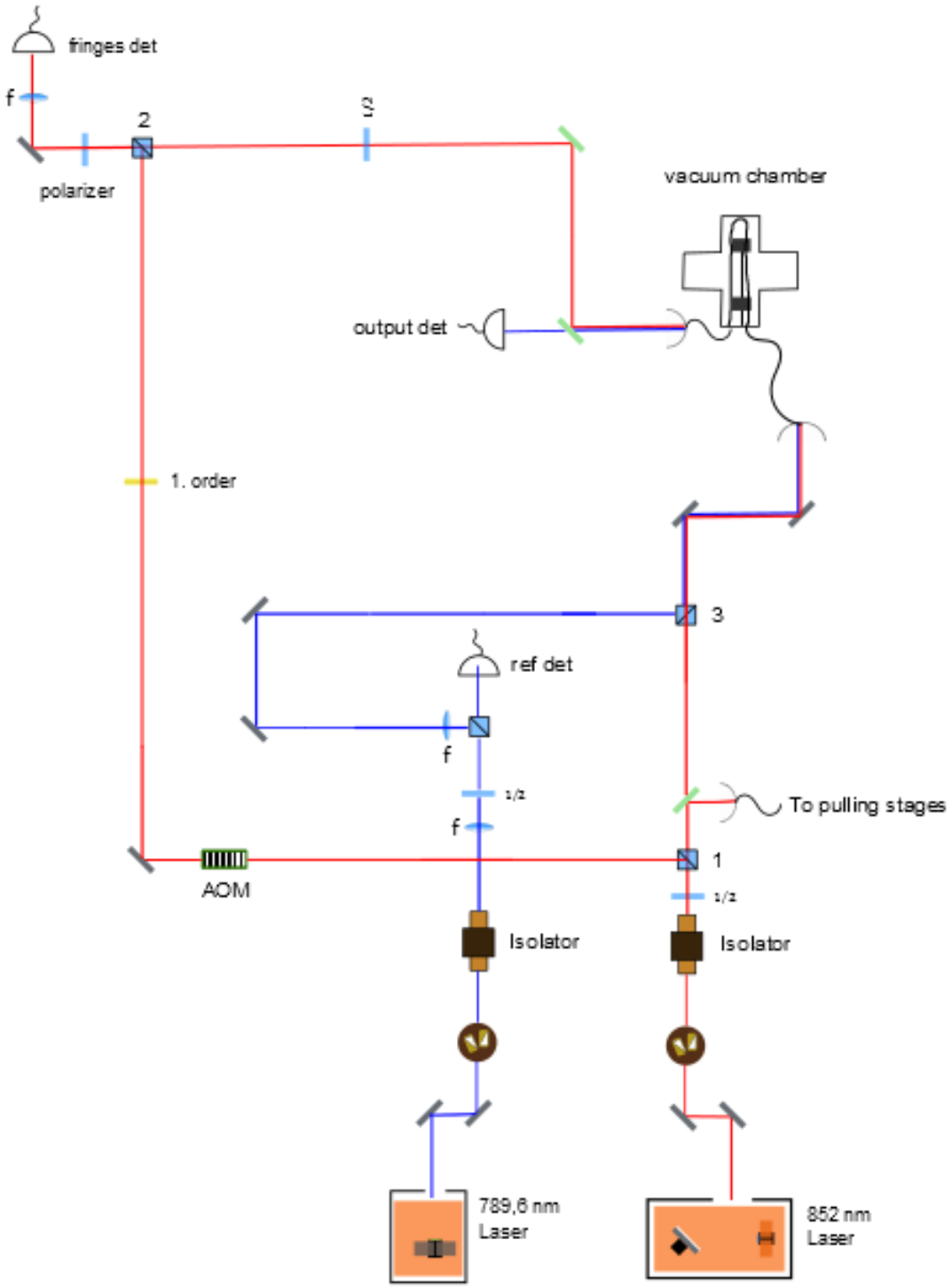

Figure 3.19: The experimental setup as it was in the autumn. The elements are described in the text.

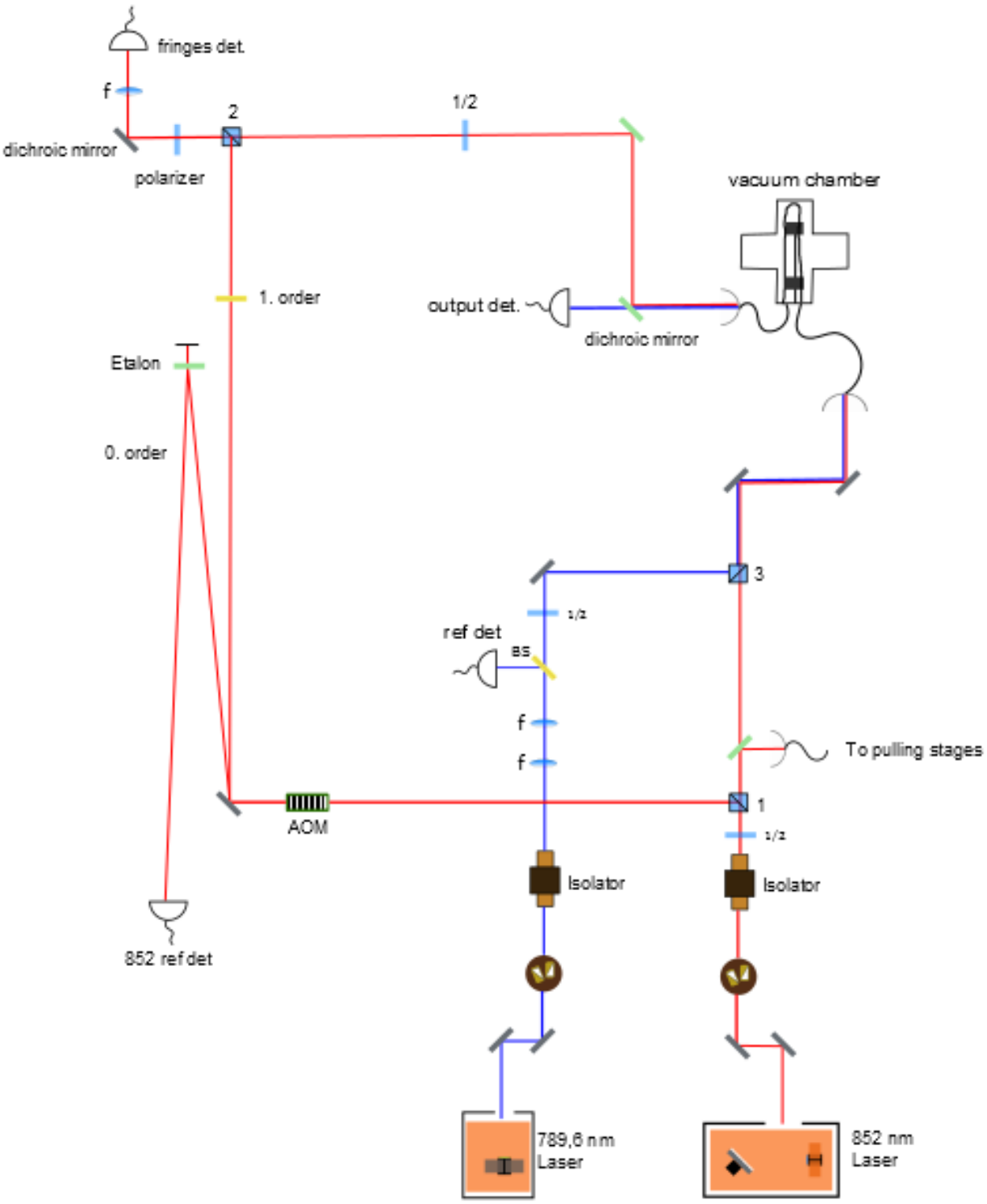

Figure 3.20: The experimental setup as it was in the spring. The elements are described in the text.

3.2.3 Heating laser (789.6 nm)

For the experiments I constructed a laser for heating and burning the fibers. It is a diode laser with a wavelength of 789.6 nm from Thorlabs (LD785-SH300) As the purpose of the laser is to heat the fibers, it is a powerful laser which can output powers up to 280 mW, see figure 3.21. The laser can according to the specs output 300 mW power. Therefore the laser does not have a grating, to narrow the linewidth of the laser, as the precision of the lasing

wavelength is not so important. A thermistor measures the temperature of the laser and a Peltier controls it using the thermoelectric effect. The lasing threshold is found from measuring the laser power with a powermeter as a function of the laser current. The measured linear part of the data (from I = 97 mA to I = 300 mA) is fitted to a linear function which gives:

$P(I) = 0.9717\frac{mW}{mA} \cdot I - 90.32mW$

So the lasing threshold is: $P(I) = 0 \Rightarrow I = 90.32/0.9717 = 92.95$ mA which fits well with the specs value of 92.9 mA.

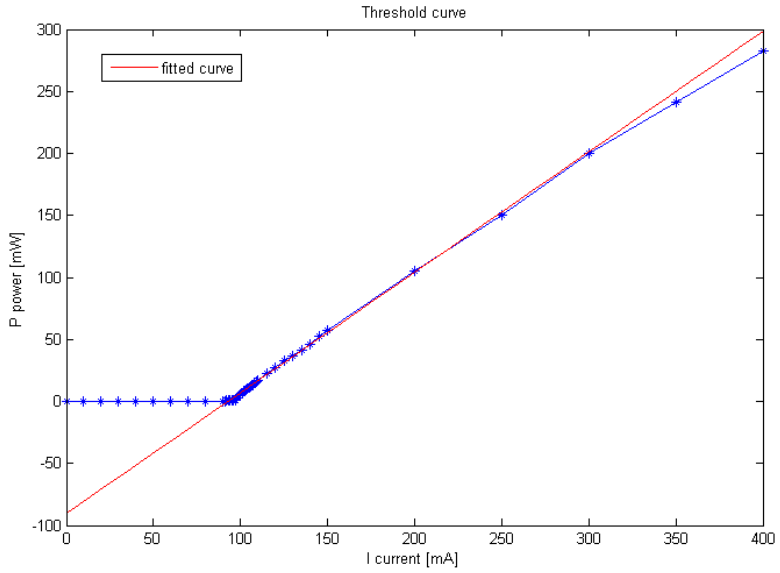

Figure 3.21: The power in [mW] as a function of the current in [mA]. The measured data (blue dots) fitted to a linear function (red curve).

As there were issues with backreflections into the laser the maximum laser current was set to 350 mA such that the maximum output power of the laser is below 250 mW.

3.2.4 Description of the experimental procedure

The air is pumped out of the vacuum chamber first using the roughing pump and then the turbo pump, see figure 3.22. First the needle valve is opened, and when vacuum is established, the bulk valve is opened. It is important to pump the air out slowly as rapid pumping can create a storm inside the chamber which can easily break the fiber at the tapered section.

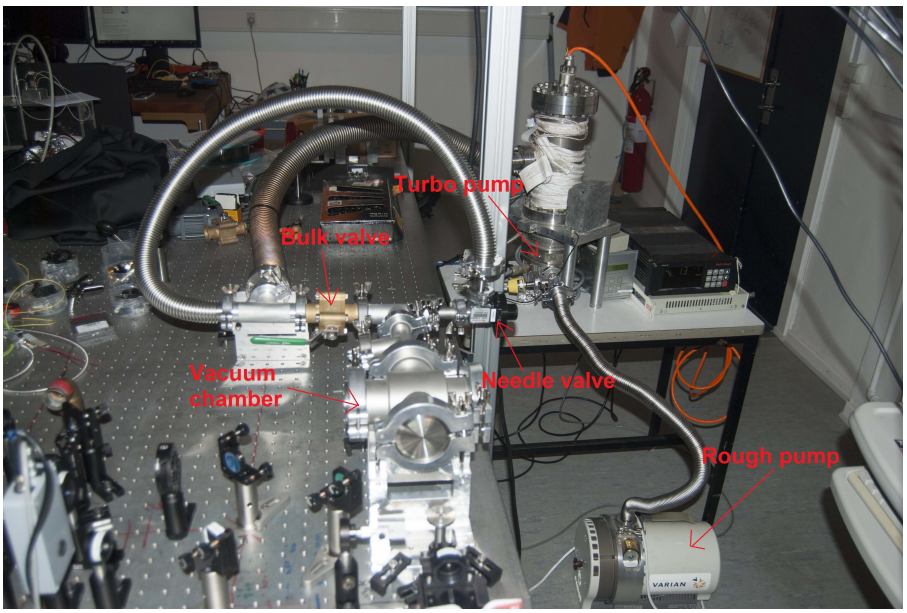

Figure 3.22: The vacuum chamber with the pumping system.

It was discovered that a proper pumping rate could be found by monitoring the transmission through the fiber while pumping. The pumping rate should then not affect the transmission through the fiber. When a vacuum is established the two laser beams are coupled into the fiber (789.6 nm with the mirrors and 852 nm with a mirror and PBS 3, see figure 3.16). The focus on the free space fiber in-coupler is optimized for the heating laser as we want to heat and eventually burn the fiber. The coupling is typically 40% for the measuring laser and 60% for the heating laser.

Then the interference signal of the two 852 arms is found by modematching the two beams. The visibility of the interference signal should be optimized, so using the two mirrors in the fiberarm the beam is "walked" into the detector to spatially overlap the fiber arm with the other arm which is already hitting the detector. It should be noted that it can help a lot on the coupling of light out of the fiber to change the position of the end of the fiber in the fibercoupler ferrule (Bullet bare fiber adapter). This is probably because the lens in the fibercoupler is not optimal for collimating the beam even though this fibercoupler was the best avaliable choice. The fiberend should of course be positioned at the place where the signal is largest. If necessary the waveplate in the fiberarm and the polarizer before the detector are changed. It is most optimal if the polarizing filter transmits approximately 50% of each beam. It can be easier to find the interference signal if an additional waveplate is inserted in the arm without the fiber to change the polarization of this beam such that the light is reflected from PBS 2, while changing the waveplate of the fiber arm such that most light is transmitted through PBS 2. Modematching of the beams can then be done at a point after PBS 2.

The interference signal should have the same frequency as the LO signal, 80 MHz, and the interference should of course disappear when one arm is blocked. It can be useful to check that the fringes moves in one direction when pushing slightly a mirror and in the other direction when pulling slightly on a mirror. When the signal is optimized such that it is much larger than the noise, the measurements can be performed. For the experiment the amount of measuring light in the fiber arm should be small, as we do not want to heat the fiber with this laser, a power of 100 µW is typically enough, while there can be several mW in the other arm. The current on the measuring laser should be chosen such that the laser is not modejumping. If the laser is mode jumping often it is enough just to change the current by $\pm$ 1 mA.

The fringes are sampled while the heating laser is blocked (causing the fiber to cool) and unblocked (causing the fiber to heat). The current on the heating laser is increased after each blocking so the power of the laser increases for each heating. The heating laser is blocked just before the f = 50 mm lens, see figure 3.16, such that there is no light on either of the heating laser detectors. During the experiment the signal on the two reference detectors and the output detector are then measured.

The interference signal from the detector is connected to an oscilloscope such that the fringes can be seen on the oscilloscope while heating the fiber. This is used to determine when the fiber burns because then the interference signal (fringes) will disappear. On the computer screen the fringes counting can be seen while doing the experiment, as the data is sampled and plotted shortly after. It is helpful to see how much the fringes counting change and whether the data sampling seems correct. Even though it can be difficult to follow everything that happens while doing the experiment because the axes on the plot changes very fast, so it is difficult to judge how much the optical path length changed and if it e.g. decreased to the initial length when the heating laser was blocked.

After the fiber is burned the actual coupling of light into the fiber can be measured by clipping and cleaving the fiber end just after the fiber (in) coupler and measure the coupling through the piece.

3.2.5 Calculation of the E-field and the intensity at the fringes detector

In the interferometer the two 852 nm beams in the two arms interfere at the detector where we see the beatnote. The optical path length change of the two arms gives a phase shift between the two beams, which at some points on the detector will be destructive and at some points will be constructive, i.e. the interference. The two beams have different frequencies, as the AOM shifts the frequency of the beam in the fiber arm from ω to $\omega + \Omega$, such that they can be mixed at the detector. The two arms have approximately the same optical path length, because while the beam in the fiber arm receives a phase shift from propagating in the fiber with a refractive index, the beam in the other arm propagates a long distance. The two beams are then shifted in phase since the beam through the fiber gets a phase shift when passing through the fiber exposed to heating.

When the fiber is heated, the fiber is elongated $l(T)$ and the fibers index of refraction $n(T)$ changes, giving rise to a phase shift of the light through the fiber. The light that goes through the fiber sees a changed optical path length $\Delta opl = \Delta(n \cdot l)$. Actually it is $\Delta opl = \int n(l)dl$ as n varies with l, so the light is phase shifted with respect to the light through the cold fiber or the other arm. The phase shift is $\Delta\phi = k \cdot \Delta opl$. When the light through the fiber is phase shifted and the optical path length changes, the interference signal moves the amount of fringes m corresponding to the changed optical path length $\Delta opl = m \cdot \lambda_0$. (1 fringe = 1 λ = 1 $\frac{\lambda_0}{n}$). From the optical path length change one could find the fibers elongation length l as; $\Delta opl = \Delta(n \cdot l) = m \cdot \lambda_0$ then $l = \frac{m\lambda_0}{n}$. The changed elongation length is then the length the empty arm should be made longer to see no moving of the fringes signal, as the fiber is heated.

In this experiment we investigate the optical path length change of the light. The elongation or contraction of the fiber should not be thought of as a physical elongation or contraction because as the fiber is pre-tensioned and glued to the metal cubes so the change in physical

length is smaller than the pre-tensioned length, as mentioned before. The optical path length change is both the length change and the refractive index change. It is difficult to say how much l changed because both l and n changes when the fiber is heated. As mentioned before the change in refractive index n is due to that n depends on temperature and strain. The change in the fibers length l when the fiber is heated will be to relax the pre-tensioned fiber a bit instead of elongating the fiber.

The E-field of the beam in the empty arm is $\overrightarrow{E}_{empty} = E_{e,0} \cdot e^{i(kz-\omega t)}\hat{z}$ where $E_{e,0}$ is the amplitude, $k = \frac{2\pi}{\lambda}$ is the wavevector, ω the frequency and t is the time. The E-field in the fiber arm with the AOM is $\overrightarrow{E}_{AOM} = E_{A,0} \cdot e^{i(kz-(\omega+\Omega)t+\phi)}\hat{z}$, where $E_{A,0}$ is the amplitude, Ω is the freqency which the AOM shifts the light with and ϕ is the phase shift the light gets when passing through the fiber.

I have assumed that both fields are plane waves and polarized in the z direction. Since we are looking at the interference in time, for this calculation the direction is not important and could be omitted.

I therefore only look at the size of the field. The total E field at the detector is then:

$$E_{total} = E_{empty} + E_{AOM} = E_{e,0} \cdot e^{i(kz-\omega t)} + E_{A,0} \cdot e^{i(kz-(\omega+\Omega)t+\phi)}$$

At the detector we measure the intensity of the field which is:

$$I = |E_{total}|^2 = E^*_{total} \cdot E_{total} =$$

$$(E^*_{e,0} \cdot e^{-i(kz-\omega t)} + E^*_{A,0} \cdot e^{-i(kz-(\omega+\Omega)t+\phi)}) \cdot (E_{e,0} \cdot e^{i(kz-\omega t)} + E_{A,0} \cdot e^{i(kz-(\omega+\Omega)t+\phi)}) =$$

$$|E_{e,0}|^2 + |E_{A,0}|^2 + E^*_{e,0}E_{A,0}e^{-i(\Omega t-\phi)} + E^*_{A,0}E_{e,0}e^{i(\Omega t-\phi)}$$

Generally the amplitudes $E_{e,0}$ and $E_{A,0}$ are complex but we can write them as $E = |E|e^{i\Phi}$.

$$I = |E_{e,0}|^2 + |E_{A,0}|^2 + |E_{e,0}|e^{-i\theta}|E_{A,0}|e^{i\psi}e^{-i(\Omega t-\phi)} + |E_{e,0}|e^{i\theta}|E_{A,0}|e^{-i\psi}e^{i(\Omega t-\phi)} =$$

$$|E_{e,0}|^2 + |E_{A,0}|^2 + |E_{e,0}||E_{A,0}|e^{-i(\Omega t-\phi+\theta-\psi)} + |E_{e,0}||E_{A,0}|e^{i(\Omega t-\phi+\theta-\psi)} =$$

$$|E_{e,0}|^2 + |E_{A,0}|^2 + |E_{e,0}||E_{A,0}| \cdot (e^{-i(\Omega t-\phi+\theta-\psi)} + e^{i(\Omega t-\phi+\theta-\psi)}) =$$

$$|E_{e,0}|^2 + |E_{A,0}|^2 + |E_{e,0}||E_{A,0}| \cdot 2\cos(\Omega t + \phi')$$

where $\phi' = -\phi + \theta - \psi$ is the total phase. We see that we measure a signal at the frequency Ω which is exactly the frequency that the AOM is driven with. Therefore the signal on the detector should in frequency be identical to the signal sent to the AOM. At the detector there is a high pass filter at 50 MHz that only allows components with frequencies > 50 MHz to pass, so the DC terms $|E_{e,0}|^2$ and $|E_{A,0}|^2$, which are constant in time, are sorted out.

Then at the detector we only have the AC term $I = 2|E_{e,0}||E_{A,0}| \cdot \cos(\Omega t + \phi')$.

At the detector the signal is demodulated into the I and Q components, i.e. the interference signal from the detector is mixed with the RF signal at 80 MHz, which is the local oscillator and is the same signal that is sent to the AOM, and then we get the I and Q signals.

In the demodulation circuit the signal is mixed with $I_\Omega = A \cdot \cos(\Omega t)$:

$I_c = I \cdot I_\Omega = 2|E_{e,0}||E_{A,0}| \cdot \cos(\Omega t + \phi') \cdot A \cdot \cos(\Omega t) =$

$2A|E_{e,0}||E_{A,0}| \cdot \frac{1}{2}(\cos(\Omega t + \phi' - \Omega t) + \cos(\Omega t + \phi' + \Omega t)) =$

$A|E_{e,0}||E_{A,0}|(\cos(\phi') + \cos(2\Omega t + \phi'))$

We have a low pass filter that sorts out the fast 2Ω frequency term such that the signal is:

$I_c = A|E_{e,0}||E_{A,0}| \cos(\phi')$

This is the I or in phase component of the signal at the detector (it is in phase with $\cos(\phi')$).

In the demodulation circuit the signal is mixed with $I_{\Omega+\pi/2} = A \cdot \cos(\Omega t + \frac{\pi}{2})$:

$I_d = I \cdot I_{\Omega+\pi/2} = 2|E_{e,0}||E_{A,0}| \cdot \cos(\Omega t + \phi') \cdot A \cdot \cos(\Omega t + \pi/2) =$

$2A|E_{e,0}||E_{A,0}| \cdot \frac{1}{2}(\cos(\Omega t + \phi' - \Omega t - \pi/2) + \cos(\Omega t + \phi' + \Omega t + \pi/2) =$

$A|E_{e,0}||E_{A,0}|(\cos(\phi' - \pi/2) + \cos(2\Omega t + \phi' + \pi/2))$

Again we have a low pass filter so the signal is:

$I_d = A|E_{e,0}||E_{A,0}| \cos(\phi' - \pi/2) = A|E_{e,0}||E_{A,0}| \sin(\phi')$

This is the Q or quadrature component of the signal (it is $\pi/2$ out of phase with the I component).

A drawing and description of the electronics used can be found in section 3.3.1 and in the appendix.

3.3 Data sampling and data analysis

In this section I will explain how the data is sampled and analysed. In the experiment the optical path length change is measured. The input from the interferometer is the fringes signal from the fringes detector.

3.3.1 Electronics

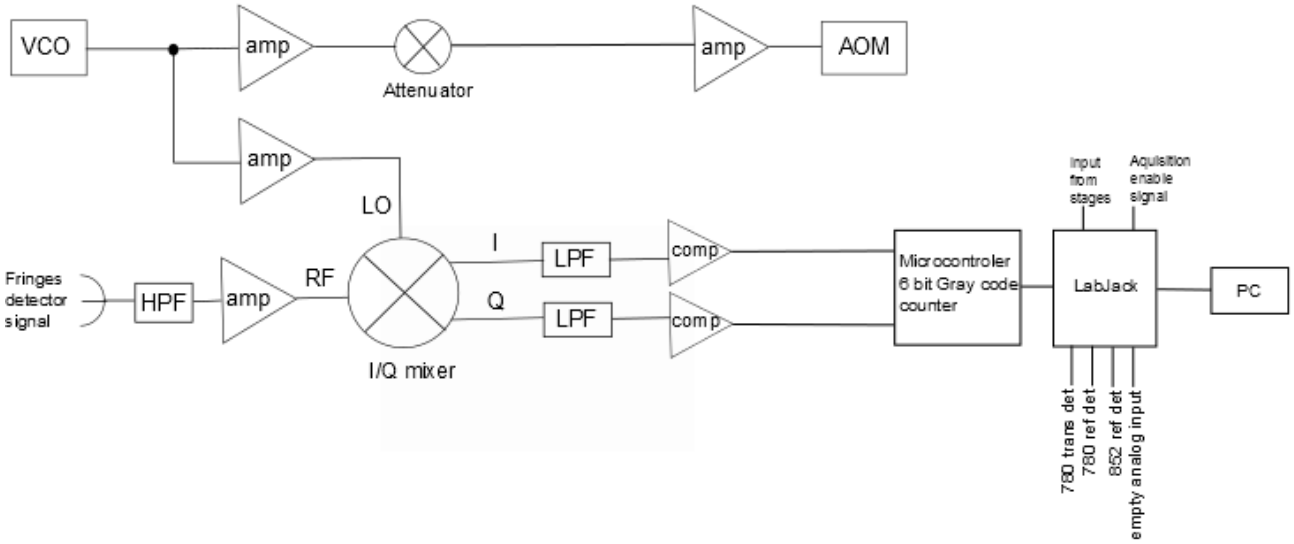

Figure 3.23: Drawing of the data sampling. VCO is voltage controlled oscillator, amp is amplifier, comp is comparator, HPF is high pass filter and LPF is low pass filter. The elements are explained in the text.

I have constructed electronics for data sampling using a design by Jürgen Appel shown in details in the appendix figure 7.1. The electronics mix the radio frequency (RF) fringes signal from the detector with the local oscillator (LO), which is the AOM driving signal at 80 MHz (also RF signal). This gives us the I and Q signals that tells if the optical path length change is increasing or decreasing.

The I and Q signals are the In phase and Quadrature components of the fringes signal. The I and Q signals are separated in phase by $\frac{\pi}{2}$ and therefore they are called quadrature signals.

When there is no change in the fringes signal the I and Q components are constant (either 0 or 1). When the fringes signal change (as the fiber is heated and cooled) the I and Q signals are alternating between 0 and 1. The I and Q signals can only change one at a time.

A schematic of the electrical circuit used to drive the AOM and mixing the RF with the LO is seen in figure 3.23. A photo of the electronics used for data sampling is seen in figure 3.24. All the electrical components are from mini circuits.

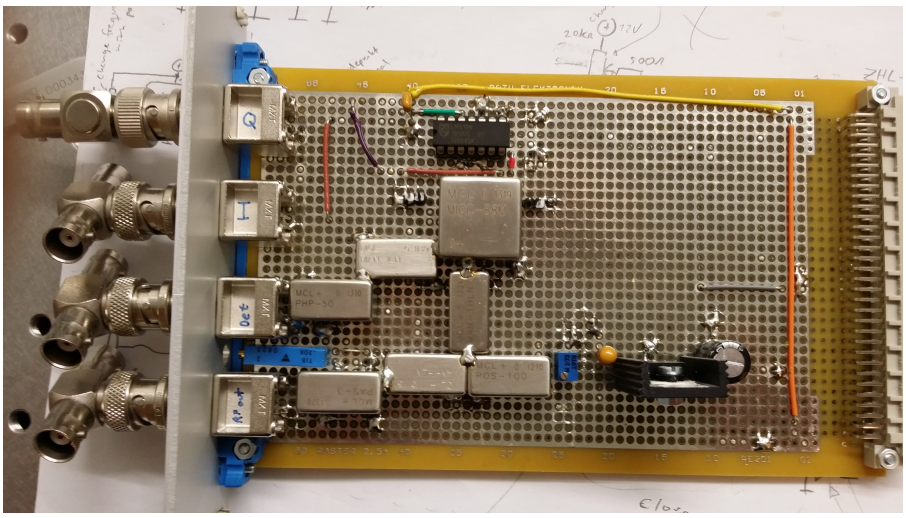

Figure 3.24: A photo of the electronics used for data sampling.

In the lower left of figure 3.23 we see the signal from the fringes detector which passes a high pass filter (PHP-50+) which allows the higher frequency components >50 MHz from the detector signal to pass. The filter is there to avoid the amplifier afterwards from saturating. Then the signal passes a low noise amplifier (MAN-1LN) which amplifies the weak signal with 28 dB. The RF signal then enters the mixer. The other signal, the LO, comes from the VCO, a voltage controlled oscillator. The frequency of the oscillating signal sent out from the VCO is controlled by the applied voltage. This voltage is set to give a signal of $\Omega = 80$ MHz. The VCO signal is split into two signals; one that goes to the mixer through an amplifier (MAN-1HLN) and one that goes to drive the AOM. The amplifier (MAN-1HLN) amplifies the signal to 10 dBm and sends it to the mixer. This signal is the strong local oscillator. The other part of the signal is also amplified to 10 dBm with the amplifier (MAN-1HLN) and then send to an attenuator (PAS-3+) which attenuates the signal below 5 dBm such that it can go to the AOM. The signal then pass through a coaxial amplifier (ZHL-1-2W-5+) connected to a heatsink. The signal is amplified with 29 dB so it is at most 33 dBm = 2W when it goes to drive the AOM. The heat sink is taking the generated heat away from the system.

At the mixer, the I&Q modulator (MIQC-88M), the LO and RF signals are mixed and the output is the I and Q signals, as calculated in the section 3.2.5. Both the I and Q signals pass a low pass filter that only allows frequencies < 3 MHz to pass so the fast oscillating terms at 2Ω are sorted out, as also found in section 3.2.5. The signals then pass a comparator. The comparator is like a switch where the voltage over the incoming signal U_s is compared with another voltage U. If U_s <U the output is 0 V ("0") and if U_s >U the output is 5 V ("1"). The I an Q signals are then measured as being either 0 or 1 and we have the possible outcome IQ values: 00, 01, 10, 11. The comparator is seen to convert the signals from analog to digital.

The I and Q signals are read by a microcontroller and then by the LabJack (LabJack U6). The microcontroller samples the data faster than the LabJack, so we do not lose data as we did when we only used the LabJack for data sampling. The microcontroller has a sample rate of 336 kHz, so we can sample the data correctly if there is always at least $\frac{1}{336\ kHz} = 3\ \mu$s between two samples, i.e. the optical path length must not change by more than 1/4 wavelength (1 count) within 3 μs. The LabJack also receives data from the three detectors: the reference detector of the measuring laser and the reference and transmission detector of the heating laser. The LabJack furthermore receives an input from the stages containing information about the position of the stages and from the stages controller. The data is then all sent to be saved in a file on the computer (PC).

3.3.2 The optical path length change from the I and Q components.

In the experiment the I and Q values are measured, and an algorithm then converts the I and Q signals to fringes counts as described below. Then the algorithm converts the fringes counts for each sample to optical path length change as a function of time, and by dividing the number of samples by the sampling rate, the duration of the experiment can be found.

The data is thus a number (counts) which change by zero or one for every measurement. Therefore the microcontroller samples the data and converts the counts to a 6 bit Gray code where only one bit is changed at every measurement. The advantage of sampling the data as Gray code is that here the data is read while the bits change so if only one bit change at every measurement then we can only lose one bit.

It is important that we measure all the data, because missing data can make it difficult to tell whether the optical path length change increased or decreased.

The gray code is then decoded to binary.

The algorithm considers the difference between the current data and adjacent data to discover how much the data has changed and in which direction, i.e. if the fiber contracted or elongated.

The fringe counts is then the cumulative sum of the differences. An example of the raw data is plotted in figure 3.25.

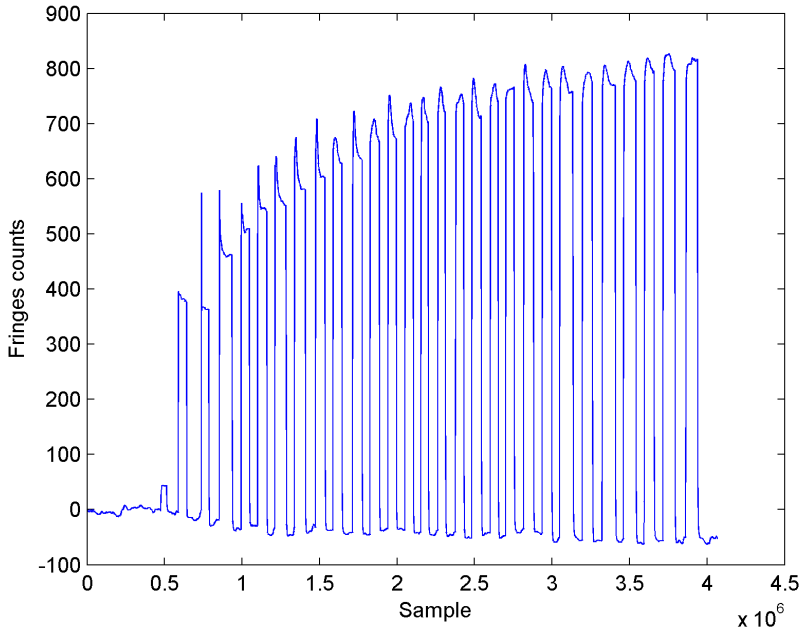

Figure 3.25: The raw data, the fringes counts versus sample. The sample rate was 8333 samples/s.

The optical path length change of the light through the fiber is calculated from the fringes counts. When the I and Q signals changes 4 times the fringes move by 1 fringe, so the fringes counts should be divided by 4. We know that 1 fringe corresponds to 1 wavelength. As we consider the interference of the two arms on the detector, the relevant wavelength of the measuring laser is the vacuum wavelength of 852 nm. The optical path length change in microns is then $L = \Delta opl = \frac{fc}{4} \cdot 0.852$ µm where fc is the fringes counts. An example of the optical path length change as a function of time is plotted in figure 3.26.

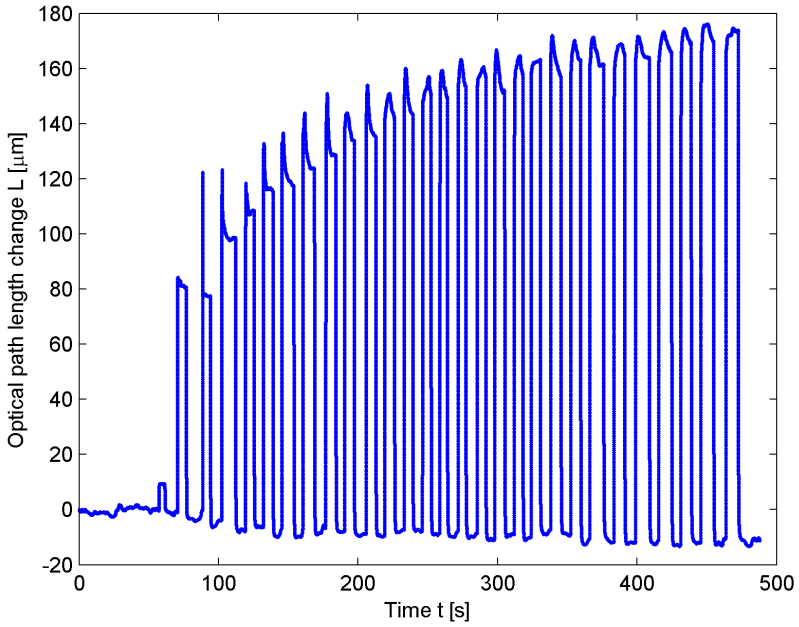

Figure 3.26: The optical path length change of the fiber as a function of time. Between each peak the fiber is heated with increasing power.

We see that the data from the experiment consists of many heating and cooling transients where the power is increased for each successive. Each peak contains a lot of data about the heating and cooling. An example of a zoom on a peak is shown figure 3.27.

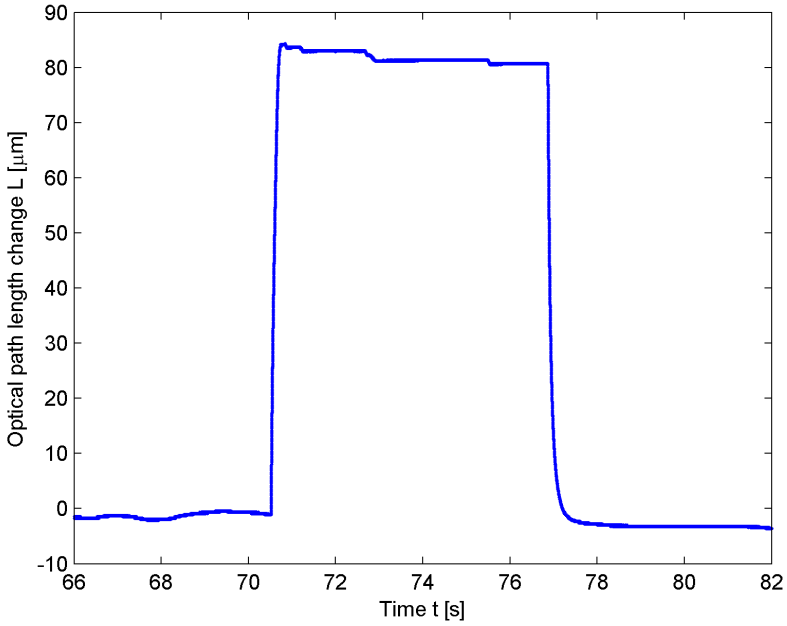

Figure 3.27: Zoom on the second peak in figure 3.26

.

3.3.3 Analysing the cooling transients.

To analyse and compare the cooling transients the algorithm allows you to zoom in on one transient and pick the sample point exactly where the cooling starts. From this point the evolution of the transient can be plotted, see figure 3.28, for the cooling transient of the peak in figure 3.27.

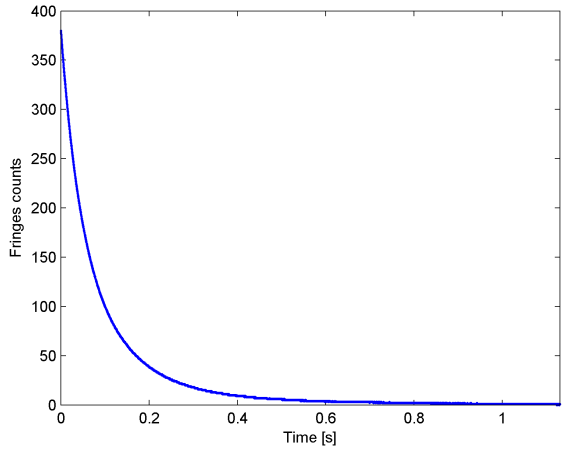

Figure 3.28: The cooling transient of the second peak (figure 3.27). The time and fringes counts are changed such that the transient starts in t = 0 and ends at fringes counts = 0.

We see that the transient lasts about 1 s. This is the typical time it takes the fiber to cool and the fringes counts to go back to the zero point.

Each transient is then analysed. The data in the transient is smoothed over 85 samples. The number 85 is chosen because the fringes counts curve is not changing dramatically over approximately 10 ms and the sampling rate times 10 ms is about 85 samples. Then the difference between every adjacent data point is found and divided by the inverse of the sampling rate to get the difference in fringes counts per sample converted to difference in fringes counts per time. This is the rate of cooling and is plotted in figure 3.29.

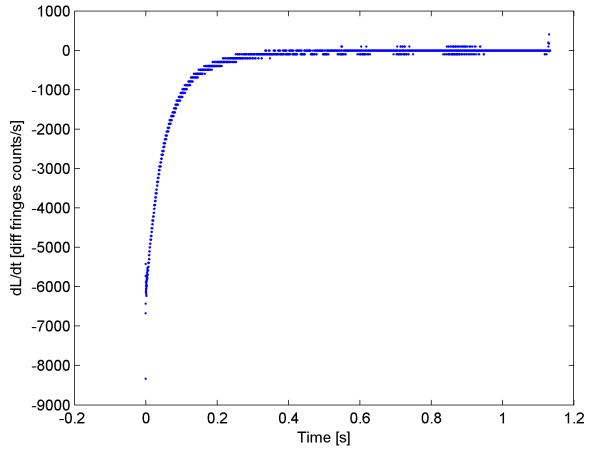

Figure 3.29: The rate of cooling $\frac{dL}{dt}$ as a function of time t.

The rate is then converted to change in optical path length change per time, and plotted as a function of optical path length change, figure 3.30.

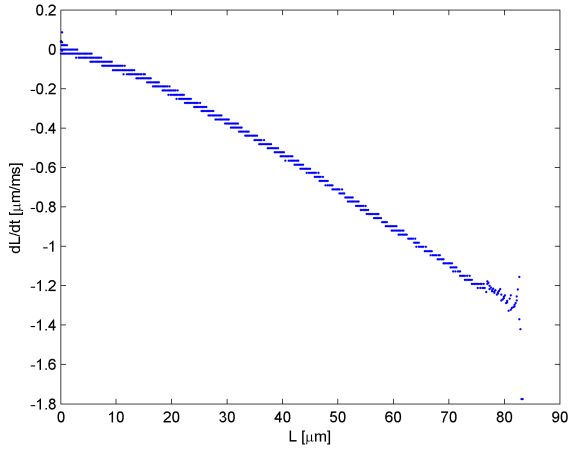

Figure 3.30: The rate of cooling $\frac{dL}{dt}$ as a function of optical path length change L.

To examine the characteristics we have plotted this as a log-log plot. To avoid diverging data, we have to neglect data equal or close to zero. For the optical path length change this is done by setting all data less than 1 µm equal to 1 µm. For the rate $\frac{dL}{dt}$ this is done multiplying all data by -1 in order to make all data positive and then setting all values smaller than 0.05 µm/ms equal to 0.05 µm/ms. Now the logarithm of $\frac{dL}{dt}$ can be plotted as a function of the logarithm of the optical path length change L, see figure 3.31.

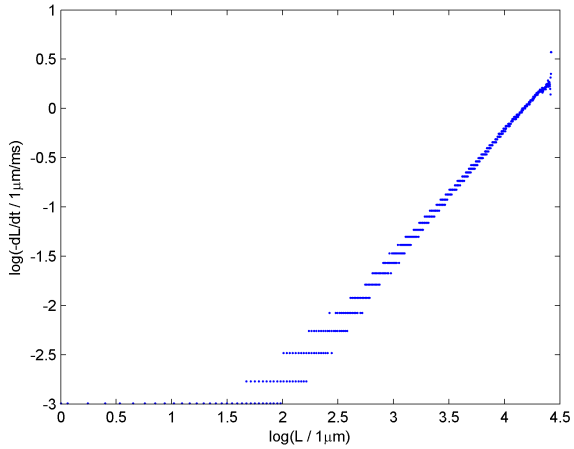

Figure 3.31: The logarithm of $\frac{dL}{dt}$ as a function of the logarithm of optical path length change L.

This is then done for all the peaks that we want to analyse.

3.3.4 Analysing the heating transients.

The heating transients are analysed in a way similar to the cooling transients. The evolution of the heating transient is chosen with the algorithm. I choose the transient from the start of the heating to the point where the optical path length change is equal to what it is when the cooling begins, because in this way I avoid the spikes in the transients.

The heating transient of the peak in figure 3.27 is shown in figure 3.32.

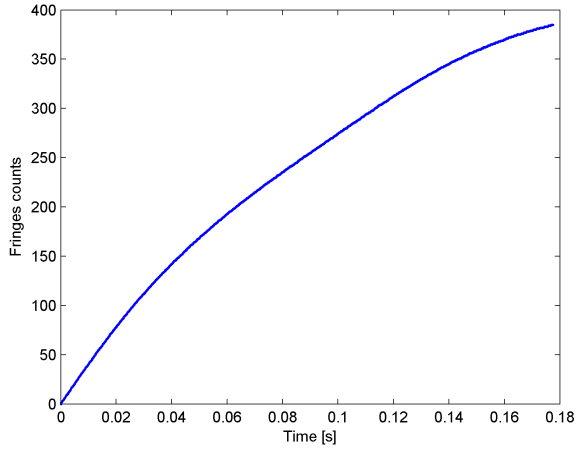

Figure 3.32: The heating transient of the second peak (figure 3.27). The time and fringes counts are changed such that the transient starts in t = 0 and at fringes counts = 0.

We see that the transient lasts about 0.18 s. This is the typical timescale on which the fiber heats.

Each transient is then analysed. The data in the transient is like the cooling data smoothed over 85 samples and then the difference between every adjacent data point is found and divided by the inverse of the sampling rate to get the difference in fringes counts pr sample converted to difference in fringes counts pr time. This is the rate of heating and is plotted in figure 3.33.

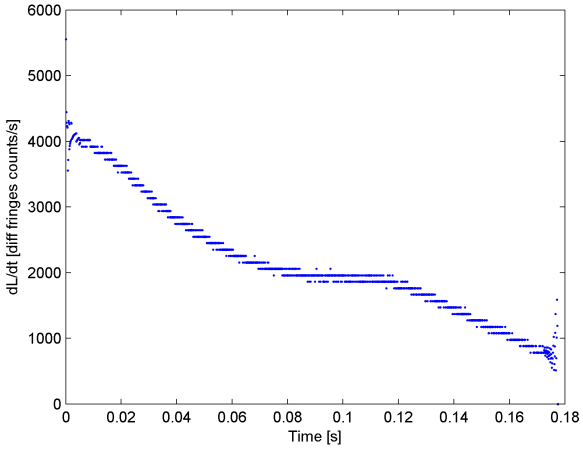

Figure 3.33: The rate of heating $\frac{dL}{dt}$ as a function of time t.

The rate is then converted to change in optical path length change pr time, and plotted as a function of optical path length change, figure 3.34.

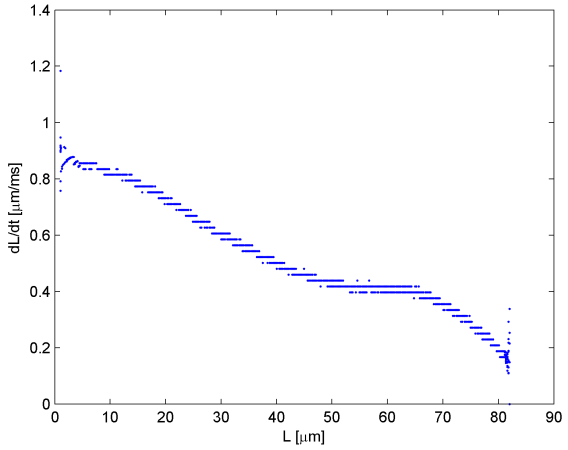

Figure 3.34: The rate of heating $\frac{dL}{dt}$ as a function of optical path length change L.

To plot this as a log-log plot if the optical path length change is less than 1 µm we set it equal to 1 µm. If the rate $\frac{dL}{dt}$ is less than 0.05 µm/ms it is set equal to 0.05 µm/ms. The logarithm of $\frac{dL}{dt}$ is plotted as a function of the logarithm of the optical path length change L, in figure 3.35.

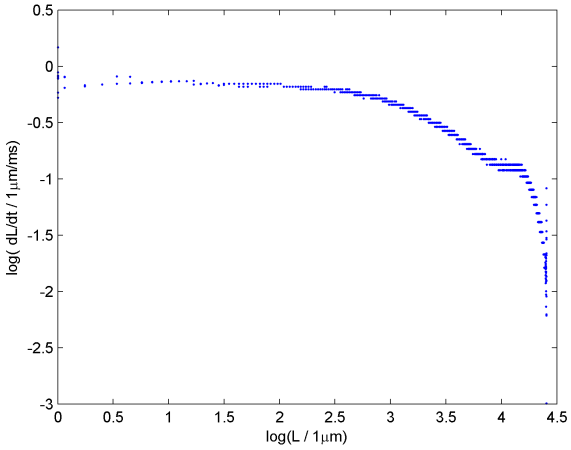

Figure 3.35: The logarithm of $\frac{dL}{dt}$ as a function of the logarithm of optical path length change L.

Again this is then done for all the peaks that we want to analyse, although it should be noted that it will turn out for the heating transients that the log-log plot is not relevant.

Chapter 4

Results and Discussion of data

In this section I will show some of the interesting results the experiment has shown and discuss what can be analysed from the data. As the setup was often changed to improve it I will relate the data shown to the setup at the time the data was measured and since I hope the thesis will be read by future students I will try to explain how and why the setup was changed. Finally I will show the data from the working setup where strange behaviour in the fringes counting (optical path length change) had been eliminated and discuss what these results show and draw some conclusions.

4.1 Measuring optical path length changes

During the first experiments when interference fringes were visible, the fringes count changed a lot, often by several thousand counts, when something in the optical path length was changed (e.g. if a mirror was just slightly touched). But the fringes counting also changed a lot when nothing in the optical path length was changed, which made it harder to identify the problem. At that time the experimental setup was as shown in figure 3.19 and it was suspected that something in the setup was not stable. The elements in the setup were each inspected with a powermeter to look for instabilities in transmitted or reflected power. Fluctuations in the transmitted power after the fiber in the vacuum chamber have always been observed, and these fluctuations are probably due to the fact that the fiber acts as a Fabry Perot resonator for the light. The huge fringe count change was seen both with a tapered fiber and with a normal optical fiber positioned in one arm of the interferometer. Several elements were realigned but the reason for the huge fringes counting change was not found.

It was, however, noticed that at the same time the fringes counting changed a lot (as seen on the computer) then the interference signal seen on the oscilloscope was jumping from big to small amplitude and back. So it could look as if the measuring laser was mode jumping. The laser current was varied but the effect was still seen. The theory was then that the laser light was backreflected from the fiber end into the laser, which could make the laser modejump. As the fiber ends are not angle cleaved the light can be backreflected from the fiber end. This optical feedback could be avoided by re-designing the experiment. If the fiber was in the same arm as the AOM there would be no backreflections because after the AOM the light is shifted in frequency, so if the light is reflected back from the fiberend into the laser then the backreflected light would have another frequency and not cause the laser to mode jump. As re-arranging the setup would take some time and because we wanted to investigate the fiber breaking power in vacuum, it was decided first to try to reduce the power of measuring light in the fiber arm, because then only a small amount of light would be backreflected into the laser. With the power reduced by a factor of 10 the change in fringes counts for the steady setup were then

only the expected fluctuations. As mentioned earlier we also only need a few times 100 µW of the measuring laser into the fiber since we should not heat the fiber with this light.

4.2 Data sampling rate

A typical result from the first fiber burning is shown in figure 4.1. The optical path length change of the measuring laser and the transmitted power and reference power of the heating laser was monitored. At that time I only experimented with heating the fiber and not cooling it. For this experiment the current of the heating laser was increased in steps of 1 mA until the fiber burned. The transmitted power data show that the fiber did burn during the measurement and the reference power signal shows how the heating laser was mode jumping. We can see that the fiber breaks as the transmitted power abruptly drops to zero and the optical path length change remains constant. This fiber burned at 15 mW of transmitted power. The measurement of this value was of course one of the experimental aims. When this experiment was done the sampling rate was only 2500 Hz (only the LabJack was used for data sampling), which we now know was too low, so probably data was lost and the optical path length change might not have been measured correctly, but at that time we did not realize that the sampling rate was too low.

The jumps seen in the power on the reference detector looks like the heating laser mode jumping. These jumps are not seen in the transmitted power, which is strange as the detectors are measuring on the same laser. This will be explained below.

The transmitted power shows fast oscillations on top of a smooth behaviour with the heating laser drive current and hence the input power to the fiber. These fast oscillations are assigned to Fabry Perot resonances of the etalon formed by the cleaved fiber endfaces. Both the optical path length of the fiber and frequency changes of the heating laser lead to rapid scanning over the transmission resonances. The fiber ends reflects 4% of the light (of both the measuring laser and heating laser) so the transmitted power is expected to oscillate with at maximum 16% because of this effect. But we also observe that the oscillations oscillate with a greater amplitude for higher power and for the highest measured power they oscillate with more than 16%.

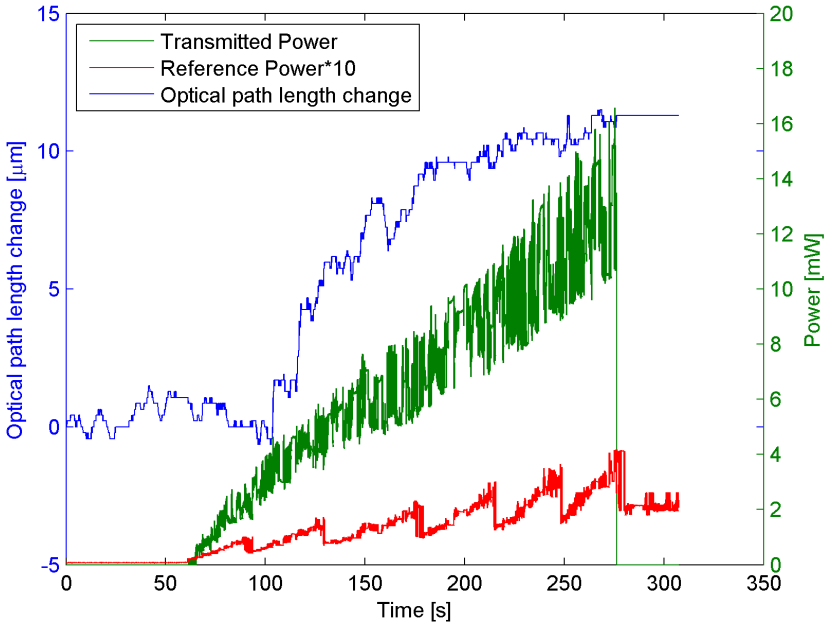

Figure 4.1: The optical path length change plotted together with transmitted power and reference power of the heating laser. The left y-axis belongs to the optical path length change and the right y-axis belongs to the transmitted power and reference power. The signal of the reference power is multiplied by 10 for clarification.

During this phase of the experiment there were sometimes problems with finding the true interference signal of the two beams. The interference amplitude should be large compared to the noise and the interference should disappear when one arm is blocked. Often when the fiber arm was blocked, there was still some interference. It was then found that the interference also contained an interference between the 0. order beam and 1. order beam from the AOM. It turned out that there was a leakage of the 0. order into the 1. order beam which also made the measured data incorrect. The leakage was avoided by removing dust from the AOM with an air spray, since the dust in the AOM scatters the 0. order beam such that it can interfere with the 1. order beam on the detector.

We then investigated cooling and heating of the fibers, by blocking and unblocking the heating laser. A typical result is shown in figure 4.2. The heating laser is blocked and the current (power) of the laser is increased and then the laser is unblocked. Therefore the data should consist of "steps" of blocking and unblocking the laser, where the optical path length change increases when the fiber is heated and we see the optical path length change decreasing when the fiber is cooled, together with the transmitted power of the heating laser increasing and decreasing.

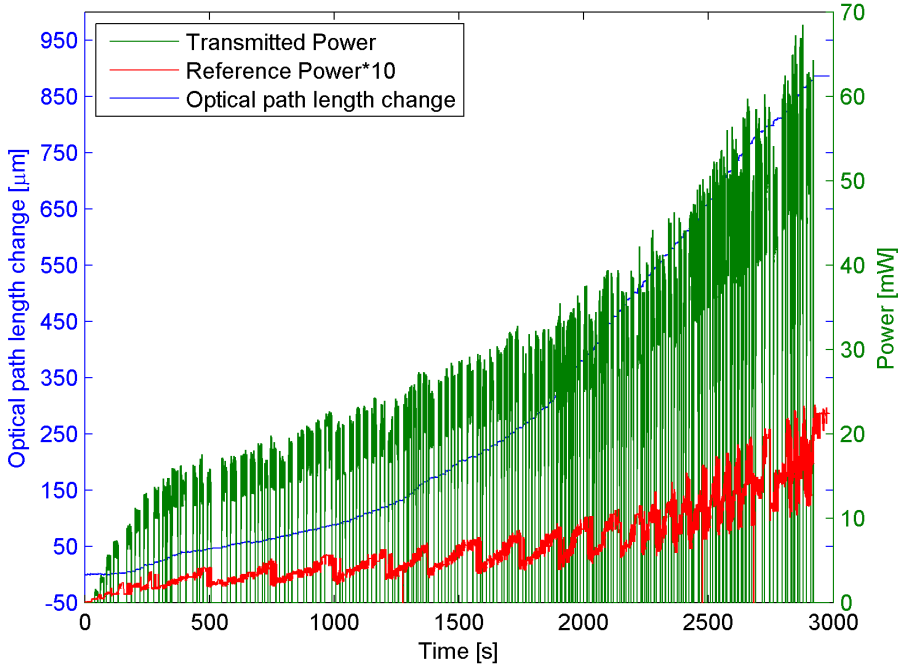

Figure 4.2: This long experiment measured the optical path length change while the fiber was heated and cooled. The sampling rate was 2500 Hz which was later found to be too low to measure all the data correctly.

In figure 4.2 we only see the optical path length change increasing during heating and not decreasing during cooling, so something is not correct, because the heating laser was blocked and unblocked during the experiment, as also seen on the transmitted power, which is dropping to zero when blocking the beam.

This fiber burned at about 60 mW as seen on the figure, but I note that just before the fiber burned it was able to withstand a power of almost 70 mW.

Later it was found that the LabJack, which was used for measuring the data, was loosing some data because the sampling rate (2500 Hz) was too low. The data were acquired but the LabJack was just to slow to catch all I/Q transitions. Therefore it was not possible with the data to tell if the optical path length change increased or decreased. It was also suspicious that the total optical path length changed by almost 1 mm as seen on the figure. This measurement also shows the mode jumps in the power on the reference detector, which will be discussed later.

During the experiment it was observed on the oscilloscope that the interference pattern, which should be steady when the optical path length does not change and move sideways when the fiber is heated or cooled, was also jumping up and down together with the amplitude decreasing and then increasing again, when the fiber was being heated. This could be because the fiber is not polarization maintaining. If the fiber is birefringent and can change the polarization of the light through it when it is heated, the interference signal may change in amplitude, as it depends on the polarisation of the two interfering beams. The amplitude is largest when the two beams have the same polarization and when the two beams have different polarisation the amplitude is smaller.

As it was observed that lost data events were detected in the data sampling and that the sampling rate of 2500 Hz was slower than the fiber response to being heated and cooled, the sampling rate was then increased to the maximum of 10 kHz.

The lost data events are defined by a change of both the I and Q signals within the same sample period. Such an event makes it impossible to decide whether the optical path length increased or decreased from the last sample and indicates that the sampling rate is too slow to track the dynamics of the fiber.

After increasing the sample rate the data looked e.g. like figure 4.3, which now also shows effects of cooling. Although data was still lost, as seen in figure 4.4 where the points where both the I and Q signals change are shown by the green lines.

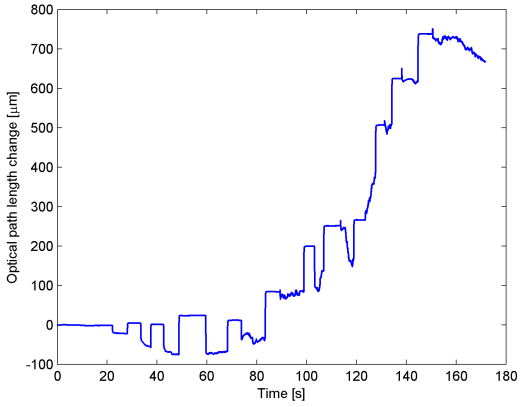

Figure 4.3: Heating and cooling the fiber. The optical path length change does not give much information as much data is lost as seen in figure 4.4.

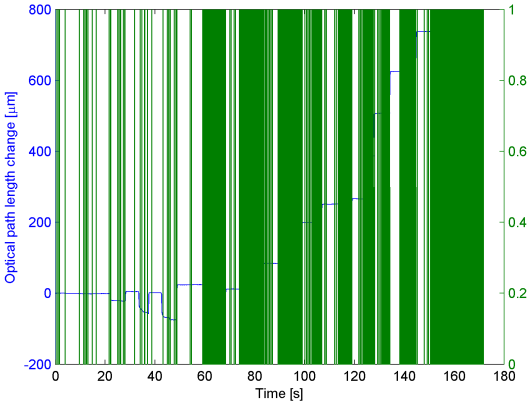

Figure 4.4: The optical path length change data from figure 4.3 with over lapped green vertical lines to mark lost data events.

We then had to change the program used for data sampling such that the total sample rate could be increased to 50 kHz and the sample rate per channel was 12012 Hz. The data were also sampled in a different way such that the data resolution was better, to prevent the sampling from losing data and measure transitions with both the I and Q signals changing.

4.3 Heating laser mode jumps

The laser modejumps which have only been seen in the power on the reference detector, figure 4.1 and figure 4.2, were still puzzling so the attention was directed to the setup and the heating laser path.

Here a $\lambda/2$ waveplate was positioned before the PBS and reference detector, see figure 3.19. This waveplate was used to change the amount of light going to the fiber and the detector respectively. The waveplate was a low order waveplate so the phase retardation, and hence the polarization transformation of the waveplate depends on the wavelength. Polarization changes are then converted into intensity changes at the output of the following PBS. Because if the laser mode jumps and the wavelength of the light changes a bit then the waveplate will transmit a different amount of light power and the calibration of the detector will be wrong, as the detector is placed after the waveplate and as it was calibrated for the waveplate positioned to transmit at a certain amount of light. This effect is especially dramatic if the PBS is oriented for almost complete extinction at the output port to the monitor detector, as it was here, so the relative error in the power on the detector was large. When the fiber heating experiment was performed the current on the heating laser was changed. At some currents the laser could mode jump to another wavelength.

Therefore the path for the heating laser was changed such that the waveplate was placed after the detector, see figure 3.20. The light then passes a beam sampler which transmits almost all the light and reflects only a few percent to the detector, which is still sufficient for the reference detector. The beam sampler is less sensitive to polarization. Also the polarization of the beam sampler was fixed by the isolator, and it consists of glass with an antireflecting coating such that it is not very wavelength dependent. The waveplate was still used for changing the polarization of the light and was positioned such that most light would be reflected from the PBS into the fiber.

4.4 A new heating laser setup

After the heating laser path was changed the data for fiber heating looked like the example shown in figure 4.5.

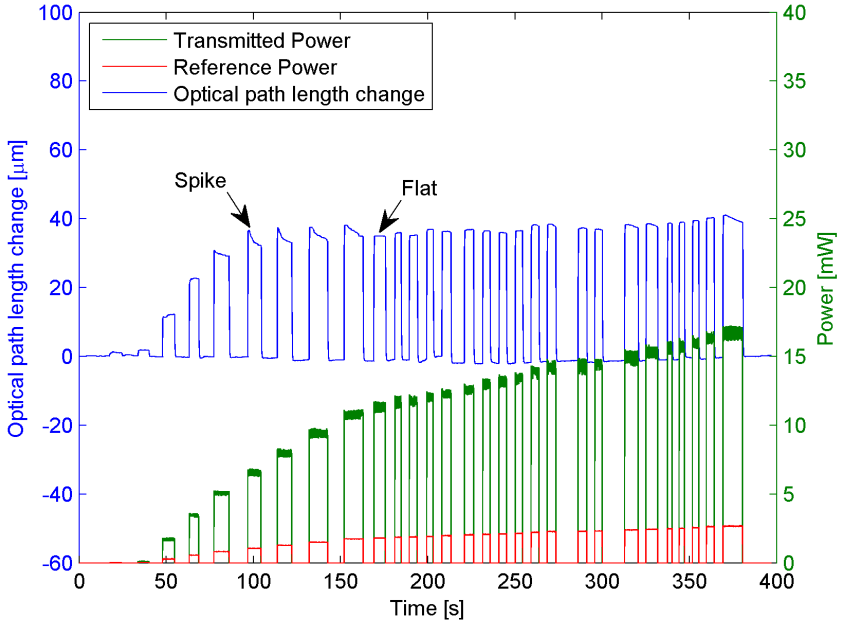

Figure 4.5: The optical path length change plotted together with the transmitted power and the power on the reference detector. Notice that the top of the transients change.

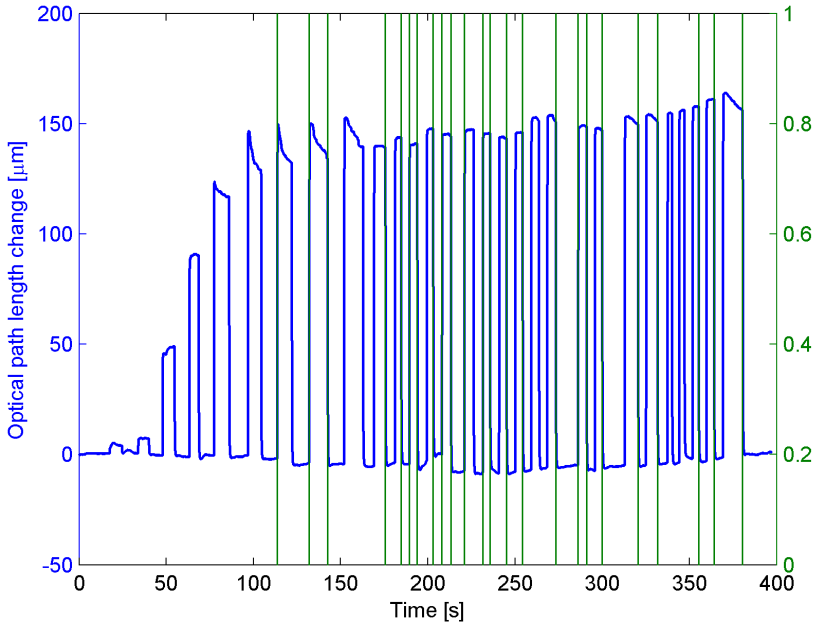

Figure 4.6: The optical path length change shown together with the green lines indicating where data is lost. This is seen to happen when the fiber is heating or cooling.

It is seen that the behaviour of the power on the reference and transmission detectors are similar, as expected, and no mode jumping in the power on the reference detector is observed. It is also seen, see figure 4.6, that the LabJack still miss some data points for higher power. However the sampling rate was now high, 12500 Hz, so lost data are now a minor fraction of all the sampled data.

Several additional explanations for the lost data were investigated. Besides that the data sampling was too slow, it could also be if the measuring laser was mode jumping and if the signal on the detector then changed too fast for the LabJack to measure it. The lost data could also be noise e.g. if the interference signal was poor then only the noise would be measured. The interference signal is always optimized before measuring and it is watched on the oscilloscope during the measuring. But it could be that it could change faster than resolved with the oscilloscope.

It is seen that the top of the transients change depending on heating power. For low power some transients shows spikes while for medium power they are flat, figure 4.5. At the same time the power signals, change from having a very steep slope to a less steep slope. This is because here I changed the increment of heating power. This is probably also why the cooling transients change from rapid heating and cooling, when the fiber is exposed to much more power than the last heating, to a less rapid heating and cooling, when the fiber is exposed to only a slightly different power than the previous heating. In this experiment the optical path length change did go back to its initial length (referred to as the zero point) when the fiber was cooled, which is also expected if the fiber is not deformed permanently by the heating.

It was also investigated if it is the same places that the data is lost. In figure 4.7, it is seen that it was usually when the fiber is heated or cooled for higher power that the optical path length change varies too fast for the LabJack to follow and we lose data.

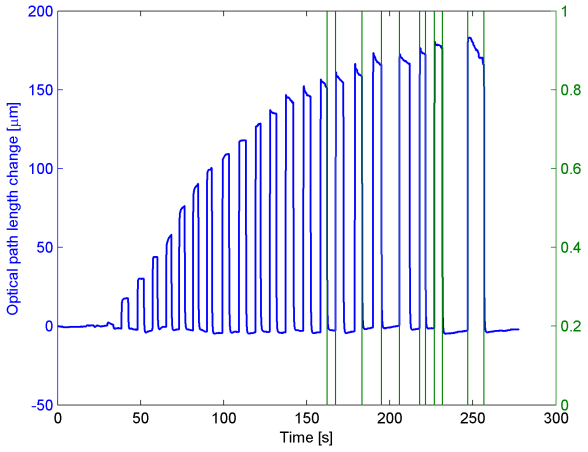

Figure 4.7: The optical path length change and data loss. We see that the data is usually lost when the fiber is heated or cooled.

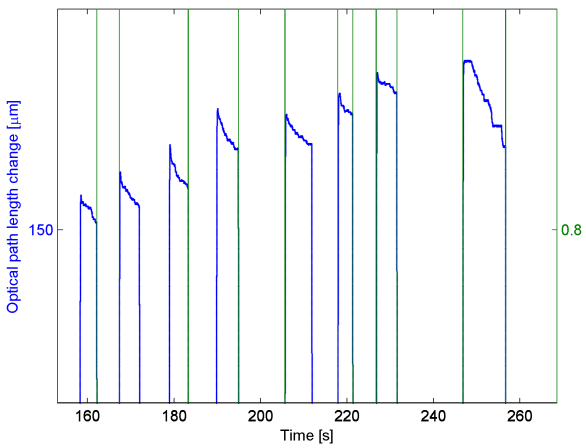

Figure 4.8: Zoom on figure 4.7, blue is the optical path length change and green is the lost data.

A subsequent experiment resulted in the data shown in figure 4.9.

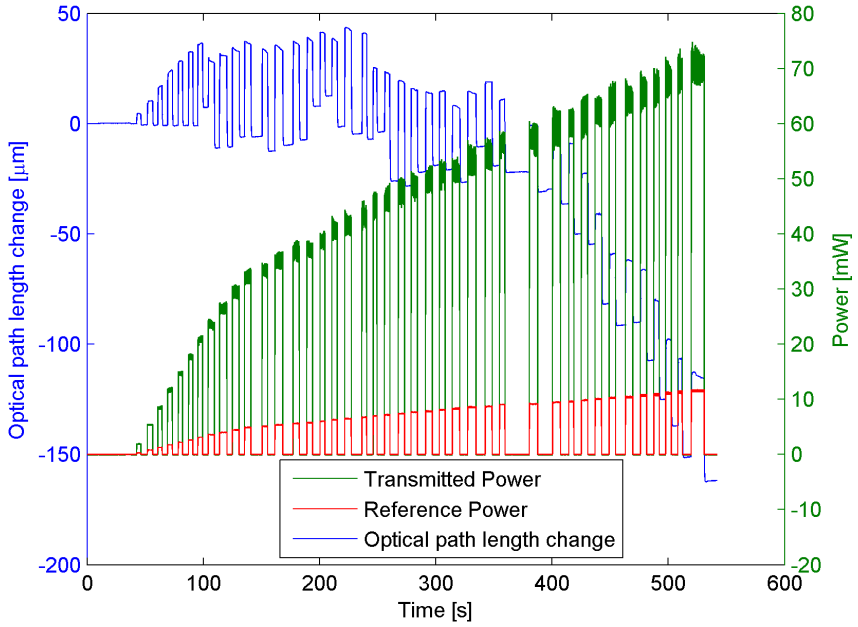

Figure 4.9: The optical path length change together with the signals on the detectors.

We see, that the optical path length change for higher heating power is decreasing, which does not make physical sense. The signals on the detectors, both changes from a very steep slope to a less steep slope around 150 s. This is again because the increment of heating power was changed during the experiment. After seeing the results of these experiments it looked like the sampling rate was still not fast enough, and it was concluded that a microcontroller for sampling the data was needed before data collection by the LabJack. The microcontroller that was acquired had a sample rate of 336 kHz, which was a lot faster than the 12.5 kHz used so far.

4.5 Saturation of the optical path length change

It was often observed that the optical path length change saturated with power, see e.g. figure 4.7. It looks like there is a maximum optical path length change. It was considered if it could be a sign that the fiber was breaking, but no correlation was observed with the breaking.

The saturation of optical path length change with power was not observed in [3]. The experiment described here and the one in [3] are different but I think it is still interesting to compare the results. As discussed before the optical path length change is observed in [3] to increase linearly with power, which they ascribe as due to the fiber being a nanofiber with $\lambda_T > d$ and therefore the thermodynamic behaviour of the fiber can not be described by Plancks law.

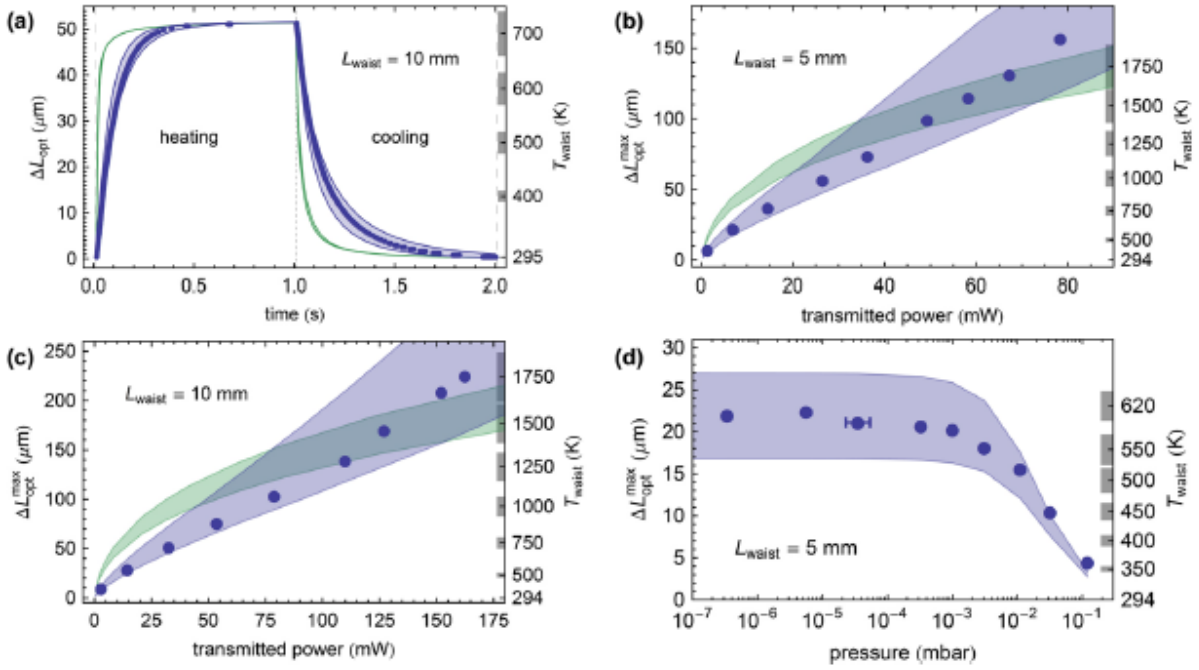

Figure 4.10: This figure show the data from [3] and is shown here to compare it with my data. The circles are the experimental data, the blue bands the FED predictions and the green bands the predictions using Plancks law. a) The optical path length change in [µm] as a function of time in [s] for one heating and cooling transient. b) The maximum optical path length change in [µm] as a function of transmitted power in [mW] for a fiber with a 5 mm long waist. c) The maximum optical path length change in [µm] as a function of transmitted power in [mW] for a fiber with a 10 mm long waist. d) The maximum optical path length change in [µm] as a function of background gas pressure for a fiber with a 5 mm long waist.

From figure 4.10 we see that the range of laser powers used for heating the fibers in [3] are similar to the powers I used for heating the fibers. The nanofibers examined by [3] had a longer waist (5-10 mm long) than my fibers which according to the simulation have a waist of 1-2 mm. It is expected that a fiber with a long waist will mainly conduct heat by radiation because there will be too much resistance along the thin waist to conduct heat in the material, whereas a fiber with a shorter waist will be more able to conduct heat to the taper region. The heating power at which the dominant effect (i.e. radiation or heat conduction) changes will depend on the length of the waist. But for high heating power, radiation is the dominant effect. This could explain why we see the saturation of the optical path length change for higher powers. The saturation of the optical path length change could be because the heating energy added to the fiber is radiated away at the same rate as it is added. As the fiber is heated to a temperature T_{max} the optical path length change will be $\Delta opl_{max} = \Delta opl(T_{max})$ and it will not increase any

more than this value. So for higher heating temperatures above T_{max} the optical path length change will maximally be Δopl_{max}.

4.6 Microcontroller for data sampling

When the data was sampled with the microcontroller a typical sample looked like figure 4.11.

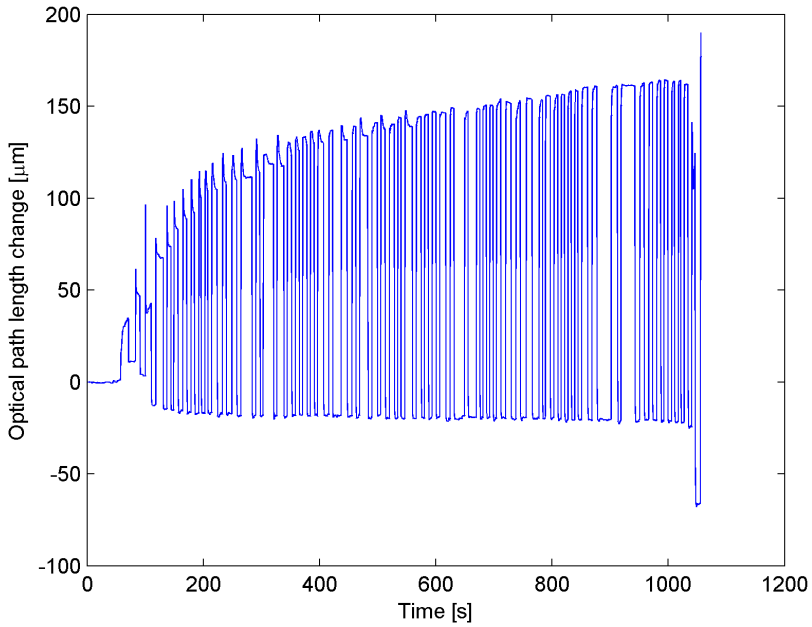

Figure 4.11: The optical path length change in [µm] as a function of time in [s]. The last measurements are not shown as here the optical path length change increases dramatically.

In the beginning of the experiment, figure 4.11, the zero point shifts and in the end the fringes counts increase dramatically. The data were sampled very fast with the microcontroller so now the extreme optical path length change is probably not an error in the data sampling.

The microcontroller samples the data with 336 kHz, so the fringes counts will be correct as long as the fringes counts does not change by more than 1 count within 3µs (1/336 kHz).

The slopes of the data (optical path length change versus time) can be resolved to see how fast the data is changing, and to determine if the data is changing faster than 1 count/3µs. The steepest slopes of the data were investigated but no data changing faster than 0.333 cts/µs was observed.

The fastest rate of change observed was 1 cts/70 µs. Hence the sample rate is high enough.

As the data sampling rate seemed to be correct we looked after parts of the setup which were not stable and could obstruct the fringes counting.

On another fiber something interesting was observed see figure 4.12.

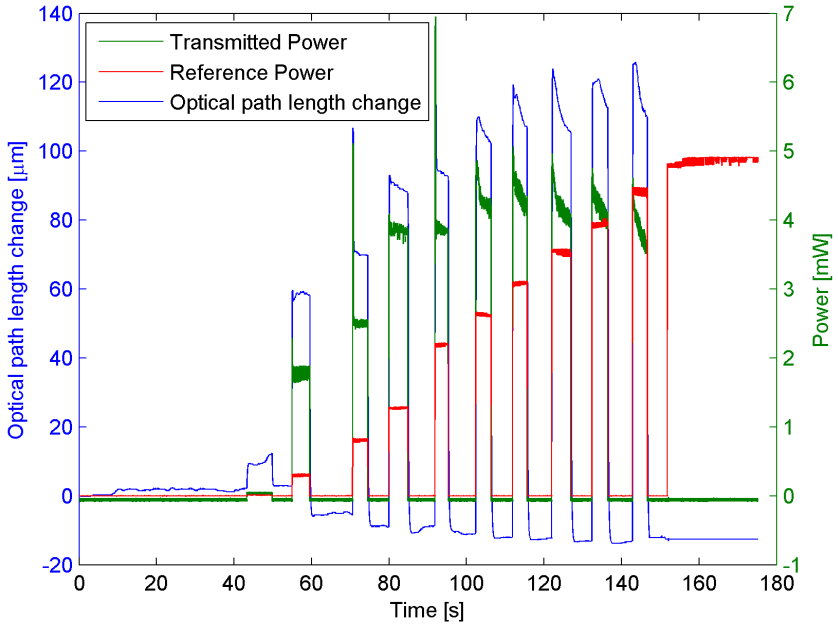

Figure 4.12: The optical path length change in [µm] together with the signals on the detectors in [mW].

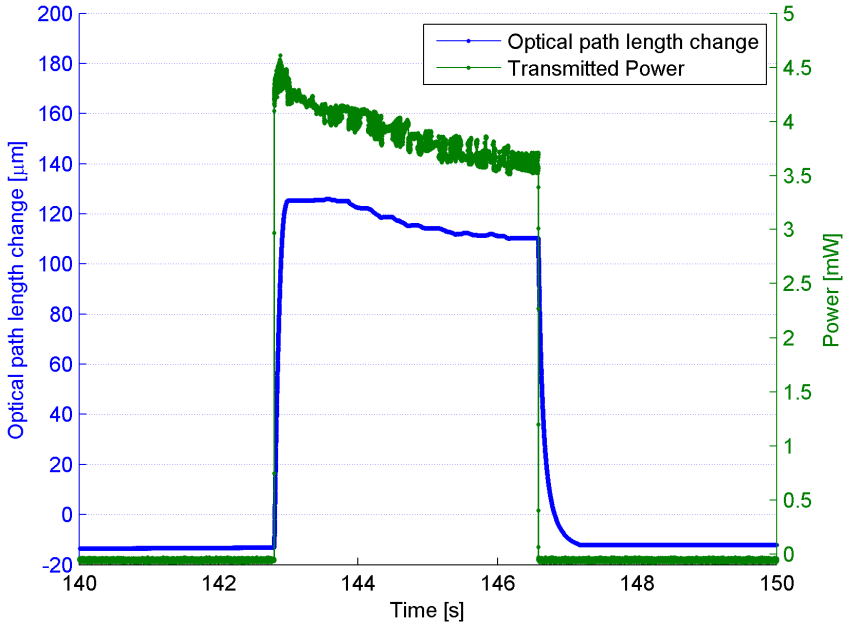

Figure 4.13: Detail zoom of fig. 4.12; the last heating/cooling transient before the fiber breaks is shown.

On figure 4.12 we see the heating and cooling of the fiber and that the fiber breaks. We see that the fiber after the last blocking contracts to the zero point (which is almost the initial length) and then it is broken while the heating laser was blocked because when the laser is unblocked the fiber is broken; there is no transmitted power and the optical path length change is constant.

On the last heating transient (shown in detail in figure 4.13) it is seen that the transmitted power decreases during the heating. The actual coupling of light into the bare fiber was measured after the experiment and it was lower than the initial coupling into the tapered fiber. The

actual coupling of the bare fiber should be higher than the initial coupling of the tapered fiber as the light is scattered at the waist of the tapered fiber. Therefore the coupling must have decreased during the experiment which is also consistent with the decrease in transmitted power.

An explanation could be that the fiber sags down such that it does not guide the light so well and then breaks. Usually when the fiber breaks it rips like a rope because the fiber is under tension, so maybe this fiber was not tensioned as much as the other fibers.

It could also be thought that a particle inside the vacuum chamber was evaporated from the fiber as the fiber was heated and then when the fiber was cooled the particle condensed on the waist, where the fiber is thinnest, and absorbed the light. This would be a very unlikely event and it could also be discussed why the particle would condense on the fiber instead of on the cold chamber walls. A particle on the nanofiber would explain the decrease in the coupling but it is not likely that it would break the nanofiber, as it takes around 1 mN of longitudinal stress to rip a nanofiber [27].

It is strange that we see spikes in the signals of both the transmitted power and the fringes counts at almost the same time. These spikes are not observed in the reference power signal. If the spikes are real and not a measurement error then at these spikes a lot of power is transmitted through the fiber and the optical path length change increases a lot. Something could have changed the coupling of light into the fiber such that at the spikes a lot of light is transmitted through the fiber and the fiber is heated a lot and the optical path length change increases.

If the laser was mode jumping we would expect to see the power jumping to a new level and not a spike.

The way the laser is blocked and unblocked is with a piece of thick paper. At the instant when the paper cuts the beam, the light will be diffracted on the paper, so the lights mode will change. If the coupling of light into the fiber was not optimized, the diffracted mode could be thought to "fit" better into the fiber and then the coupling would increase together with the amount of transmitted light through the fiber, in this instant of time. This could explain the spikes and that we do not see the spikes for every blocking/unblocking because as the light is blocked by hand with a piece of paper it is not possible to do it exactly the same way each time. But as the duration of the spikes is approximately 0.5-1 s it could be discussed if not the diffraction effect would happen on a much shorter time scale (as it takes no more than 1 s to block the beam).

The amplitude of the interference signal during this experiment was low compared to typical values in the experiment so it is possible that the interference signal was so small that the detector mostly measured noise. The interference signal was optimized before the experiment but dropped to 1/3 of its amplitude during the second heating. Later it was discovered that when the experiment was started the current of the heating laser was 90 mA. The current was low because we did not want to burn the fiber immediately (and we did not know how much power it could stand). This current is actually below the threshold (92.95 mA) so the laser is not lasing as well yet. When the current was increased above threshold of the heating laser (in the second heating) and the fiber was heated the fiber could have rotated the polarization of the light and the amplitude of the interference signal would change.

The spikes in the transmitted power of the heating laser are also seen in the optical path length change, and could indicate that the fringes detector measures light from the heating laser. At the dichroic mirror before the transmission detector, figure 3.20, a small part of the heating laser light is reflected towards the fringes detector. It could be that for high power this

light locally saturates the fringes detector, which fits with the interference signal decreasing. If the detector is locally saturated for high power this could explain why we saw the extreme optical path length change of the fiber in figure 4.11. When the heating laser is at the maximum current (maximum output power) a total of 3.6 mW hits the fringes detector. Hereof 1.2 mW is actually from the heating laser.

4.7 Local saturation of the fringes detector

Many of the experiments showed an extreme increase in the optical path length change of the fiber for high powers, as we saw in figure 4.11. It could look like the measuring laser made a mode jump. As there, at that time, was no reference detector for the measuring laser it was not possible to check that. Most of the experiments had a low coupling of the measuring laser light into the fiber because the fiber coupling is optimized for the heating laser light, and it was therefore discussed to increase the power of the measuring laser in the fiber arm.

For high powers it was also often seen that the amplitude of the interference signal decreased when the fiber was heated and then it re-appeared at normal height when the fiber was cooled.

During some experiments it was tried to change the rotation of the waveplate (in the fiber arm after the fiber before PBS 2, figure 3.20) as the fiber was heated at high power and when the interference signal decreased, to see if the amplitude of the interference signal could be increased. If the fiber does change the polarization of the measuring light in the fiber arm, such that it does not interfere as well at the detector with the empty arm, then it should be possible to change the amplitude of the interference signal back by changing the lights polarization with the waveplate.

It was discovered that when the fiber was heated and the amplitude of the interference decreased, the interference signal could get back to almost the same amplitude as it was by changing the waveplate. Only for very high power was it difficult to get a good signal when the fiber was heated.

As it looks like the fringes detector was locally saturated by the heating laser the position of the lens in front of the detector was changed such that the light was not focused directly at the detector. Then the interference signal did not change in amplitude during the experiment, and the data now looked like figure 4.14.

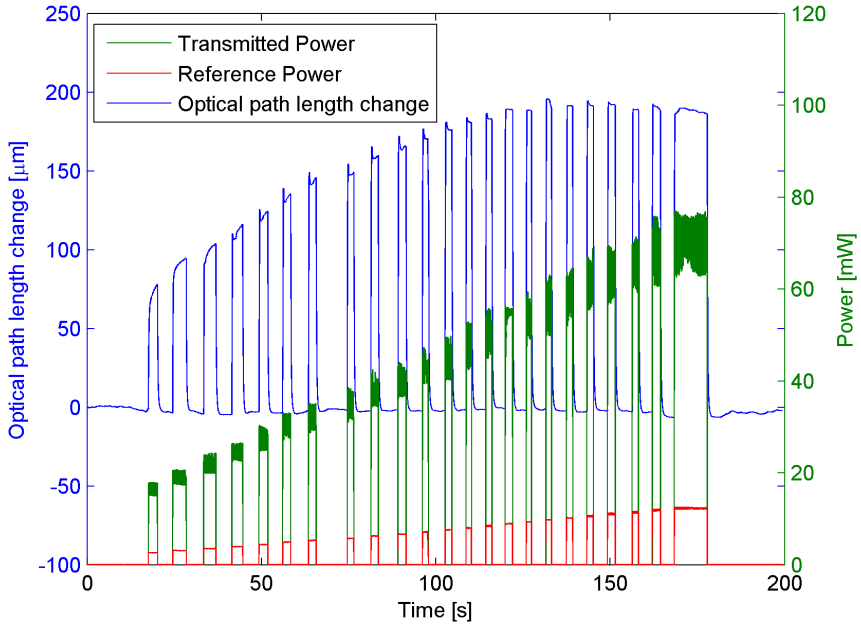

Figure 4.14: The optical path length change in [µm] together with the signals on the detectors in [mW] as a function of time in [s].

Here the optical path length change increases as the fiber is heated more and decreases to the initial length as the fiber is cooled. The oscillations in the transmitted power through the fiber are always observed, due to the fiber behaving as a Fabry Perot resonator for the light. We see that the optical path length change saturates, and as discussed earlier this was not expected according to [3], and this indicates that there is a maximum optical path length change of the fiber. In [3] it was observed that the optical path length change depended linearly on the heating power but here we always first seen a linear dependence on power and then saturation (figure 4.14). With this fiber, figure 4.14, it actually looks like that the optical path length change decreases a bit again for higher powers, indicating that there is a maximum optical path length change for a certain power.

4.8 Adding a dichroic mirror in front of the fringes detector

The extreme optical path length changes did, however, return in subsequent measurements so in order to completely avoid the possible saturation of the fringes detector, which was thought to be the reason for the extreme optical path length changes, the mirror in front of the detector was replaced with a dichroic mirror such that the heating laser light is removed from the beam before it arrives at the detector. The dichroic mirror reflects the measuring laser and transmits the heating laser.

After adding the dichroic mirror, different optical path length changes were then observed as shown in figure 4.15 and figure 4.16. In these experiments the amplitude of the interference signal did not change, which could be an indication that the amplitude fluctuations observed earlier were actually caused by the heating laser saturating the detector.

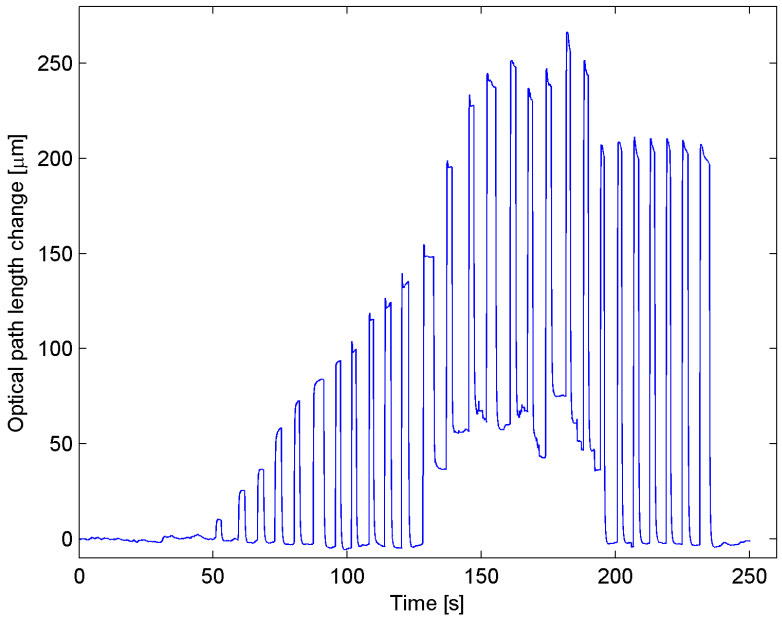

Figure 4.15: The optical path length change in [µm] as a function of time in [s] for the first heating and cooling experiment on the fiber.

In figure 4.15 it is seen that the zero point of the optical path length change is changed during the experiment but ends at the initial zero point again. An explanation is that the measuring laser was mode jumping to another mode, when the zero point changed, and then back.

I notice that when the heating laser is blocked the fringes moves continuously over time. But when the heating laser is unblocked the fringes jump in discrete steps. Probably because of the optothermal effect i.e. that the fiber acts as a Fabry Perot resonator for the heating laser light, so the increasing temperature (power) changes the length of the fiber which is the length of the Fabry Perot resonator, so the transmitted power of the transmitted frequencies are changed, and the change in reflected and transmitted power inside the fiber heats the fiber and again changes the fiber length (fringes moving).

Another measurement afterwards on the same fiber is shown in figure 4.16.

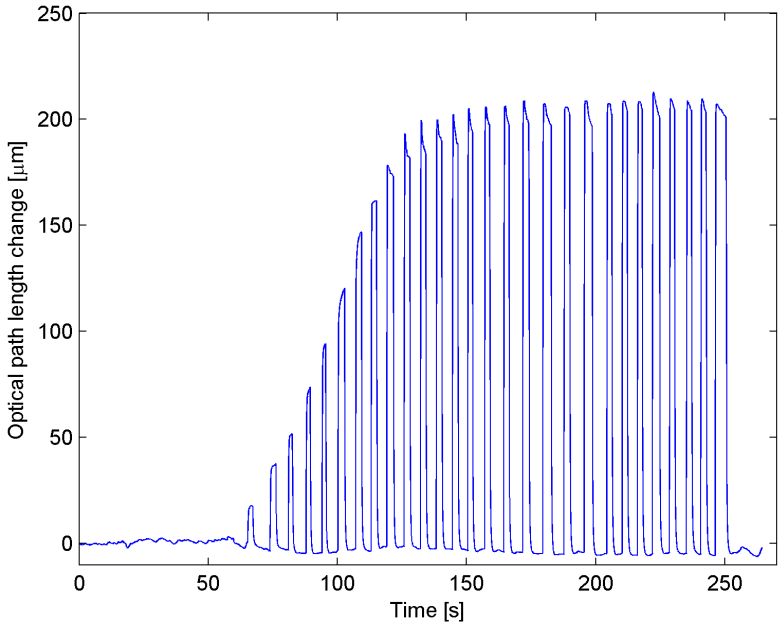

Figure 4.16: The optical path length change in [µm] as a function of time in [s] for the second heating and cooling experiment on the fiber.

Here there is no changing of the zero point of the optical path length change. The saturation of optical path length change with power is very clear. If the first heating (figure 4.15) and second heating (figure 4.16) are compared it is seen that the optical path length change has almost the same size and behaviour if the shifting zero point is subtracted from the data (figure 4.17).

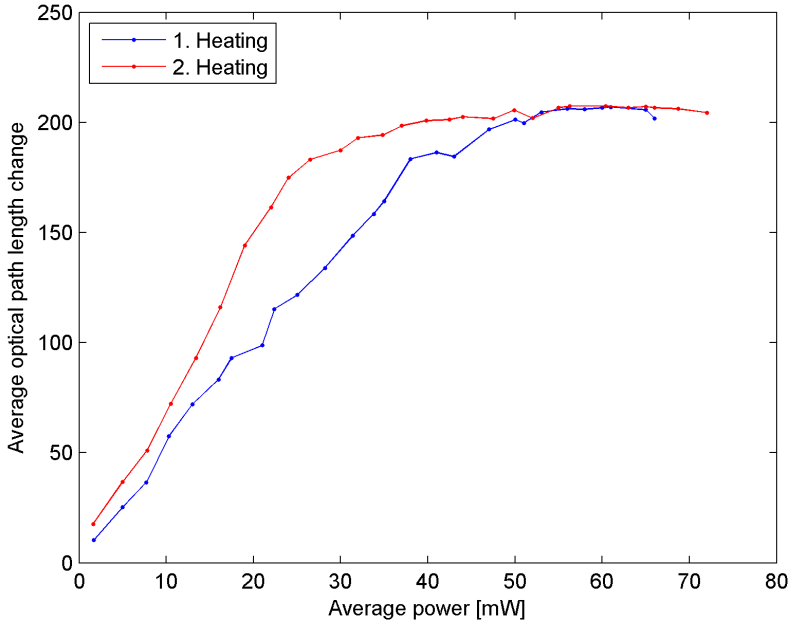

Figure 4.17: Average optical path length change as a function of average transmitted power for the first heating (blue dots) and second heating (red dots) of the fiber.

4.9 Investigation of memory effects

The previous observations inspired to test if the fiber has memory, i.e. if the fiber would be affected by being heated a second time shortly after the first heating (figure 4.18).

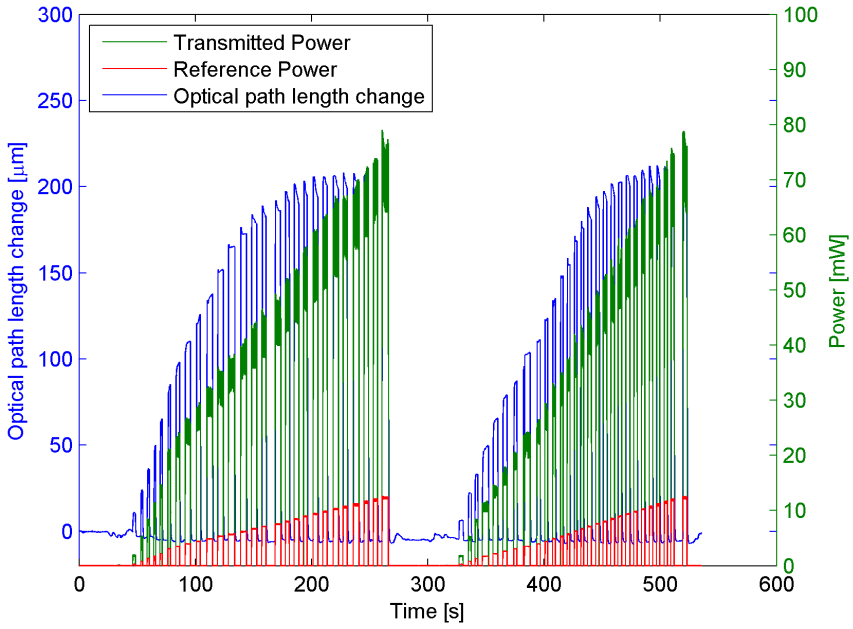

Figure 4.18: The optical path length change in [µm] together with the signals on the detectors in [mW] as a function of time in [s] for the two successive heating and cooling experiments on the fiber.

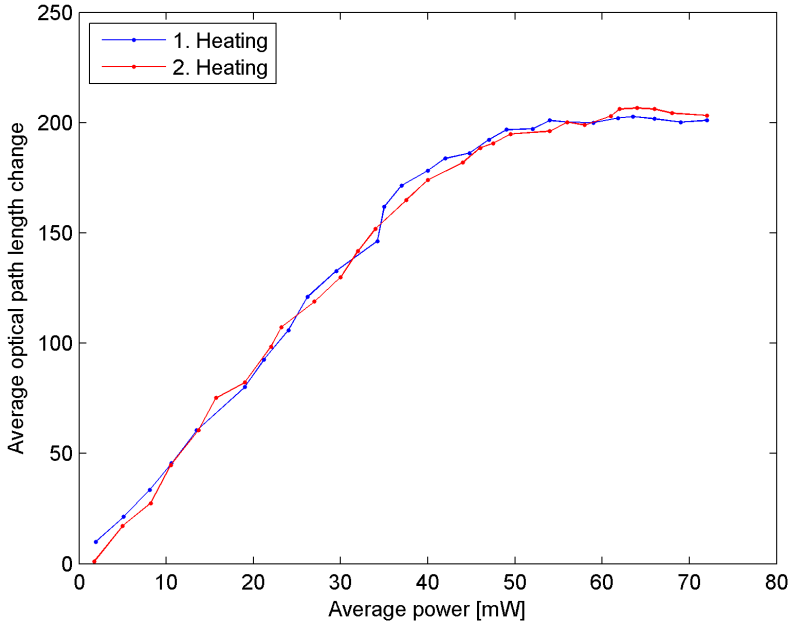

Figure 4.19: Average optical path length change as a function of average transmitted power for the first heating (blue dots) and second heating (red dots) of the fiber.

In figure 4.19, the average transmitted power versus average optical path length is shown. For the average optical path length the deviation from zero is subtracted (just before the optical

path length change increases) so all peaks have the same zero point for the two memory test heatings.

The first and second heating look similar so it looks like the fiber is not changed by the first heating i.e. it does not have memory about the first heating. The top of the heating and cooling peaks also look similar for both heatings, and the top of the peaks change in the same way for high and low power. In a zoom it is observed that for low power they increase gradually whereas for high power they have a steep increase and then a decrease.

Another memory test on the same fiber is shown in figure 4.20. Here something changes the optical path length and the three heatings do not look the same. The optical path length change does not go back to the zero point when the fiber is cooled. No change was observed in the interference signal during the experiment.

The difference in the zero point of the optical path length change could be because the measuring laser was mode jumping because of optical feedback, and adjusting the optical path length change for the zero offsets show that they are rather similar.

Other possible explanations for the shift in zero points could be that the glue was heated such that the fiber is not so tensioned as we expect. It could also be a deformation of the fiber. If the fiber is deformed while it is heated, i.e., the heating changes the fibers shape, it could be thought that it would be observed as a changing of the zero point of optical path length change. But the deformation would then be expected to happen at a high power close to the fibers melting temperature, and here the zero point starts to change already at low power. As discussed earlier the fiber should also be pre-tensioned such that when it is heated it is expected to relax and then rip so it is not expected that it will deform. The measuring laser mode jumping is therefore a more probable explanation.

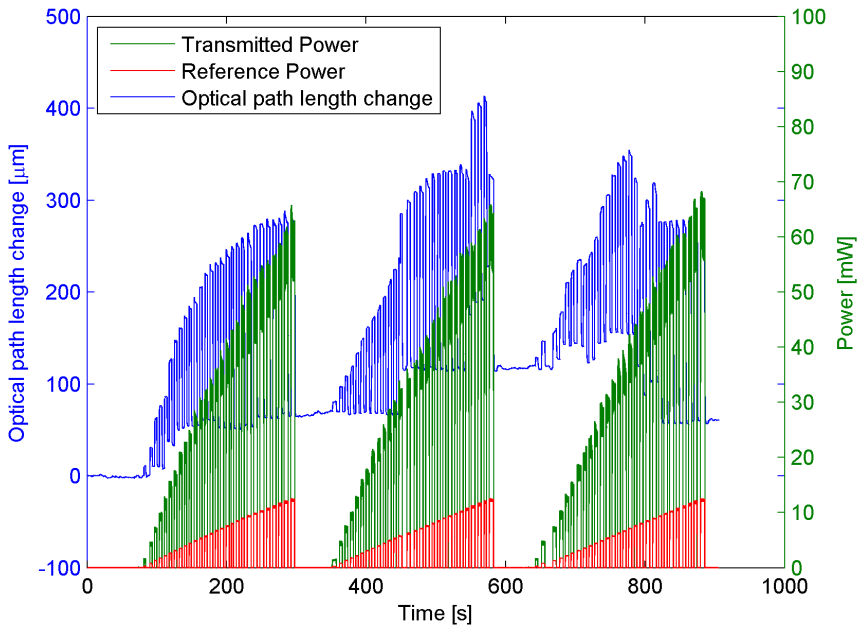

Figure 4.20: The optical path length change in [µm] together with the signals on the detectors in [mW] as a function of time in [s] for the three successive heating and cooling experiments on the fiber.

We have seen that it does not seems that the fiber show memory effects. The time between the measurements should also be sufficient for the fiber to cool. If the fiber was affected by the first heating it would probably be seen as a deformation the fiber.

4.10 Analysis of a 400 nm diameter tapered fiber

In this section we analyse data from a fiber with a waist diameter of 400 nm. The fiber was heated to observe if and when it would break (figure 4.21). The fiber did not break since it could stand the maximum avaliable heating power of 55 mW.

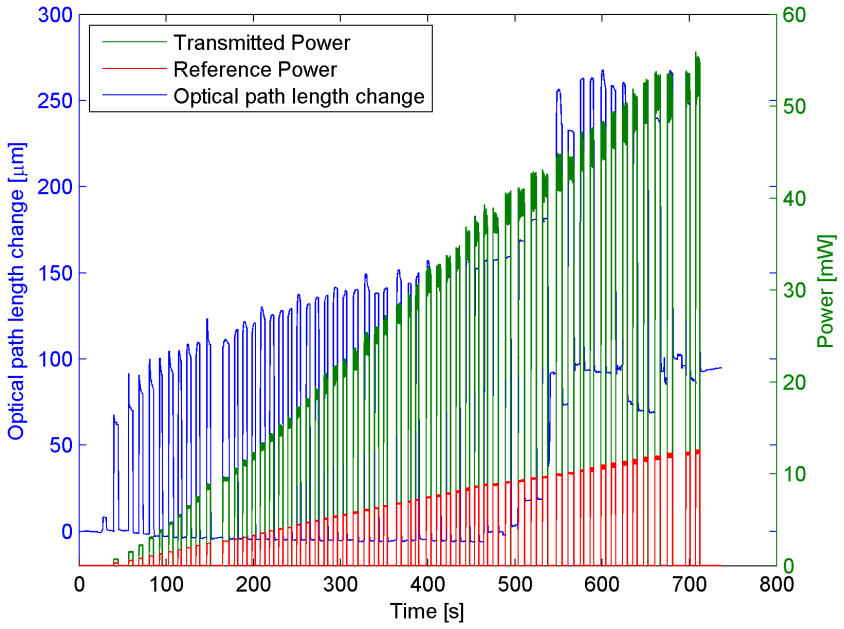

Figure 4.21: The optical path length change in [µm] together with the signals on the detectors in [mW] as a function of time in [s]

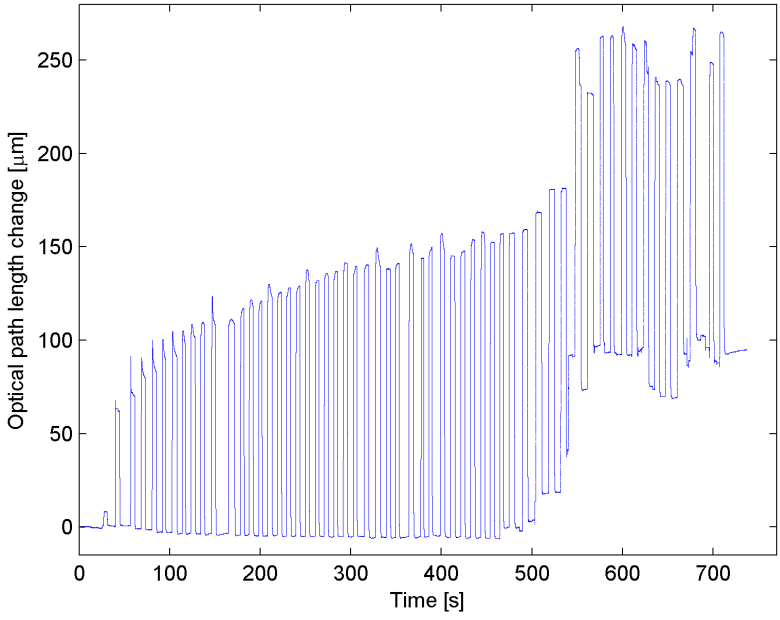

Figure 4.22: The optical path length change as a function of time when the fiber is heated and cooled. (Shown here since the red and green curves in figure 4.21 partly overlaps with this curve).

We observe that the optical path length change suddenly increases when the transmitted power reaches about 40 mW, figure 4.21, and at this point does not go back to the zero value

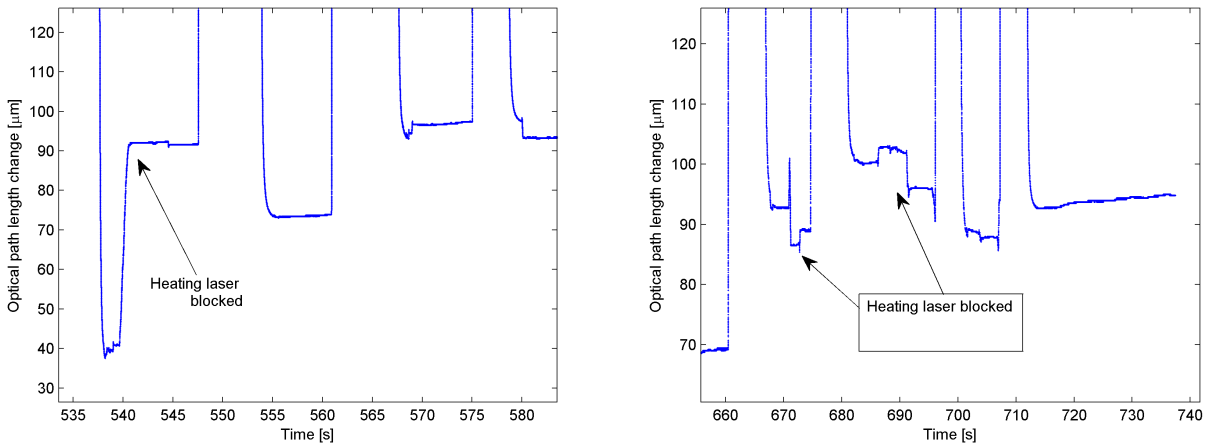

Figure 4.23: Zoom on the optical path length changes on figure 4.22. When the heating laser is blocked, the optical path length changes.

again. This behaviour is what would be expected if the fiber was deformed during the heating. The fringes counts were all measured and the slope of the optical path length change as a function of time was not above the maximum rate, so the behavior could not be ascribed to counting errors.

It was also observed, figure 4.23, that the optical path length change fluctuates when the heating laser is blocked and the fiber has cooled off. Here the fringes counts (optical path length change) should be constant, so this may be due to an unstability in the setup and will be discussed later. The fluctuations were not in the same direction and when they were inspected closely it was seen that the changes were continuous and not jumps, which also indicates that it was an unstability and not a sampling error.

The optical path length change is plotted as a function of the average power in figure 4.24. The optical path length change is taken as the last point when the fiber has been heated and just before the laser is blocked and the cooling begins. The background is subtracted, where the background is the deviation from the zero point after cooling at the right hand side of the peak.

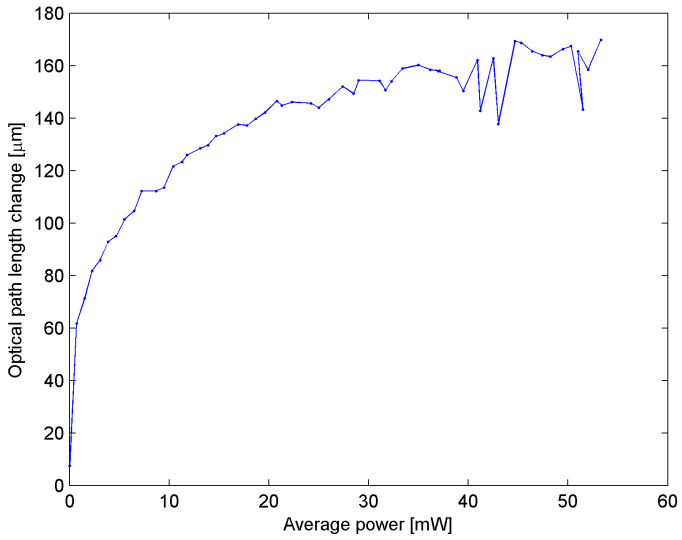

Figure 4.24: The maximum optical path length change in [µm] as a function of the average transmitted power in [mW] through the fiber.

We here observe the saturation of the optical path length change and also note that some fluctuations arise for high power where the optical path length change differs more for each heating.

4.10.1 Cooling transients

As explained in the data analysis section, every 5th peak of the heating transients are analysed starting from the 2nd peak (the 1st peak is also included in the following two figures but the optical path length change of this peak is small probably because the current for this heating was just above the threshold of the laser).

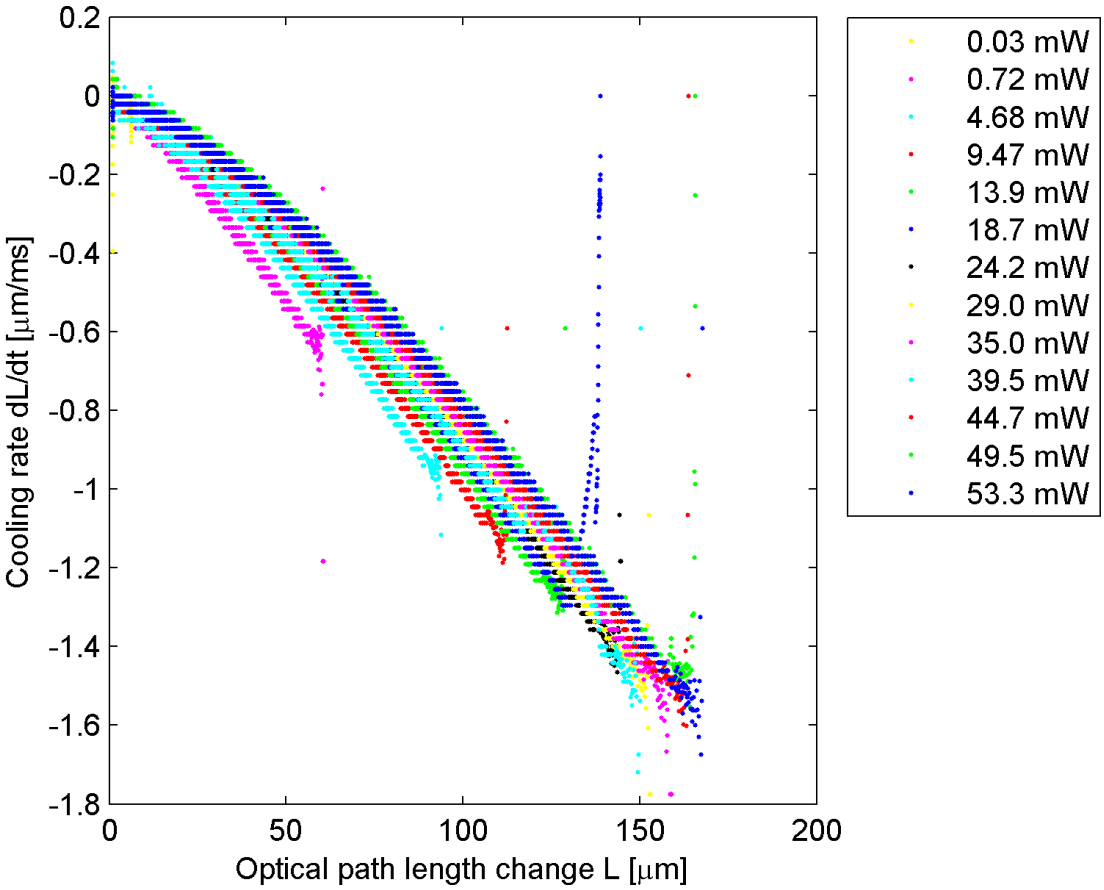

Figure 4.25: The cooling rate dL/dt as a function of optical path length change L for every 5th of the cooling transients in figure 4.22.

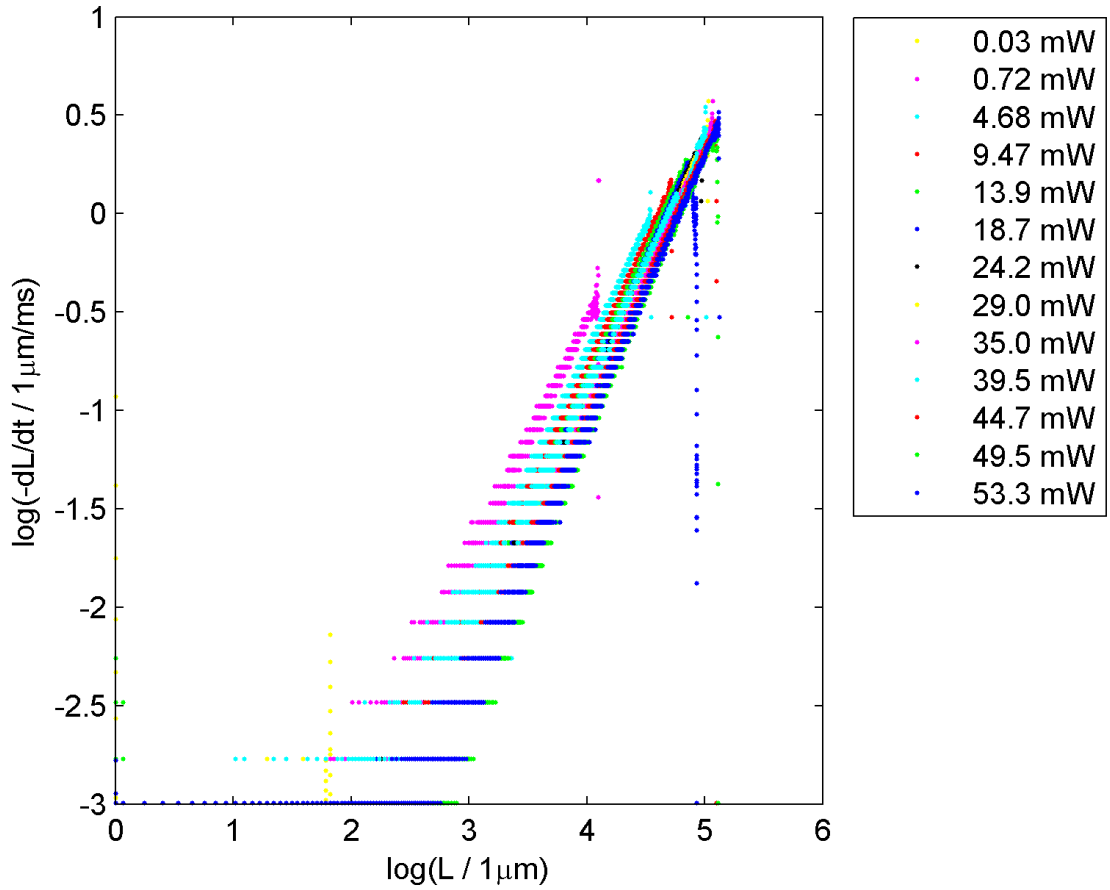

Figure 4.26: The logarithm of the cooling rate -dL/dt as a function of the logarithm of the optical path length change L for every 5th of the cooling transients in figure 4.22.

We find, as shown in figure 4.25, that the cooling rate dL/dt is numerically largest when the fiber starts cooling, i.e. for the initial optical path length change L, and then the rate decreases towards zero as the fiber cools to zero optical path length change. We also find that the cooling rates dL/dt are different depending on the heating power used to obtain the optical path length change L. Note for example that for a given optical path length change L the cooling rate dL/dt depends on the power the fiber was heated with, so that the cooling rate is smaller for higher heating power. This means that the fiber cools faster when it has been heated with less power for a given optical path length change. This I will discuss later. A priori one might have expected that the cooling transients were similar and that the fiber would cool in the same way independent of the power used to heat it.

If the fibers cooling was exponential the rate of cooling dL/dt would depend linearly on L. As seen on figure 4.25 the slopes are not linear and as described in [3] the thermodynamics of the fiber is also expected to be more complicated. That the curves are shifted vertically tells us that the fibers cooling is also a function of the fibers history i.e. of the power it was heated with and not only a function of the optical path length change of light that the fiber gives rise to. (It should be noted that the offliers in figure 4.25 appears in the beginning of the cooling and are related to the sudden decrease in heating that causes some initial disturbance in the fiber).

In figure 4.26 the logarithm of the cooling rate -dL/dt is plotted as a function of the logarithm of the optical path length change L, and these plots are now linear. While the slopes of

the curves are rather similar, the different cooling transients (curves) are shifted horizontally depending on the power, i.e. they do not have the same intersection with the y-axis.

Inspired by figure 4.25 we describe the rate of cooling dL/dt as a function of optical path length change L by a power law

$$\frac{dL}{dt} = -(\alpha \cdot L)^{\beta} = -\alpha^{\beta} \cdot L^{\beta} \tag{4.1}$$

with α and β positive constants. Taking the logarithm on each side of this gives

$$\log(-\frac{dL}{dt}) = \beta \cdot \log(\alpha \cdot L) = \beta \cdot \log(\alpha) + \beta \cdot \log(L) \tag{4.2}$$

which gives the linear function as seen in figure 4.26. By fitting the linear part of the curves in figure 4.26 to a linear polynomial the coefficients a and b can be found. Using $y = a \cdot x + b$ where $y = \log(-\frac{dL}{dt})$, $x = \log(L)$, we find for the slope $a = \beta$ and for the intersection with the y-axis $b = \beta \cdot \log(\alpha)$. From b we can find $\alpha = \exp(\frac{a}{b})$. The units of the fits are found with the optical path length change L in µm and the time t in ms.

The results of the fits are shown in table 4.1. The measurement with the lowest power of 0.03 mW has been excluded from the fit since it was close to the noise level.

Table 4.1: Table of cooling transient data.

Cooling transients						
Power	$a = \beta$	b	α	L^{max}	τ_{init} [ms]	τ_{final} [ms]
0.72 mW	1.188	-5.31	0.0114	61.8	100	130
4.68 mW	1.230	-5.65	0.0101	95.0	108	149
9.47 mW	1.277	-5.92	0.0097	113	111	163
13.9 mW	1.297	-6.05	0.0094	130	111	168
18.7 mW	1.328	-6.22	0.0093	140	111	175
24.2 mW	1.330	-6.26	0.0090	146	114	181
29.0 mW	1.345	-6.35	0.0089	154	114	184
35.0 mW	1.338	-6.35	0.0087	160	116	185
39.5 mW	1.281	-6.02	0.0091	150	111	164
44.7 mW	1.337	-6.39	0.0084	169	119	190
49.5 mW	1.351	-6.52	0.0080	166	128	208
53.3 mW	1.360	-6.51	0.0083	170	121	199
Average	1.305	-6.13	0.0091	-	-	-

From the data in table 4.1 we can calculate average values of α and β that could be used in equation 4.1 as $\alpha = 0.0091$ and $\beta = 1.305$. However we also see that both a and b (numerically) increases with power, but since the absolute value of b increases faster than a, the value of $\alpha = \exp(\frac{a}{b})$ decreases. The results are shown graphically in figure 4.27 and figure 4.28, where it is observed that the cooling coefficients β and α have a clear power dependence.

We can now improve equation 4.1 by fitting a logarithm to β, see figure 4.27. The fit is good, except for one peak which was more difficult to fit. I have checked this fit but it does not change significantly when the fitting interval is changed.

The β coefficients are fitted to the formula $\beta = c_1 \cdot \log(P) + c_2$ and this gives $\beta = 0.0389 \cdot \log(P) + 1.1952$. The α coefficients are fitted to a linear formula $\alpha = d_1 \cdot P + d_2$ which gives $\alpha = -5 \cdot 10^{-5} \cdot P + 0.0104$.

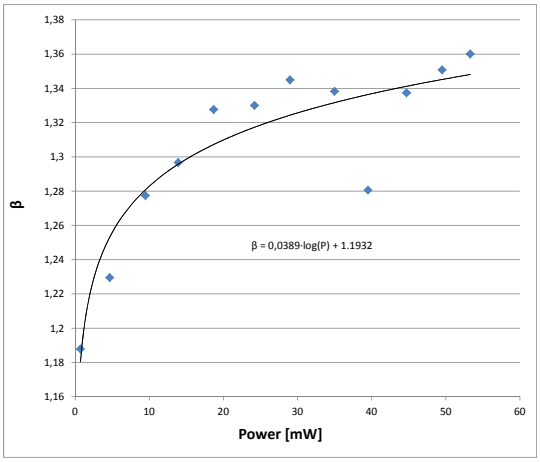

Figure 4.27: The quantity β as a function of power in [mW]. The data is fitted to a logarithm.

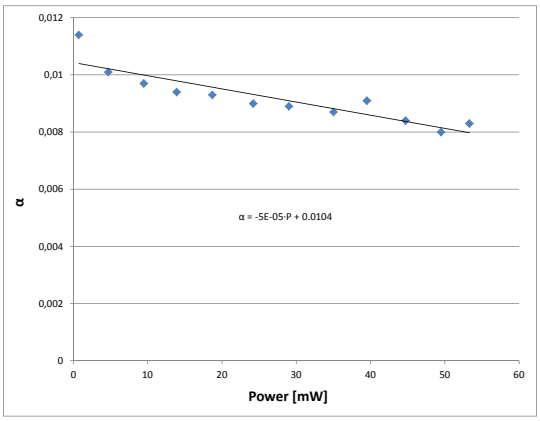

Figure 4.28: The quantity α as a function of power in [mW]. The data is fitted to a linear function.

In [3] they also investigated the time constants for the heating and cooling transients and compared them to the FED prediction and Plancks law. They obtained figure 4.29 and showed that their data followed the FED prediction. The time constants were obtained by considering the heating rise times in the interval 10%-50% of maximum optical path length change of the heating and in the interval 75%-90% of maximum optical path length change of the heating. For the cooling time constants they considered the cooling fall times in the interval 90%-50% of maximum optical path length change of the cooling and in the interval 25%-10% of maximum optical path length change of the cooling.

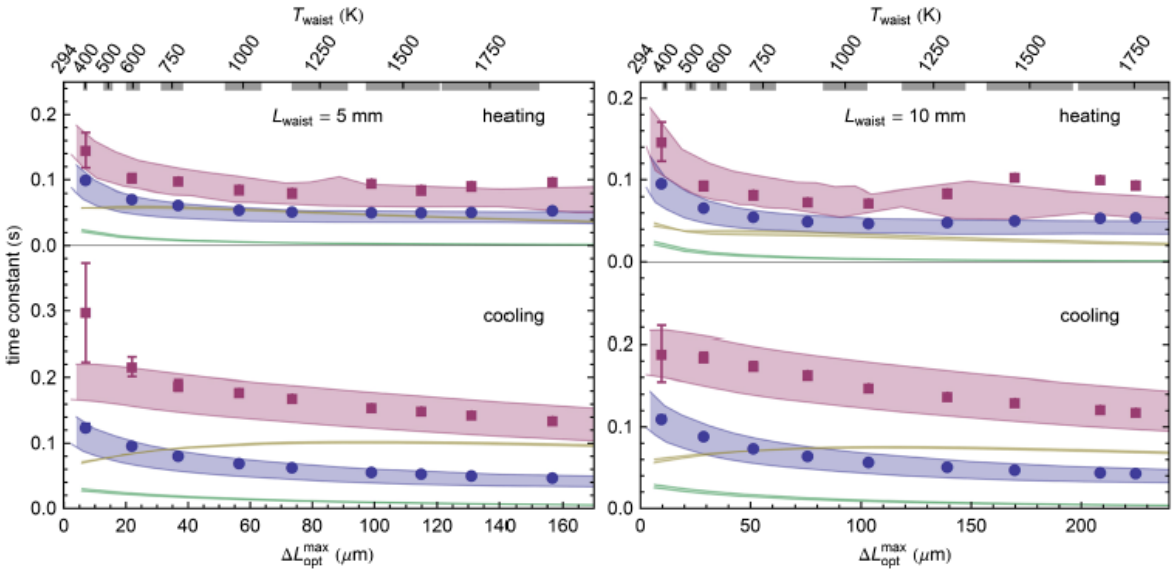

Figure 4.29: This figure shows the time constant data from [3] and is shown here to compare with my data. Left (right) side: heating and cooling time constants in [s] as a function of maximum optical path length in [µm] for a nanofiber with a 5 mm (10 mm) long waist. The blue circles (red squares) are the measured initial (final) time constants. Blue (red) bands is the FED prediction for the initial (final) time constants, green (yellow) bands is the predictions for the initial (final) time constants using Plancks law.

The cooling time constants τ are found from the rate dL/dt as $\tau = -\frac{L}{\frac{dL}{dt}} = \frac{-L}{-(\alpha \cdot L)^{\beta}} = ((\alpha \cdot L)^{-\beta}) \cdot L$ where the minus sign is due to that it is cooling. To compare my data to the data found in [3] I will consider τ_{init} the time constant for when the fiber has cooled to 70% of its initial optical path length change (i.e. of the maximum optical path length change L^{max}) and τ_{final} the time constant for when the fiber has cooled to 17.5% of its initial optical path length change (i.e. of the maximum optical path length change L^{max}). These times are thus the average of the intervals considered by [3]. The maximum optical path length change is shown in figure 4.24.

We then have:

$\tau_{init} = (\alpha(P) \cdot 0.7L^{max})^{-\beta(P)} \cdot 0.7L^{max}$ and $\tau_{final} = (\alpha(P) \cdot 0.175L^{max})^{-\beta(P)} \cdot 0.175L^{max}$

To calculate τ_{init} and τ_{final} I use the values from table 4.1 where the obtained values of τ_{init} and τ_{final} are also given. The found time constants are shown in figure 4.30.

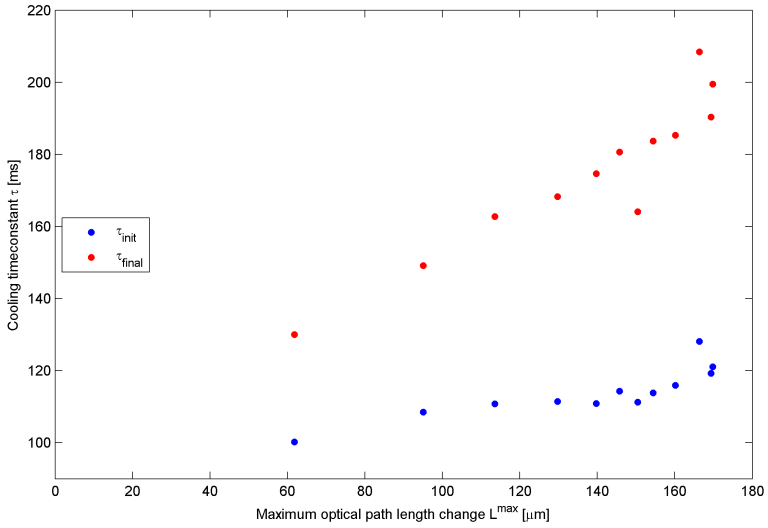

Figure 4.30: Initial and final cooling time constants in [ms] as a function of the maximum optical path length change of the cooling in [µm].

We see that $\tau_{init} < \tau_{final}$ i.e. $(\frac{dL}{dt})_{init} > (\frac{dL}{dt})_{final}$ so the fiber cools faster in the beginning of the cooling. This is also found in [3] both for the FED and Planck predictions. For my fibers τ_{init} is almost constant whereas τ_{final} increases with maximum optical path length change (heating power). This is in contradiction to what [3] observes as for their fibers both τ_{init} and τ_{final} decreases with maximum optical path length change which they claim is because their fibers follow the FED prediction. As seen in figure 4.29 the Planck prediction for τ_{init} and τ_{final} is almost constant in the interval 60-180 µm (the same maximum optical path length changes as my fibers have). This could indicate that my fibers follows Plancks law more than the FED prediction. The values of the time constants are in the same interval for my fiber and [3]. But both my τ_{init} and τ_{final} are greater than the FED and Planck predictions, although τ_{final} is a bit closer to the FED prediction. Here it is important to remember that my setup and the setup in [3] is not the same and also that my fiber has a waist length much shorter than [3]. The shorter waist length could influence the time needed for cooling.

The reason why the cooling rate dL/dt for a given optical path length change L is different, depending on the heating power, is probably due to the way the fiber cools, where the rate of cooling depends on the fibers temperature.

When the fiber is heated the temperature distribution as a function of the fibers length will be expected to be a function with the peak temperature centred at the thinnest point of the fiber i.e. at the waist. When the fiber is cooled, the fiber waist, which is hottest and thinnest, will cool faster than the rest of the fiber.

In figure 4.31 a sketch of the fiber and its temperature distribution is shown. If the fiber is heated with high power it will start with the red temperature distribution and if the fiber is heated with less power it will start with the blue temperature distribution. A fiber with the initially red temperature distribution will, when it is cooled, cool very fast in the beginning (peaked red distribution), and then slow down (flatten red distribution) as it is very hot and all the heat from inside the fiber has to travel to the fiber surface to radiate away. This fiber has more heat to radiate so it will take a longer time to cool than a fiber with the initially (peaked) blue temperature distribution will need.

The measured optical path length change will depend on the temperature distribution of the fiber. The initially hot fiber will in the beginning (peaked red distribution) give rise to a longer optical path length change than the initially colder fiber (peaked blue distribution), because it is hotter, but as it is cooled (flatten red distribution) it will give rise to a shorter optical path length change. At some point the two fibers will give rise to the same optical path length change. If the two fibers are compared at the time when the initially hot fiber (flatten red distribution) has reached the optical path length change that the initially cold fiber (peaked blue distribution) gives rise to, i.e. the optical path length change in the moment the cold fiber starts cooling, then here the initially hot fiber will be cooling at a rate lower than the initially cold fiber, because the initially hot fiber has been cooling for a while.

This could be why we observe in figure 4.25, that the cooling rate dL/dt is faster for lower heating power than for higher heating power for a given optical path length change L.

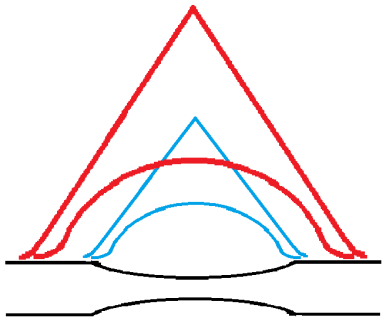

Figure 4.31: Sketch of how the temperature distribution of the fiber (black) could be visualized. The red temperature distribution is of a fiber heated with high power and the blue temperature distribution is a fiber heated with lower power. The initial temperature distribution is peaked and concentrated at the waist whereas the temperature distribution after some time flattens out.

We have seen that a power law can describe the fiber cooling where the shifting factor $b = \beta \cdot \log(\alpha)$ accounts for that the rate of the optical path length change dL/dt depends not only on the optical path length change L but also on the initial heating power through the coefficients α and β.

We have also seen that we could explain the fact that the rate of the optical path length change dL/dt depends on the initial heating power by the fiber radiating the heating energy from its surface. This is what is expected from Plancks law for macroscopic objects. It is in contradiction to what [3] observes, as they find that to explain the nanofibers radiation of heating energy they have to consider the volume of the nanofiber. So it seems that the cooling of the fibers, used in this experiment, despite that they are nanofibers, actually obeys Plancks law.

4.10.2 Heating transients

The heating transients of the same peaks as the cooling transients are analysed as explained in the data analysis section. Again the 1st peak is included in the next two figures but not in the following figures due to the low signal.

The rate of the heating transients dL/dt versus the optical path length change L are shown in figure 4.32. It is seen that the heating rates increases as the fiber is heated more, so the fiber heats faster when it is heated more, which is also what is expected. The heating rate is largest when the heating starts and then it decreases towards zero as the fiber heats. For a

given optical path length change L the heating rate dL/dt is higher for higher heating power. Figure 4.33 shows the logarithm of dL/dt vs the logarithm of L.

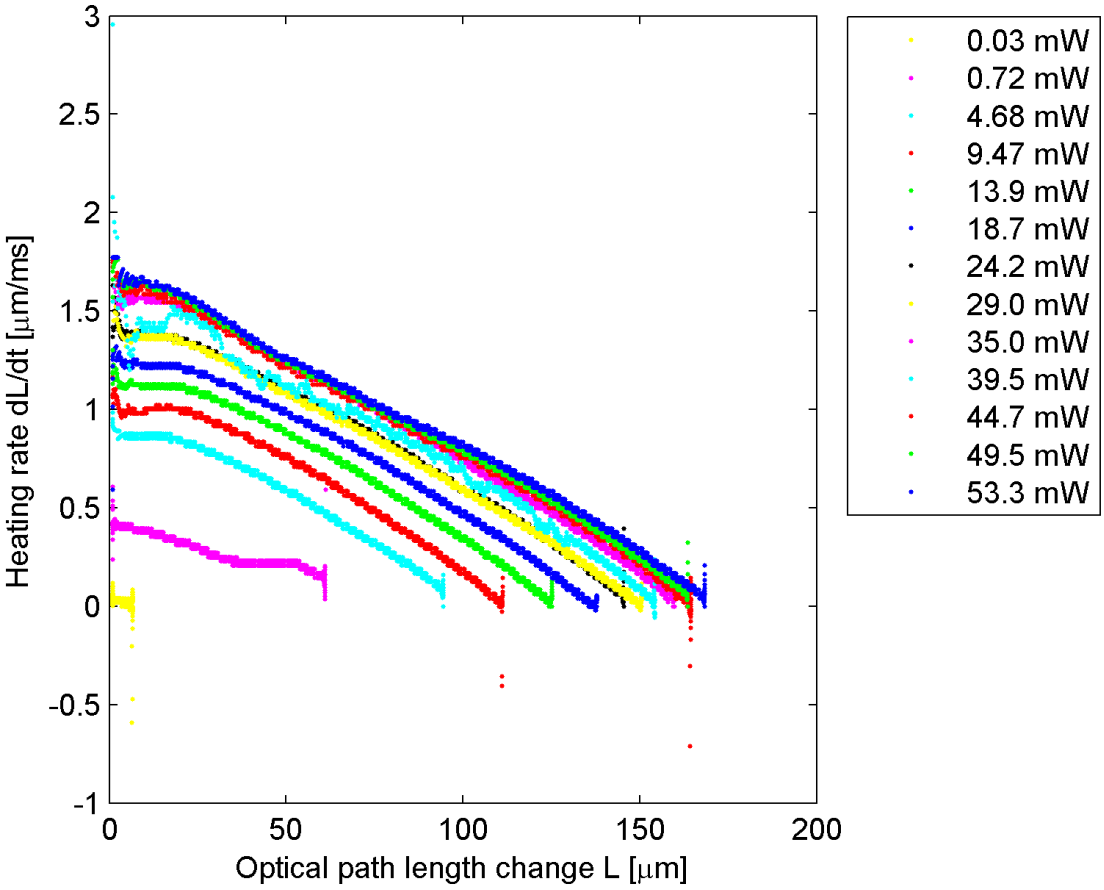

Figure 4.32: The heating rate dL/dt as a function of optical path length change L for every 5th of the heating transients in figure 4.22.

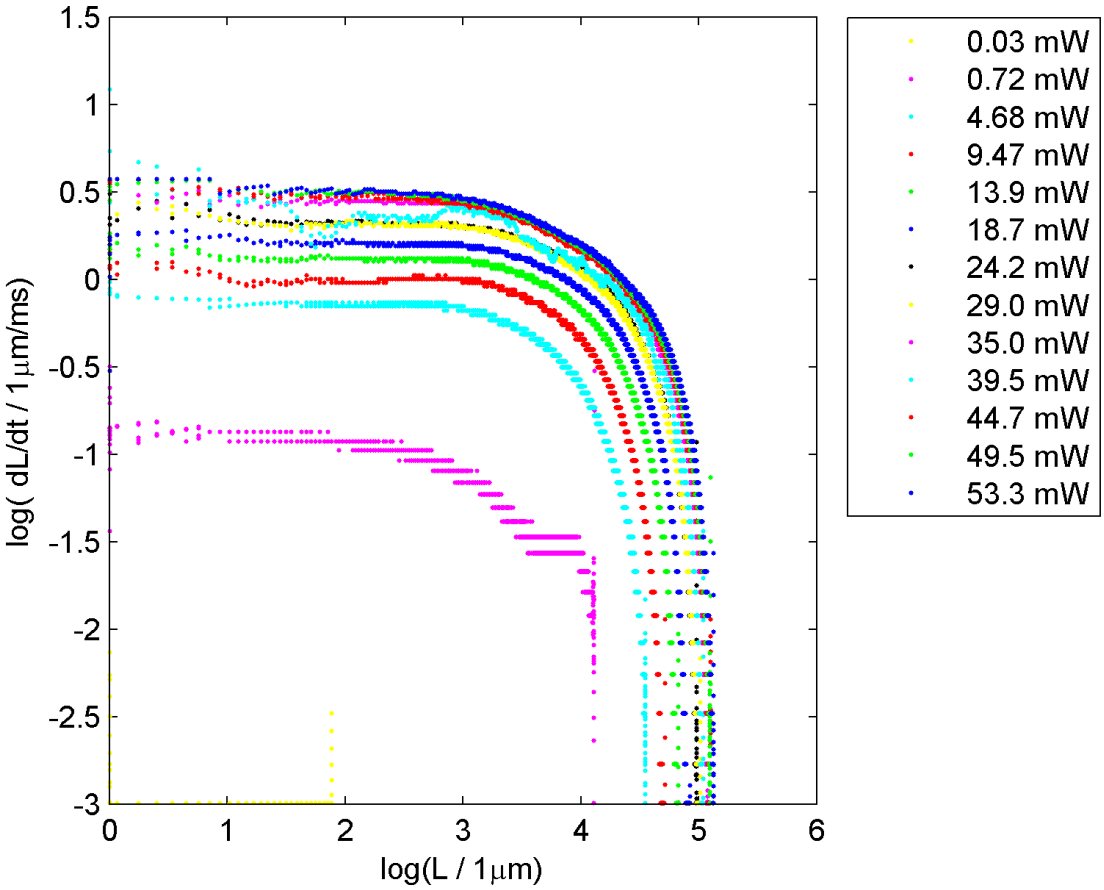

Figure 4.33: The logarithm of the heating rate dL/dt as a function of the logarithm of the optical path length change L for every 5th of the heating transients in figure 4.22.

As the heating rates dL/dt in figure 4.32 are almost linear, the linear part of the data is fitted to a linear function $y = ax+b$ where $y = dL/dt$ and $x = L$. The slopes a and intersections b of the linear fits are given in table 4.2 and plotted as a function of power in figure 4.34 and figure 4.35 respectively. It was chosen to omit the first data point as the power of this transient was so low that the signal was not good (the 2nd heating transient). It is seen that the values of the slopes a are similar but the intersections b differ more.

Table 4.2: Table of heating transient data.

Heating transients					
Power	a	b	L^{max}	τ_{init} [ms]	τ_{final} [ms]
4.68 mW	-0.0106	1.106	95.0	35.4	284.2
9.47 mW	-0.0117	1.339	113	36.2	385.7
13.9 mW	-0.0114	1.464	130	38.1	438.7
18.7 mW	-0.0113	1.575	140	38.1	423.2
24.2 mW	-0.0108	1.658	146	36.9	334.3
29.0 mW	-0.0107	1.646	154	40.3	450.8
35.0 mW	-0.0107	1.795	160	37.5	347.1
39.5 mW	-0.0105	1.694	150	37.0	316.8
44.7 mW	-0.0104	1.781	169	40.5	425.1
49.5 mW	-0.0103	1.791	166	39.1	363.3
53.3 mW	-0.0102	1.806	170	39.6	370.9
Average	-0.0108	1.605	-	-	-

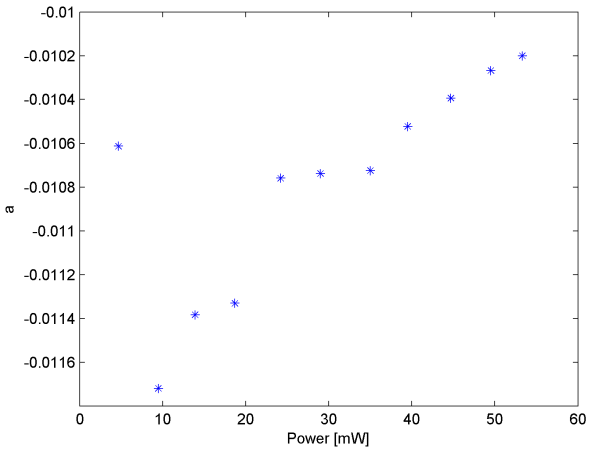

Figure 4.34: The slope a of the fits of figure 4.32 as a function of power in [mW].

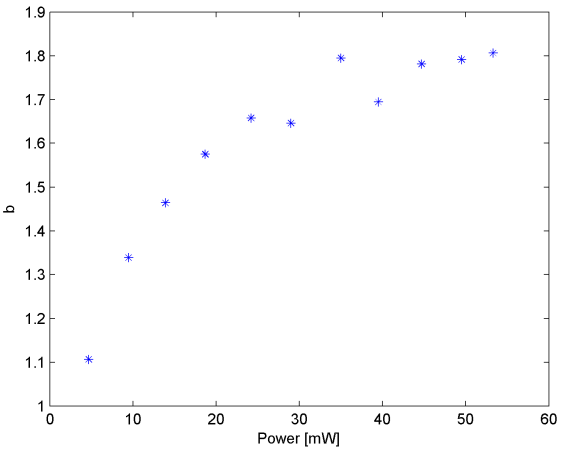

Figure 4.35: The intersections b of the fits of figure 4.32 as a function of power in [mW].

Again to compare my data to [3] I will consider τ_{init} the time constant for when the fiber has heated to 30% of its maximum optical path length change L^{max} and τ_{final} the time constant for when the fiber has heated to 82.5% of its maximum optical path length change L^{max}. These times are thus again the average of the intervals considered by [3].

For the heating we have the time constant $\tau = \frac{L}{\frac{dL}{dt}} = \frac{L}{a \cdot L + b}$ so $\tau_{init} = \frac{0.3 \cdot L^{max}}{a(P) \cdot 0.3 \cdot L^{max} + b(P)}$ and $\tau_{final} = \frac{0.825 \cdot L^{max}}{a(P) \cdot 0.825 \cdot L^{max} + b(P)}$

The obtained values of τ_{init} and τ_{final} are shown in table 4.2 and plotted in figure 4.36.

We see that $\tau_{init} < \tau_{final}$ i.e. $(\frac{dL}{dt})_{init} > (\frac{dL}{dt})_{final}$ so the fiber heats faster in the beginning of the heating, which is expected and also seen from figure 4.22 where dL/dt is maximum for zero optical path length, i.e. at the beginning of the experiment. This [3] also finds both for the FED and Planck predictions.

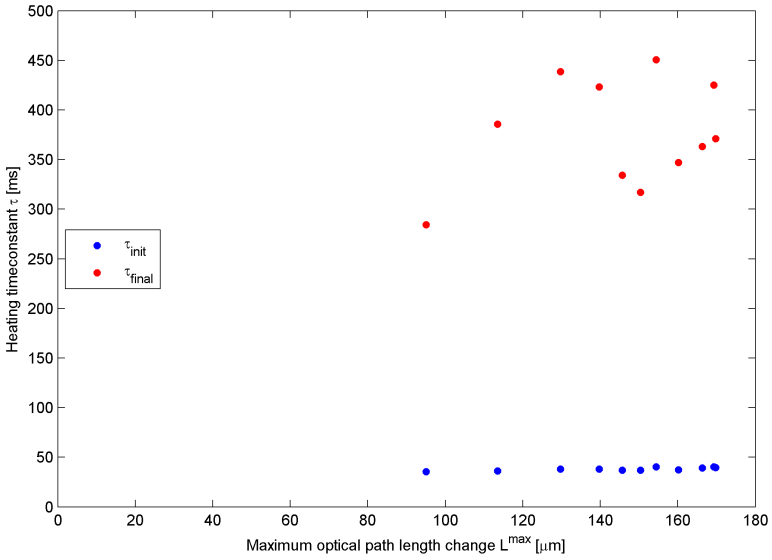

Figure 4.36: Initial and final heating time constants in [ms] as a function of the maximum optical path length change of the heating in [µm].

The initial heating time constants τ_{init} are constant while the final heating time constants τ_{final} lies within the same interval but show no obvious tendency. Also in [3] almost constant time constants for the heating for both the FED and Planck prediction for the same maximum optical path length changes as considered here is observed. The values of τ_{init} are below the FED prediction and above the Planck prediction, whereas the values of τ_{final} are much above both the FED and Planck prediction. So this fiber heats fast in the beginning, when it has reached 30% of its initial optical path length change, and it heats very slowly as it has reached 82.5% of its maximum optical path length change. From figure 4.32 we also observe that the heating rates dL/dt when the optical path length change L has reached 82.5% of its maximum value are very close to zero, i.e. here the heating is very slow.

From figure 4.25 and figure 4.32 it is seen that the numerical rates of cooling and the rates of heating are in the same interval. We see that as expected, for both heating and cooling the initial rate is larger when the heating power is higher. Also we observe that a fiber heated at a power P in the beginning of the heating, heats at almost the same rate as it cools when it is cooled.

For both heating and cooling processes we saw that $\tau_{init} < \tau_{final}$ i.e. $(\frac{dL}{dt})_{init} > (\frac{dL}{dt})_{final}$ so the fiber heats and cools fastest in the beginning of the heating or cooling but the laws describing the heating or cooling were different.

4.11 Preheating the fiber

In [3] the fibers were preheated before the experiment. The fibers were preheated at a high heating laser power (80-160 mW [3]) for 30 seconds before each heating and cooling. This was done to ensure that the fiber was thermalized at the not tapered parts, i.e. that the fiber had the same temperature at all places except at the nanofiber section (the waist). According to [3] the thermalization time of the not tapered fiber parts is 8 seconds so the 30 s preheating should be enough time for thermalization. After preheating the heating laser was switched of for 2 seconds before the heating and cooling experiment was started. The 2 seconds is according

to [3] enough time for the nanofiber section to cool so that the fiber was at ambient temperature before the experiments.

With my setup it takes much more than 2 seconds to block the heating laser and increase the current (power) on the heating laser. An improvement to the setup would be to have a mechanical blocking mechanism and a switch to control the heating laser power in which case this could be done in a short time. This was not implemented in this work, so here the non-tapered parts of the fiber might also start cooling when the heating laser is blocked.

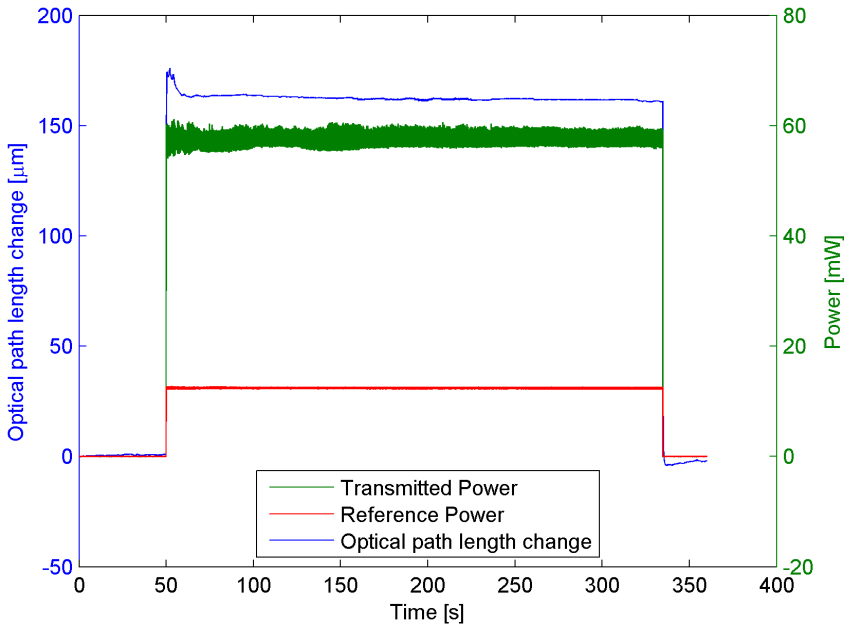

Figure 4.37: Preheating a fiber for 5 min at maximum power. The optical path length change in [µm] plotted together with the transmitted power and reference power of the heating laser both in [mW].

In this experiment, figure 4.37, a fiber was heated for 5 min at maximum power and the behaviour of the fringes signal was observed. During the first 10 s the optical path length change increases a lot then decreases and after that it is almost constant, but a little decreasing. This decreasing could be due to the interferometer drifting in time. This spike in optical path length change have often been seen before, at the moment when the heating laser is unblocked and the fiber is heated. The oscillations in the transmitted power fluctuates more in the beginning of the measurement where the optical path length change also fluctuates. It is seen that 30 s of preheating is enough time for the fiber to thermalize as the optical path length change is approximately constant after 10 s.

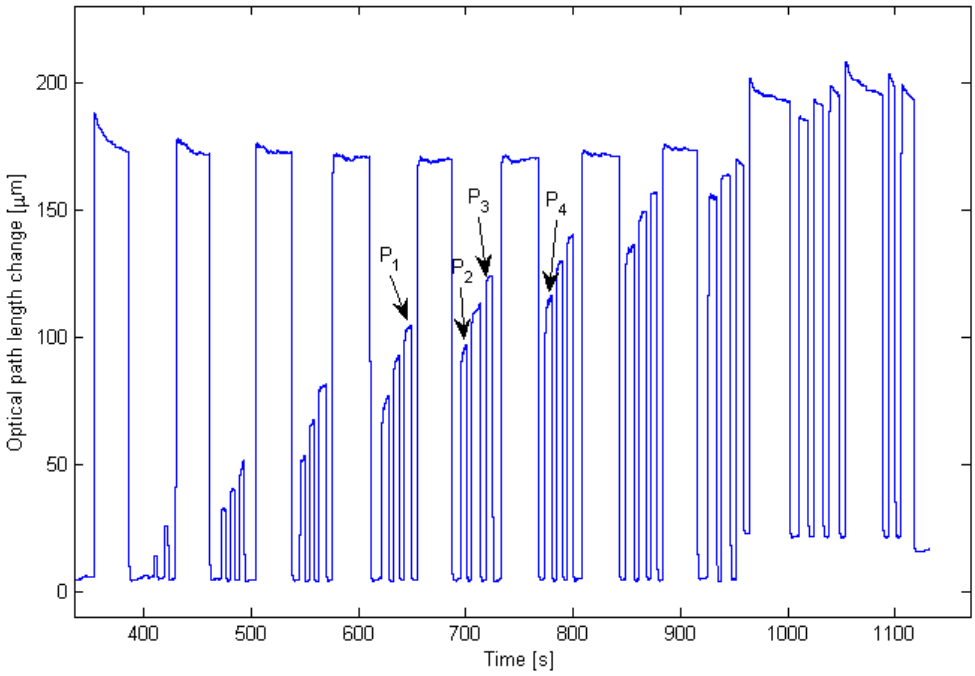

Figure 4.38: The preheated fiber. It is noticed that the optical path length change does not increase with power after the fiber is preheated as the heating powers P have the relation: $P_4 > P_3 > P_2 > P_1$.

Figure 4.38 shows measurements on a fiber which has been preheated. The fiber is preheated with the maximum avaliable power for approximately 30 s and then the heating and cooling transients follow. Afterwards the fiber is preheated between every 3rd measurement.

It is seen that the top of the preheated transients change with power just like the top of the heating transients. The spike in the first preheat was also observed in figure 4.37. In the beginning of the experiment when the heating power is low, the preheated transients increase relatively fast, see figure 4.39, then the rate is reduced until the end of the experiment where the heating power is almost the same as the preheating power, the rate again increases.

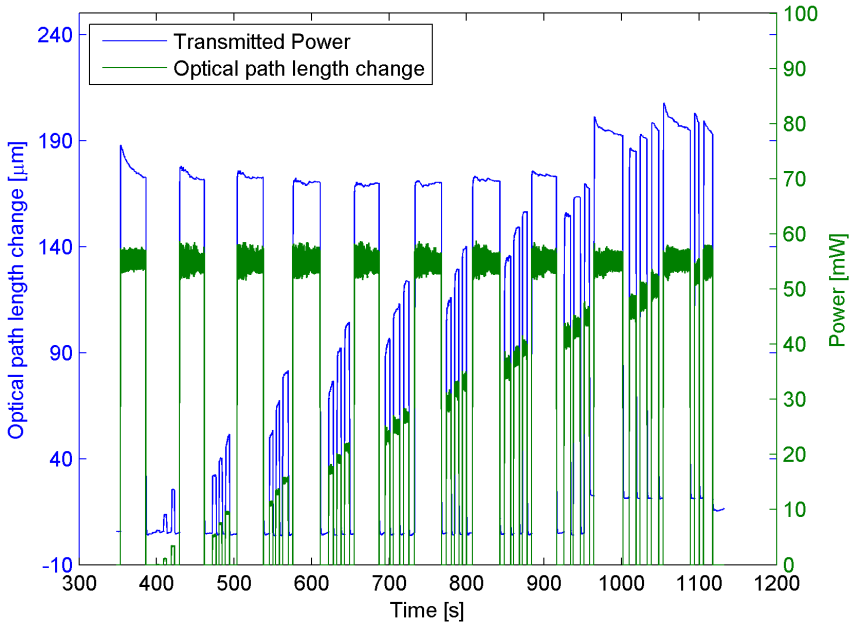

Figure 4.39: The optical path length change in [µm] plotted together with the transmitted power of the heating laser in [mW].

It is noticed, figure 4.38, that the optical path length change does not increase with power after the fiber is preheated, because we see in figure 4.39 that the relation between the heating powers P are $P_4 > P_3 > P_2 > P_1$. This behaviour is unexpected as the optical path length change does go back to the zero point so we would expect that higher heating power causes an increase in the optical path length change. This seems to show that the preheating of the fiber actually results in a decreased optical path length change when the fiber is heated again. But as it does takes a longer time to change the power of the laser after the preheat, than between each successive heating and cooling, it might be possible that the whole fiber has time to cool after the preheat and then it does not matter if it is preheated. The observations might then be explained if the non tapered parts of the fiber before the preheat does not have time to cool and then it is already hot as it is heated so the optical path length change is longer (P_1 and P_3) than after the preheat where the non tapered parts of the fiber have time to cool and then the optical path length change is smaller (P_2 and P_4).

For the present setup and our fibers it therefore does not seem to be an advantage to preheat the fibers as described in [3]. The preheating is done to obtain an initial temperature condition of the fiber, but this seems already be the condition with the cold fiber, because the cold fiber in the vacuum chamber should have the same temperature everywhere when the experiment is started.

4.12 Reference detector for the measuring laser

As there were doubt about if the measuring laser was mode jumping it was decided to add a detector to the setup to be able to monitor the measuring laser while heating the fiber. The detector is seen on figure 3.20 where an etalon reflects the 0th order beam from the AOM into the reference detector. On the detector the interference of the light reflected from the surface of the etalon and the light reflected inside the etalon is observed. The interference fringes will change when the laser modejumps. The LabJack then samples one more channel but since the

sample rate was then 8333 Hz and with the microcontroller for data sampling, this should still be high enough to measure all optical path length changes.

4.13 Changing the two arms in the interferometer

As discussed before the sudden changes of the optical path length change could be due to optical feedback into the laser. When the optical path length changes (as the fiber is heated or cooled) the optical feedback into the laser changes and then the frequency of the laser can change (mode jumping). The mode jumping will elongate and contract the fiber differently, which can change the optical path length.

To avoid the optical feedback it was decided to change the setup, such that the AOM was positioned in the fiber arm, see figure 3.16. This should reduce the feedback, as the beam in the AOM arm is shifted in frequency and will therefore not make the laser mode jump if this beam is feedback. At the same time the optical path lengths of the two arms were changed to make them equal because then the fringes counting on the detector will be more stable to frequency changes.

4.14 Analysis of a 500 nm diameter tapered fiber

In this section we analyse data from a fiber with a waist diameter of 500 nm. The data were obtained from after the two arms in the interferometer were switched. The fiber had a transmission of 90.5% after it was pulled. As the fiber was pulled it is interesting that we could actually see that the measuring laser was mode jumping. This is seen both in the transmitted power (blue) and in the reference power (red) in figure 4.40.

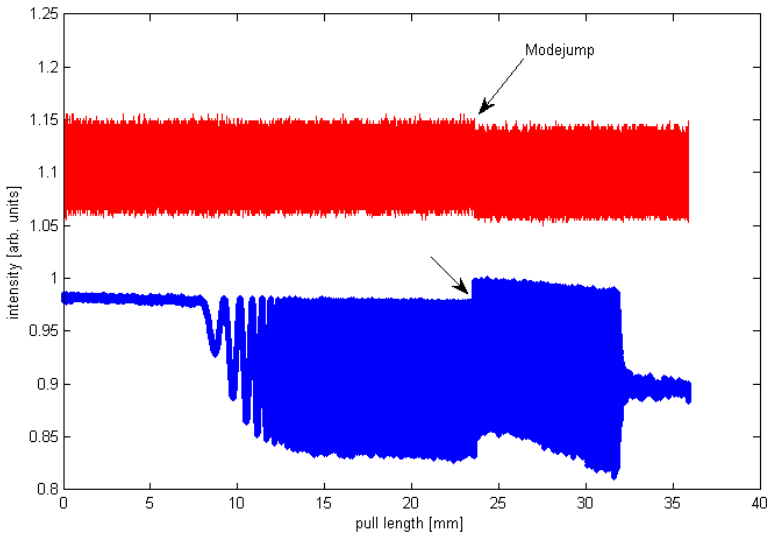

Figure 4.40: Raw data from the experiment. The intensity as a function of pulling length in [mm]. The laser is modejumping seen in the transmission through the fiber (blue) and in the power on the reference detector (red).

At a pull length of approximately 24 mm we suddenly observe a change as more light is transmitted through the fiber while less light is measured at the reference detector. That the change is simultaneous in both detectors indicates that it is a mode jump.

Figure 4.41 shows the optical path length change plotted together with the reference power and the transmitted power of the heating laser, and we observe that it looks like a typical measurement series.

We also see that the fiber did not break in the experiment and from figure 4.41 it is seen that the fiber could withstand the maximum avaliable power of about 67 mW.

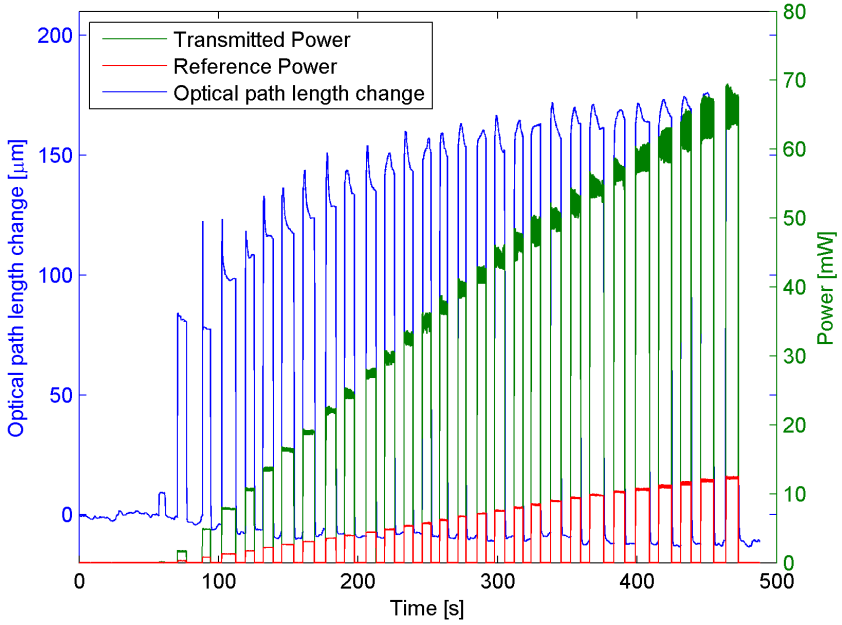

Figure 4.41: The optical path length change plotted together with the reference power and the transmitted power of the heating laser.

We do not see anything unusual in the detector signals while performing the experiment. Figure 4.42 shows the signal on the reference detector for the measuring laser. The measuring reference signal usually changes by ±0.01 V and always shows some spikes, which we ascribe to electronic noise in the detector, since the spikes often occur both when the heating laser is turned on or off, as seen in figure 4.43.

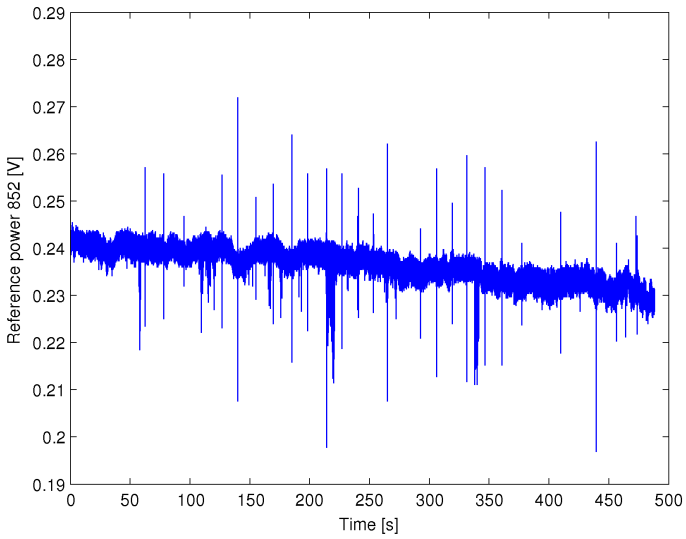

Figure 4.42: The signal on the reference detector in [V], for the measuring laser, as a function of time.

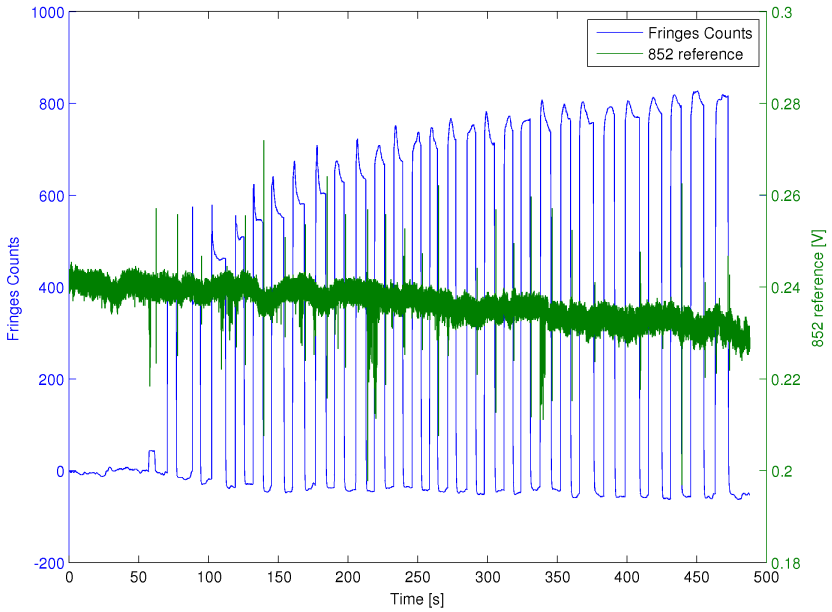

Figure 4.43: The fringes counts together with the reference signal of the measuring laser. The spikes in the signal on the detector occur briefly when the heating laser is turned on or off.

The saturation of the optical path length change is still observed, see figure 4.44. Here the blue curve is the average optical path length change while the green curve is the final optical path length change just before the fiber is cooled. The curves are observed to be similar but the green curve is a bit below the blue, because the average curve also includes the spikes often appearing in the beginning of the heating. The optical path length change saturates around 160 μm or 40 mW of transmitted power.

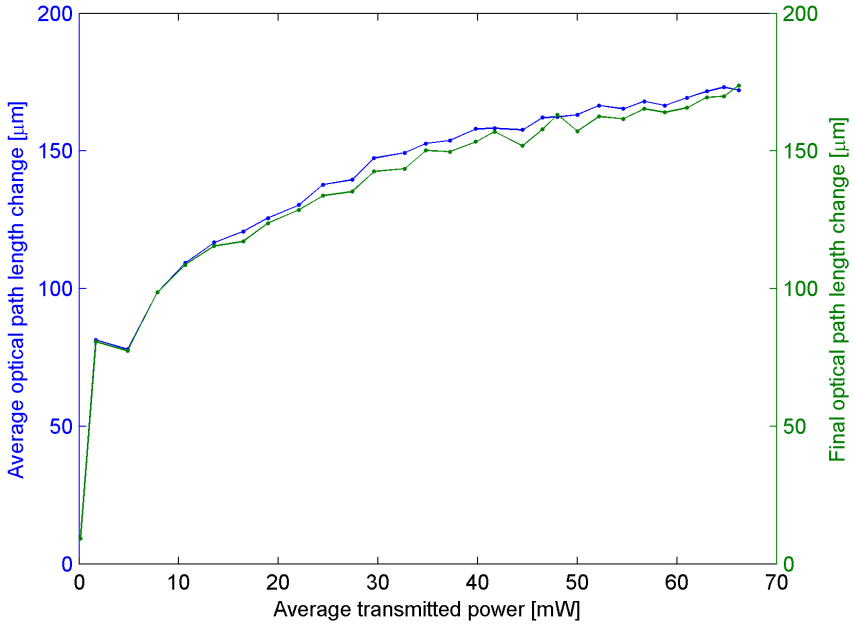

Figure 4.44: The optical path length change as a function of the average transmitted power through the fiber. The blue curve is the average optical path length change while the green curve is the final optical path length change before the fiber is cooled, it is this curve that I refer to as the maximum optical path length change.

We also observe, figure 4.45, that during the whole experiment the optical path length change returns to the zero point as the fiber is cooled. Furthermore we do not observe any sudden fluctuations in the optical path length change when the heating laser is blocked and the fiber has cooled of. This indicates that the switching of the two arms in the interferometer, did improve the measurements, and made the setup more stable. It also indicates that it was probably backreflections of the measuring laser which made the zero point of optical path length change.

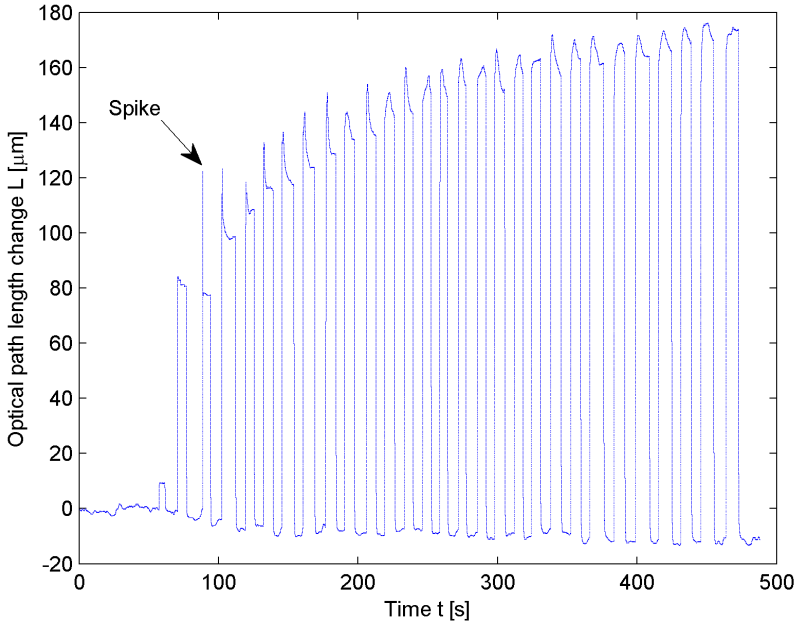

Figure 4.45: The optical path length change in [µm] as a function of time in [s] when the fiber is heated and cooled.

But we still observe the spikes in the optical path length change as the fiber is heated, indicated on figure 4.45. Since the setup is now more stable the spikes are probably real and not due to measurement errors. We see that the spikes do not appear for all transients. This could indicate that the spikes appear when the fiber is heated above a certain temperature T_c or when the fiber is heated above T_c again after it has been cold for a while. As the power is increased, we note that the spikes become smaller and even disappear, which is interesting as one might have expected that the spikes would occur with sudden heating with high power. This could therefore be an effect of the whole fiber being heated up gradually during the experiment. Also as the optical path length change begins to saturate, the spikes are fewer and the small peaks at the maximum power begins to level out.

4.14.1 Cooling transients

Figure 4.46 shows the rate of optical path length change dL/dt as a function of optical path length change L for some of the cooling transients. We see, that we observe the same behaviour as with the 400 nm fiber, as discussed earlier. In particular we observe that for the same optical path length change L the cooling rate depends on the fibers initial heating power and that the rate is slower for higher heating powers.

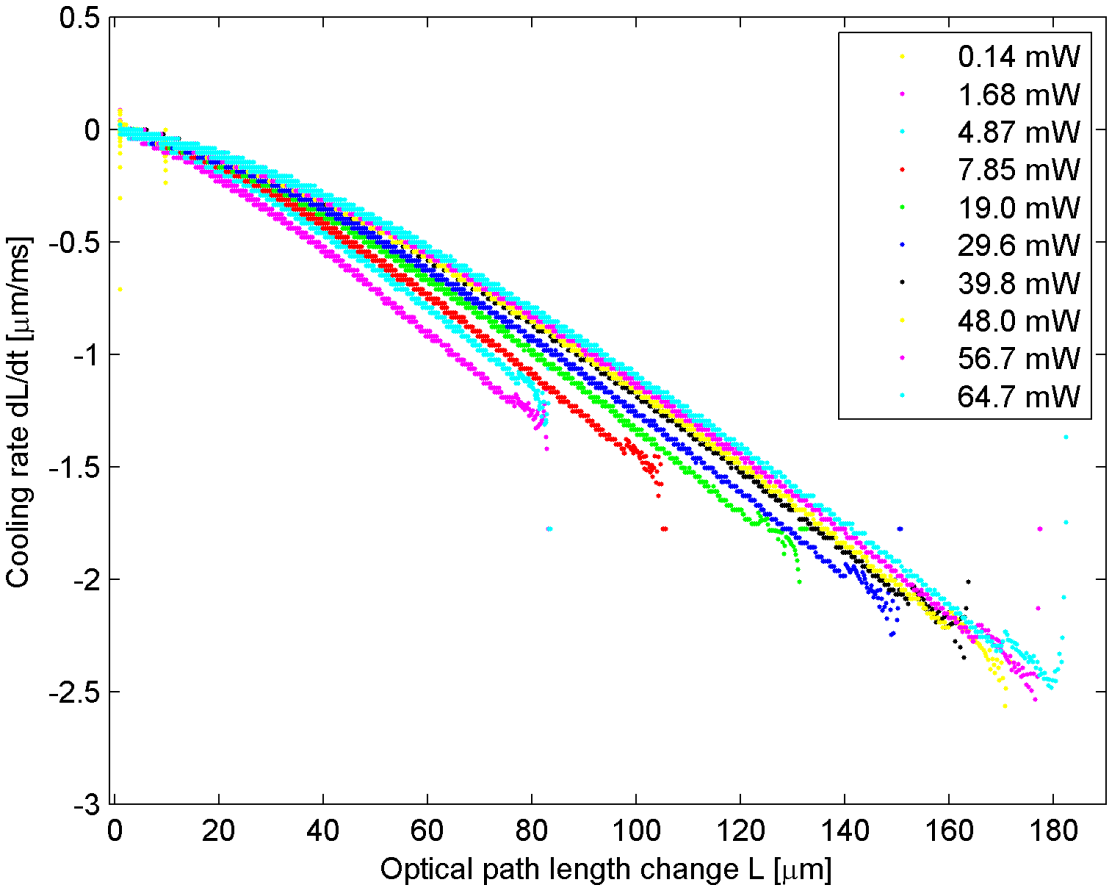

Figure 4.46: The rate of optical path length change dL/dt as a function of optical path length change L for some of the cooling transients in figure 4.45.

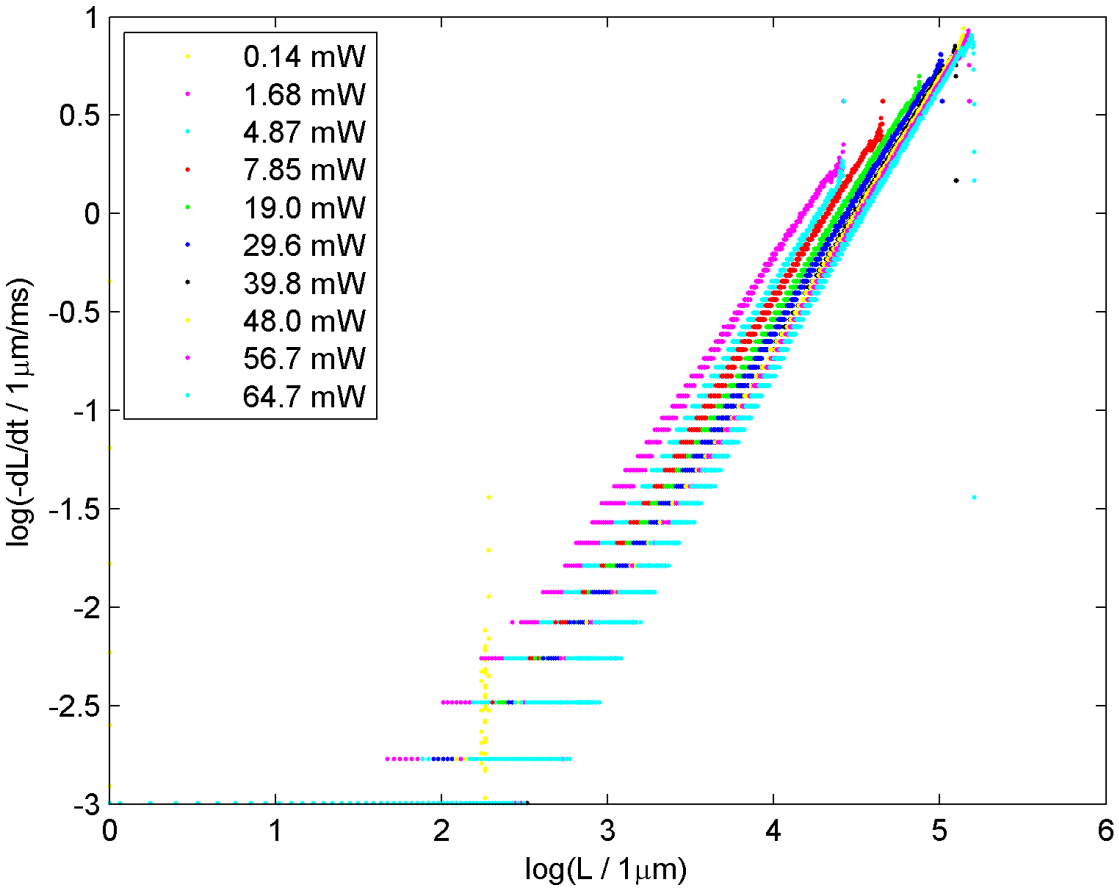

Figure 4.47: The logarithm of the cooling rate -dL/dt as a function of the logarithm of the optical path length change L for some of the cooling transients in figure 4.45.

Figure 4.47 shows the log plot of the data which like the 400 nm fiber indicates that the cooling of the fiber follows the power law 4.1.

It again looks as the peaks have the same slope but that they are shifted in the intersection with the y axis. The cooling data for the analysed peaks are shown in table 4.3, except the data for the 1st peak which was very weak.

Table 4.3: Table of cooling transient data.

Cooling transients						
Power	$a = \beta$	b	α	L^{max}	τ_{init} [ms]	τ_{final} [ms]
1.68 mW	1.277	-5.35	0.0152	80.7	68.6	101
4.87 mW	1.326	-5.65	0.0138	77.3	79.7	125
7.85 mW	1.373	-5.95	0.0132	98.6	78.4	132
19.0 mW	1.361	-6.00	0.0122	124	80.3	133
29.6 mW	1.351	-6.02	0.0117	142	81.0	132
39.8 mW	1.386	-6.26	0.0109	153	86.3	147
48.0 mW	1.377	-6.22	0.0109	163	84.5	142
56.7 mW	1.370	-6.21	0.0107	165	86.4	144
64.7 mW	1.382	-6.29	0.0105	169	87.5	149
Average	1.356	-6.00	0.0120	-	-	-

The power dependence of the coefficients β and α from the power law are shown in figure 4.49 and figure 4.48 where the fits are also shown. It is found that the β coefficients follow $\beta = 0.0237 \cdot \log(P) + 1.2868$. The α coefficients are fitted to the formula $\alpha = d_1 \cdot P + d_2$ which gives $\alpha = -6 \cdot 10^{-5} \cdot P + 0.0141$.

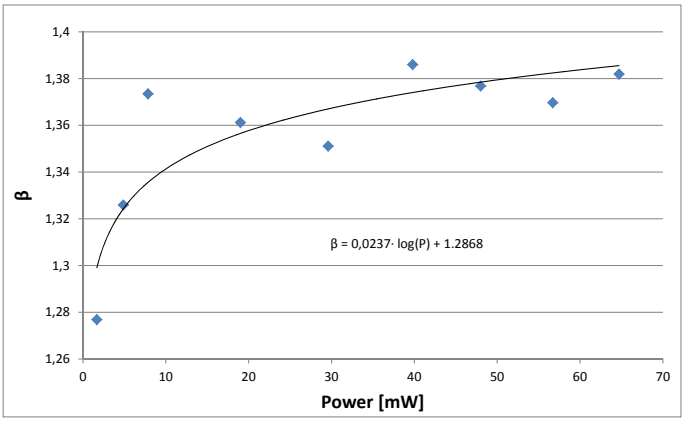

Figure 4.48: The quantity β as a function of power in [mW]. The data is fitted to a logarithm.

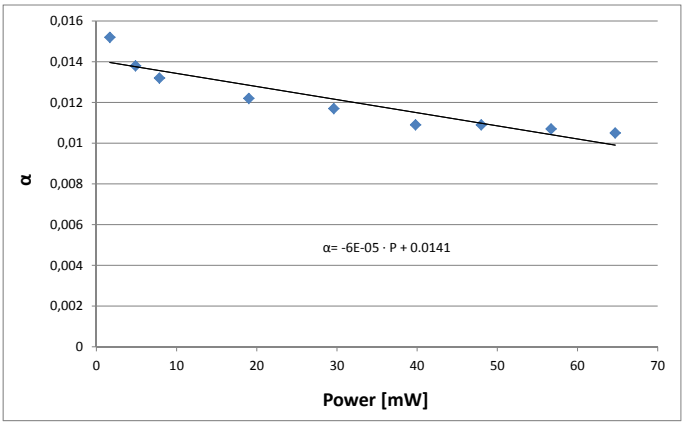

Figure 4.49: The quantity α as a function of power in [mW]. The data is fitted to a linear function.

The initial and final time constants for the cooling are shown in figure 4.50. The maximum optical path length change is found from figure 4.44. It is seen that both τ_{init} and τ_{final} are almost constant and τ_{final} is increasing slowly for higher maximum optical path length change, so they look more like the Planck prediction than the FED prediction from [3]. The 2nd data point deviates, due to the decrease in maximum optical path length change of this peak, and as τ depends on L, τ for this peak is reduced.

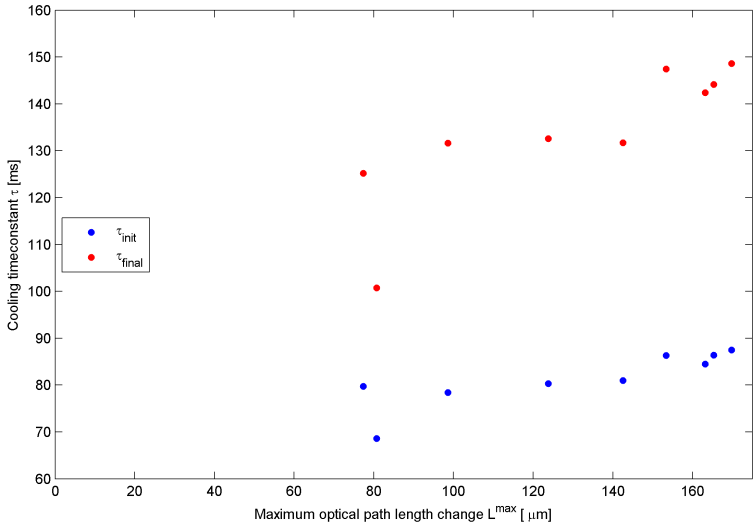

Figure 4.50: Initial and final cooling time constants in [ms] as a function of the maximum optical path length change of the cooling in [µm].

We see that τ_{init} is close to but greater than the constants found by and the FED prediction and is also greater than the Planck prediction. Whereas τ_{final} is between the time constants of the FED and Planck prediction.

The tendencies of the cooling time constants are similar to the 400 nm diameter fiber discussed earlier so it looks like they follow the Planck prediction. But we observe that this 500 nm diameter fiber cools faster than the 400 nm diameter fiber.

4.14.2 Heating transients

The heating rates dL/dt as a function of optical path length change L are shown in figure 4.51. Figure 4.52 shows the logarithm of the data.

The heating rates dL/dt are not as linear as for the 400 nm diameter fiber, figure 4.32. The linear part of the data is fitted to a linear function. For higher power the data is approximately linear until a sudden "bump" around L = 110 μm and then the data is again linearly decreasing towards zero. So it could look like the data follows two linear functions, but here I have only fitted the first linear part of the data, which for high powers is the data approximately from 20 to 110 μm. The fitting coefficients a and b are given in table 4.4 and their power dependence is shown in figure 4.53 and figure 4.54 respectively. We have again omitted the 1st peak as the signal was very weak.

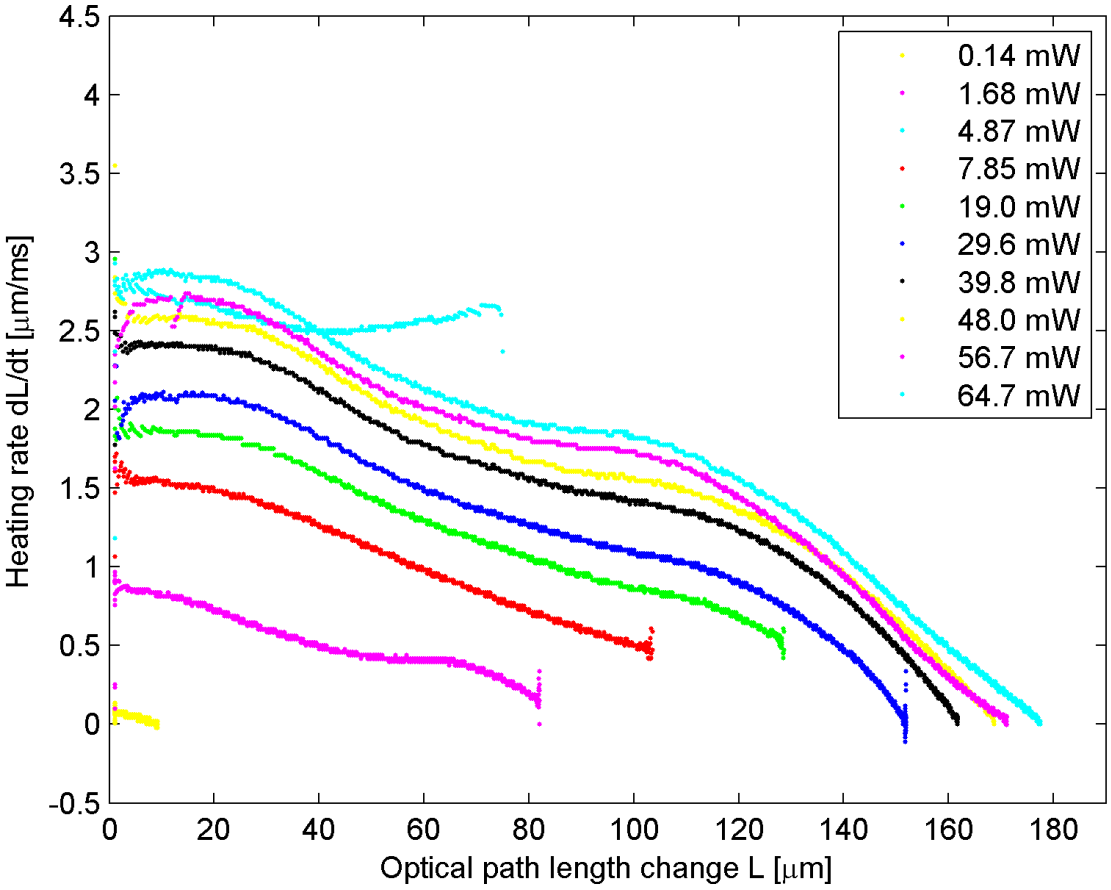

Figure 4.51: The heating rate dL/dt as a function of optical path length change L for some of the heating transients in figure 4.45.

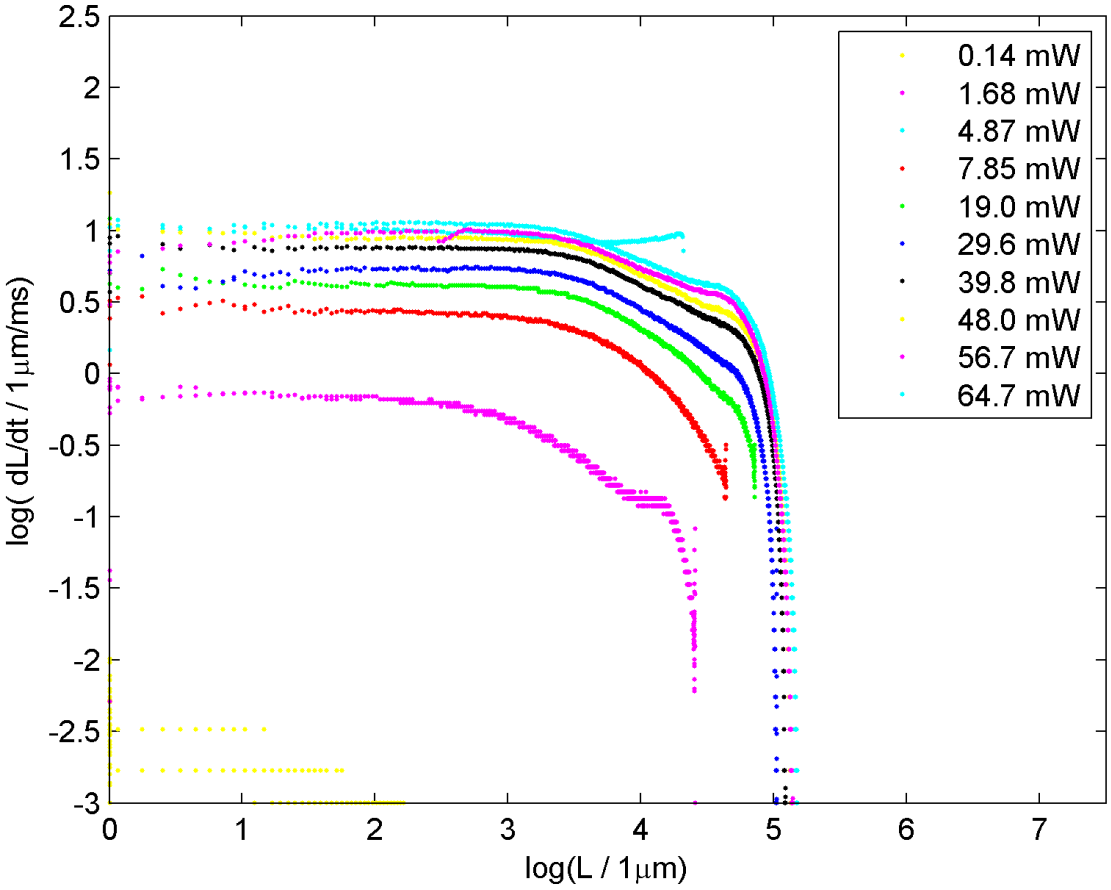

Figure 4.52: The logarithm of the heating rate dL/dt as a function of the logarithm of the optical path length change L for some of the heating transients in figure 4.45.

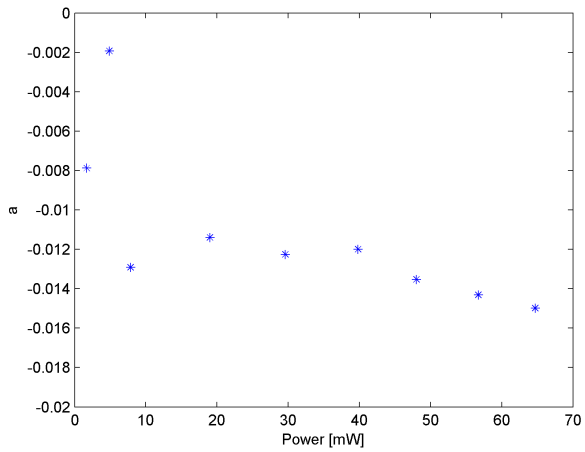

Figure 4.53: The slope a of the fits of figure 4.32 as a function of power in [mW].

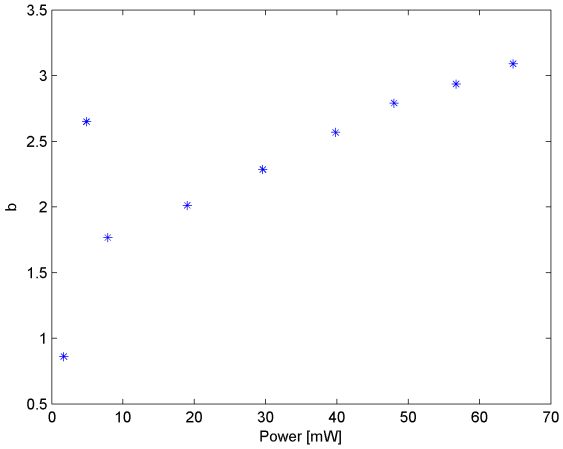

Figure 4.54: The intersections b of the fits of figure 4.32 as a function of power in [mW].

Table 4.4: Table of heating transient data.

Heating transients					
Power	a	b	L^{max}	τ_{init} [ms]	τ_{final} [ms]
1.68 mW	-0.0079	0.8604	80.7	36.2	199
4.87 mW	-0.0019	2.649	77.3	8.9	25.2
7.85 mW	-0.0129	1.766	98.6	17.1	49.0
19.0 mW	-0.0114	2.012	124	18.9	54.0
29.6 mW	-0.0123	2.285	142	19.1	54.7
39.8 mW	-0.0120	2.568	153	18.2	52.9
48.0 mW	-0.0135	2.791	163	17.9	51.5
56.7 mW	-0.0143	2.936	165	17.3	49.7
64.7 mW	-0.0150	3.090	169	16.8	48.4
Average	-0.0112	2.329	-	-	-

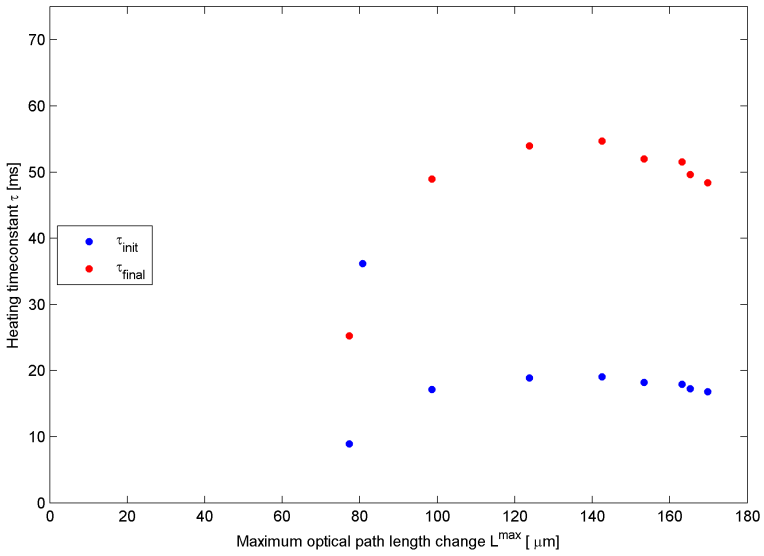

Figure 4.55: Initial and final heating time constants in [ms] as a function of the maximum optical path length change of the heating in [µm].

The time constants are shown in figure 4.55. I have omitted a data point for τ_{final} in the plot as this point was very high compared to the other final time constants. From figure 4.51 it is also seen that this point (1.68 mW) heats very slowly (τ high). We see that the time constants are first increasing then decreasing (when we neglect τ_{init} for 1.68 mW). The values of the time constants fit very well with the Planck predictions in [3]. It is also noticed that this fiber heats very fast compared to the 400 nm diameter fiber.

4.15 Example with dust on the fiber

Ideally the fiber should always be inspected for dust before transferring it to vacuum. Figure 4.56 shows an example of a dust particle on a fiber. After the fiber was pulled it was inspected with the camera and a bright spot was noticed, which was identified as a dust particle. The pattern looks almost like a diffraction pattern.

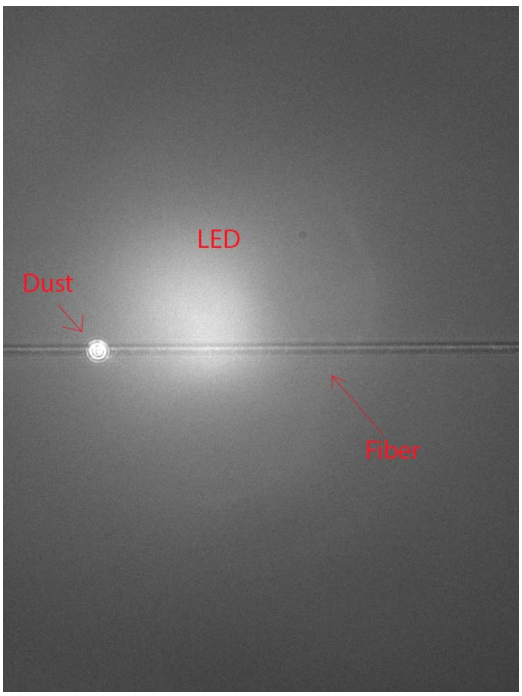

Figure 4.56: Dust particle on the fiber. The picture is taken with the CCD camera. The light from the LED is seen in the background.

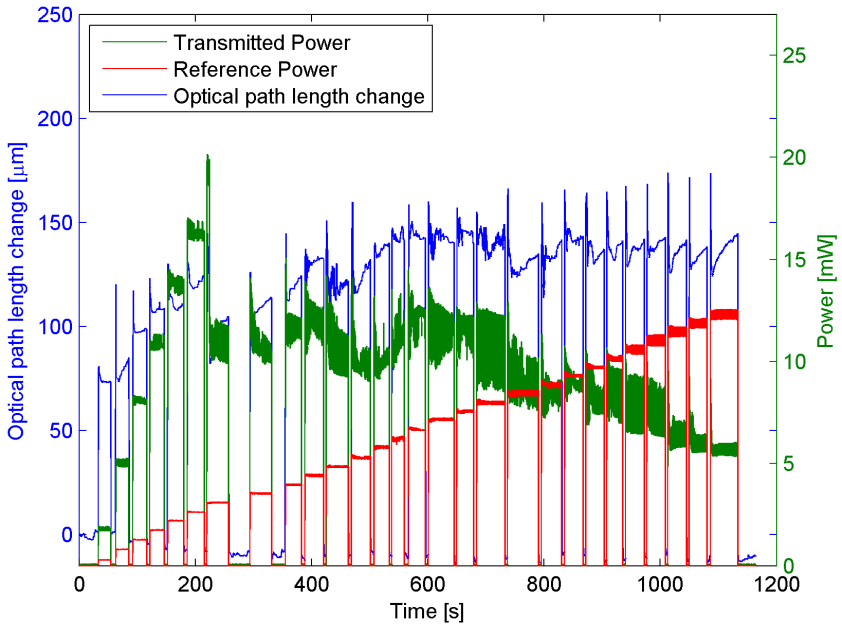

Figure 4.57: The optical path length change plotted together with the reference power and the transmitted power of the heating laser.

The fiber was still transferred to the vacuum chamber for burning it as we thought it could be interesting to see if the dust particle affected the fiber burning. During the 7th heating, figure 4.58, the interference signal decreased a lot in amplitude. Here the transmitted power, figure 4.57, also decreases.

If the fiber was deformed due to the heating we would not expect the fringes counts to go back to the same zero point which they do here. It looks like a dust particle on the fiber

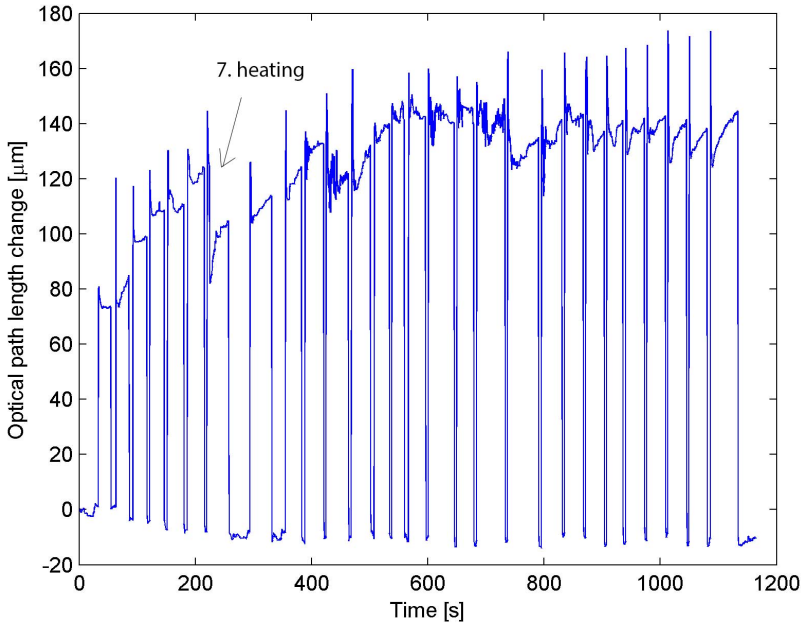

Figure 4.58: The optical path length change in [µm] as a function of time in [s] when the fiber is heated and cooled. The 7th heating is indicated with an arrow.

absorbs and scatters the light which is why the transmitted power is low. But we see that the dust particle first affects the fiber in the 7th heating. Also as the coupling of light into the fiber before the experiment was good the particle seen in figure 4.56 could not have affected the coupling. Maybe the dust burned to the fiber at this power. With an infrared viewer a bright point to the left of the fiber was visible which was scattering the light. This could very well have been the dust particle.

The particle must also be on the left side (in coupling of light) of the fiber because then when the fiber is heated the dust will absorb the light, and as the heating is blocked and unblocked the optical path length change will not increase and decrease any more than it did just before the dust burned to the fiber. This is also what we observe in figure 4.57. If the particle was on the right side (out coupling of light) then as the heating is blocked and unblocked the optical path length change should be able to increase and decrease more than before the dust burned to the fiber when the power is increased.

The coupling when the experiment started was 63% for the heating laser. The actual coupling through the bare fiber (the fiber is clipped before the fibercoupler and here the actual coupling is measured) was 69%. The transmission through the fiber (with tapered part) was only 7.3% after the experiment. As the transmission before the experiment was 90% this low transmission after the experiment indicates that the dust particle absorbed the heat.

4.16 Breaking power of the nanofibers

A purpose of the experiment was to see how much power the fibers could stand in vacuum before they broke and if there were any characteristics of the fiber burning, i.e. if we could tell in advance by looking at the fringes counts that the fiber was going to burn during the next heating. As discussed before, in section 2.2.2, the breaking power is expected to depend on the thickness of the waist, while it is not expected to depend on the fiber shape, as the fiber will break at its thinnest part where it is hottest, i.e. the waist. As the project time was mostly spend on building the experiment and make it work and explain why it was behaving as it was and as it also quickly turned out that the good fibers could stand a lot more power than needed for the atom trap experiment (15 mW), the project focus moved from reproducing fibers for burning them, to investigate the optical path length change and to understanding the heating and cooling transients. The experiments also showed that the breaking power of the fibers where indeed very different; either they could stand a lot of power or they would break immediately at only a few mW of power. I think that this difference in breaking power is due to how clean the fibers are.

The measurements I have achieved (since the experiment, both the fiberpulling and fiberbruning, was working) shows that 46% of the fibers could stand > 15 mW as required for the atom trap experiment. Hereof 82% could stand > 50 mW. The highest power sent through a fiber without the fiber breaking was 108 mW. Often the high transmission fibers could not break even with the maximum avaliable power (the maximum avaliable power depends on the coupling of light into the fiber). Of the fibers that could not stand more than 15 mW, they all burned at powers less than 5 mW. I think that these fibers might have been polluted during the transfer into the vacuum chamber.

A total of 60% of all the fibers were burned or tried to be burned with the highest avaliable power. The other 40% broke during fabrication either during the pulling or during the transfer to vacuum. When the fibers broke during the pulling, it was usually at different pull lengths that they broke, which indicates that it was not a systematic error in the pulling procedure. The fact that approximately every second to third fiber will break during fabrication is a factor which must be taken into account when doing the experiments.

Since the initial purpose of the work was to investigate the fiber breaking, I will here show some of the many examples observed.

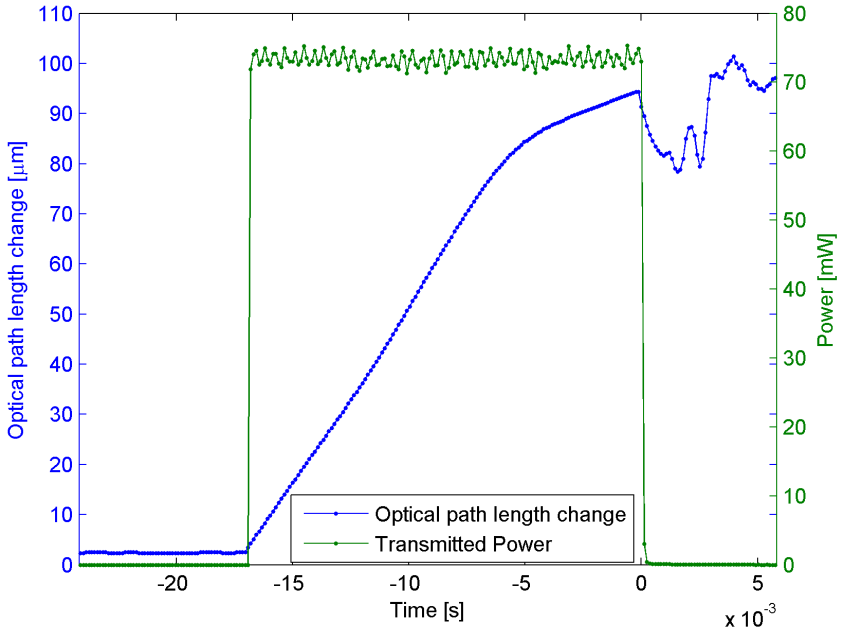

Figure 4.59: Fiber burning of 500 nm diameter fiber. The optical path length change and transmitted power is plotted as a function of the time where the time is set to zero at the breaking time.

Figure 4.59 shows a typical fiber burning at 75 mW of power. We see the optical path length change increases fast and then the slope of optical path length change versus time becomes slower before the fiber breaks (when the transmitted power drops). When the fiber breaks the optical path length change drops a bit and afterwards the fringes detector only measures noise. As the fiber breaks the rate of change of the counts is less than the maximum rate for the data sampling to be correct (1 cts/3 μs), so we do measure all data on the fiber breaking correctly. The fiber breaks fast and the transmitted power only changes within one sample period while the fiber breaks. The transmitted power is measured with the LabJack with a sample rate of 8333 Hz. If the sample rate was even faster we could see more features in the transmitted power when the fiber breaks.

Another fiber that broke at high power is seen in figure 4.60. This fiber broke at 80 mW. The optical path length change follows the same characteristics as figure 4.59 but on a longer time scale. Usually the thin fibers broke at lower power than the thick fibers probably because a thick fiber can hold more power for a longer time than a thin fiber. But figure 4.60 shows an example of a thin fiber which could stand a lot of power.

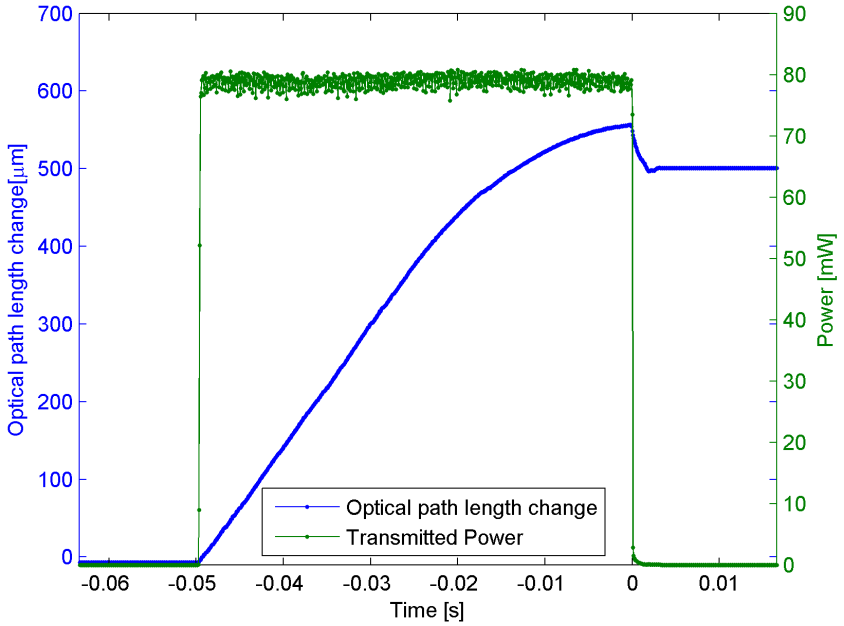

Figure 4.60: Fiber burning of 400 nm diameter fiber. The optical path length change and transmitted power is plotted as a function of the time where the time is set to zero at the breaking time.

The breaking plots can be compared to how a heating transient for a fiber that does not break, acts on the same timescale, shown in figure 4.61 and figure 4.62. It is observed that the slope of the optical path length change as a function of time is increasing.

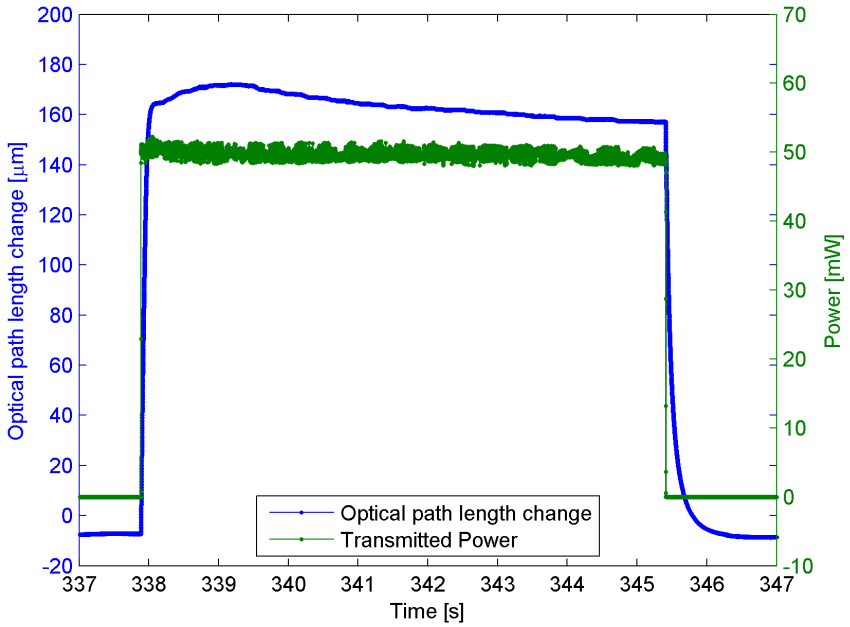

Figure 4.61: A usual heating and cooling transient of a fiber that did not burn. The optical path length change and transmitted power is plotted as a function of the time.

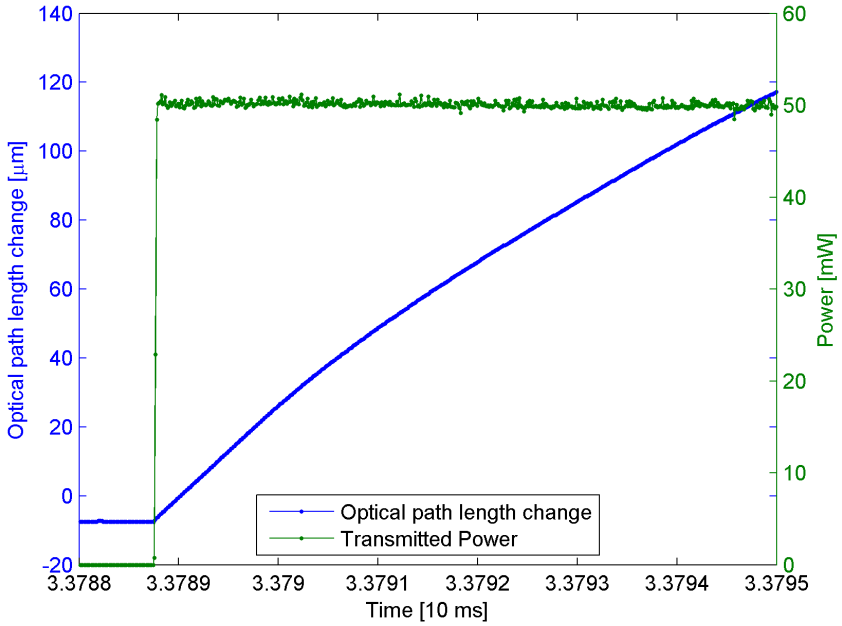

Figure 4.62: A zoom of figure 4.61.

Figure 4.63 shows a typical 500 nm fiber that broke at very low power. The slope of the optical path length change as a function of time is not changing as much as for the 500 nm fiber that broke at high power, figure 4.59, but just before the fiber breaks the slope is constant. It is observed that this fiber breaks at a longer timescale than the 500 nm fiber at high power. It could indicate that the time the fiber is heated before it breaks depends on the breaking power.

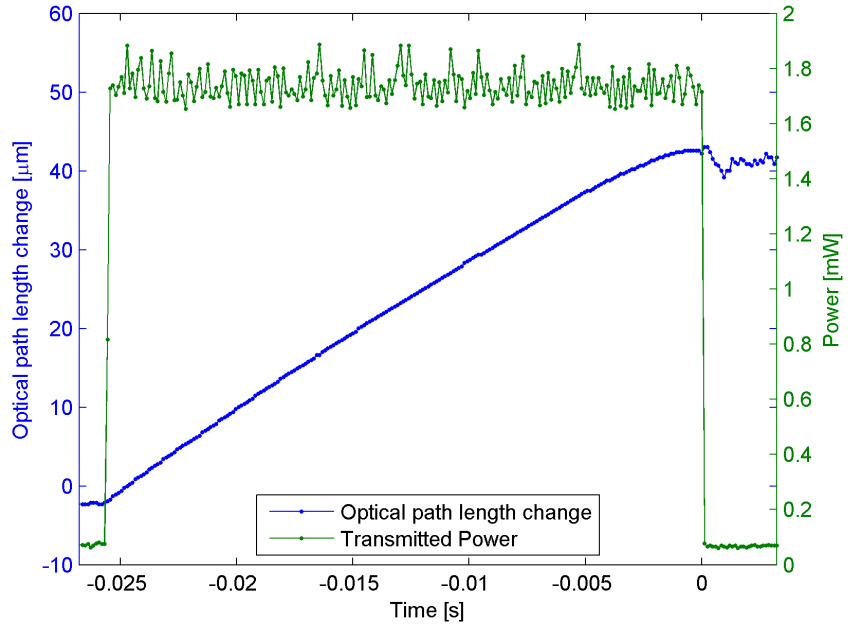

Figure 4.63: Fiber burning of 500 nm diameter fiber. The optical path length change and transmitted power is plotted as a function of the time where the time is set to zero at the breaking time.

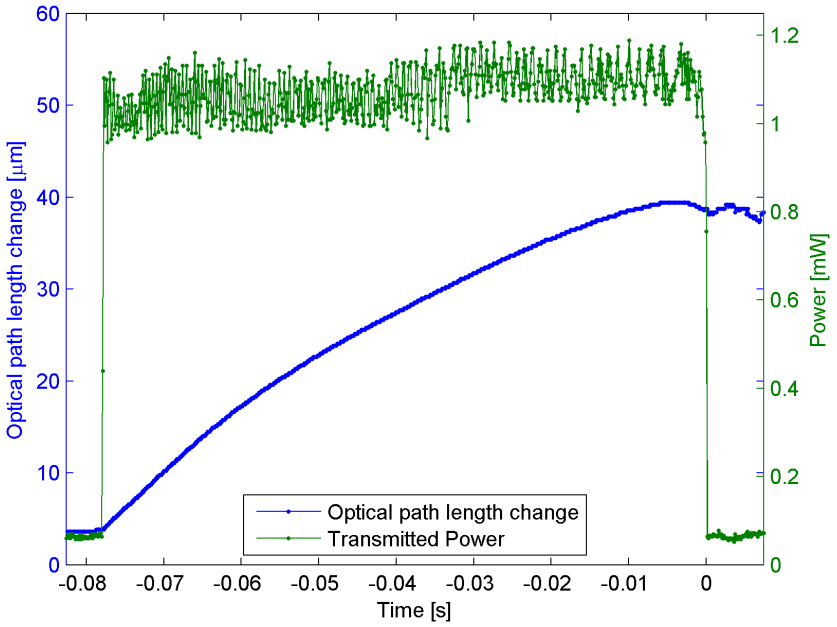

Figure 4.64: Fiber burning. The optical path length change and transmitted power is plotted as a function of the time where the time is set to zero at the breaking time.

The fiber in figure 4.64 took longer time to break, and at very low power. The slope of the optical path length change as a function of time decreases until it becomes constant and just before the fiber breaks it is seen that the (now negative) slope increases, and the optical path length change decreases a bit.

It could look like it is possible to divide the breaking curves into two types for high breaking power and low breaking power. For high power the slope decreases and then the fiber breaks whereas for low power the slope becomes constant and maybe it shifts sign and then the fiber breaks. But not all fibers showed this.

From all the investigated fiber breakings it looks like the time the fiber is heated before it breaks depends on the power. For high power the fiber breaks on a short timescale while for low power the fiber breaks at a longer time scale. It also makes sense that the fiber needs to be heated a longer time with low power to get to the breaking temperature. But if the power is above the breaking temperature the fiber will break immediately.

The thin 400 nm fibers usually broke at lower powers than the thicker 500 nm fibers, which we also expect, as the thinner fiber is more sensitive to defects that could heat and make the fiber break.

Figure 4.65: One of many broken nanofibers.

There is an uncertainty in the breaking power which comes from the uncertainty in the detector calibration. Besides the breaking power is determined as the average transmitted power measured in the interval when the fiber was breaking.

As mentioned before, in the first experiments, a picture of the fibers was always taken with the camera before they were transferred to vacuum. When this was done the fibers did not stand much power afterwards in vacuum. But when the fibers were not pictured they survived a lot more power. This shows that it is very important to get the fibers transferred to the vacuum chamber quickly.

I have noticed that the best fibers, i.e. the fibers that were cleaned easily and the fibers that could stand very high power, where produced during holidays or weekends. I think this was because at these times there were very few people in the fiber lab, so there was not much changing in the air. It is an important observation because it shows how sensitive the experiment and fiber production is to the environment.

We did not see any characteristics in the optical path length change before the fiber burned, so it must be concluded that it is not possible to tell in advance from the optical path length change when the fiber is going to burn. We actually saw all types of behaviour of the optical path length change as a function of time: increasing slope, flat slope and decreasing slope. In all cases the slope was changing before the fiber broke but there was no tendency. It can then be concluded that the characteristics of the fiber breaking in the optical path length change and the breaking power depends on each individual fiber.

Chapter 5

Conclusion

We have found that for the fibers investigated in this experiment the numerical rates of cooling and the rates of heating are in the same interval. We have seen that as expected, for both the heating and cooling the initial rate is larger when the heating power is higher. Also we observe that a fiber heated at a certain power in the beginning of the heating, heats at almost the same rate as it cools, when the heating is discontinued.

For both the heating and cooling process we saw that $\tau_{init} < \tau_{final}$ i.e. $(\frac{dL}{dt})_{init} > (\frac{dL}{dt})_{final}$ so the fiber heats and cools fastest in the beginning of the heating or cooling, but the analytical expressions describing the heating and cooling were found to be different.

The conclusion with regard to the thermal properties of the tapered nanofibers investigated in this experiment is that the rate of heating dL/dt as a function of optical path length change L can be described by a linear function whereas the rate of cooling dL/dt as a function of optical path length change L can be described by a power function.

That the rate of heating dL/dt as a function of optical path length change L can be described by a linear function means that the fiber heats exponentially (L is in µm and t is in ms).

$$\frac{dL}{dt} = -\Gamma \cdot L + b \Rightarrow L(t) = L_0 \cdot (1 - e^{-\Gamma \cdot t}) \tag{5.1}$$

where $\Gamma = -a$ in tables 4.2 and 4.4. A typical value of Γ is 0.01.

That the rate of cooling dL/dt as a function of optical path length change L can be described by a power function means that the fiber also cools by a power law.

$$\frac{dL}{dt} = -(\alpha \cdot L)^{\beta} \Rightarrow L(t) = c_1(c_2 + t)^{\gamma} \tag{5.2}$$

where $\gamma = \frac{1}{1-\beta}$ and β is given in tables 4.1 and 4.3. A typical value of γ is -3.

Even though it is not possible to compare my experiment completely to the experiment in [3] I still think it is interesting and informative to look at the data together, with the combined results shown in figure 5.1.

We have observed that the time constants for heating and cooling were in the same range as observed by [3]. The general increasing trend of the cooling time constants for the fibers in this experiment looks more like the data predicted by Plancks law than for FED theory (see center panel of figure 5.1). The trend of the fibers heating time constants did not show the

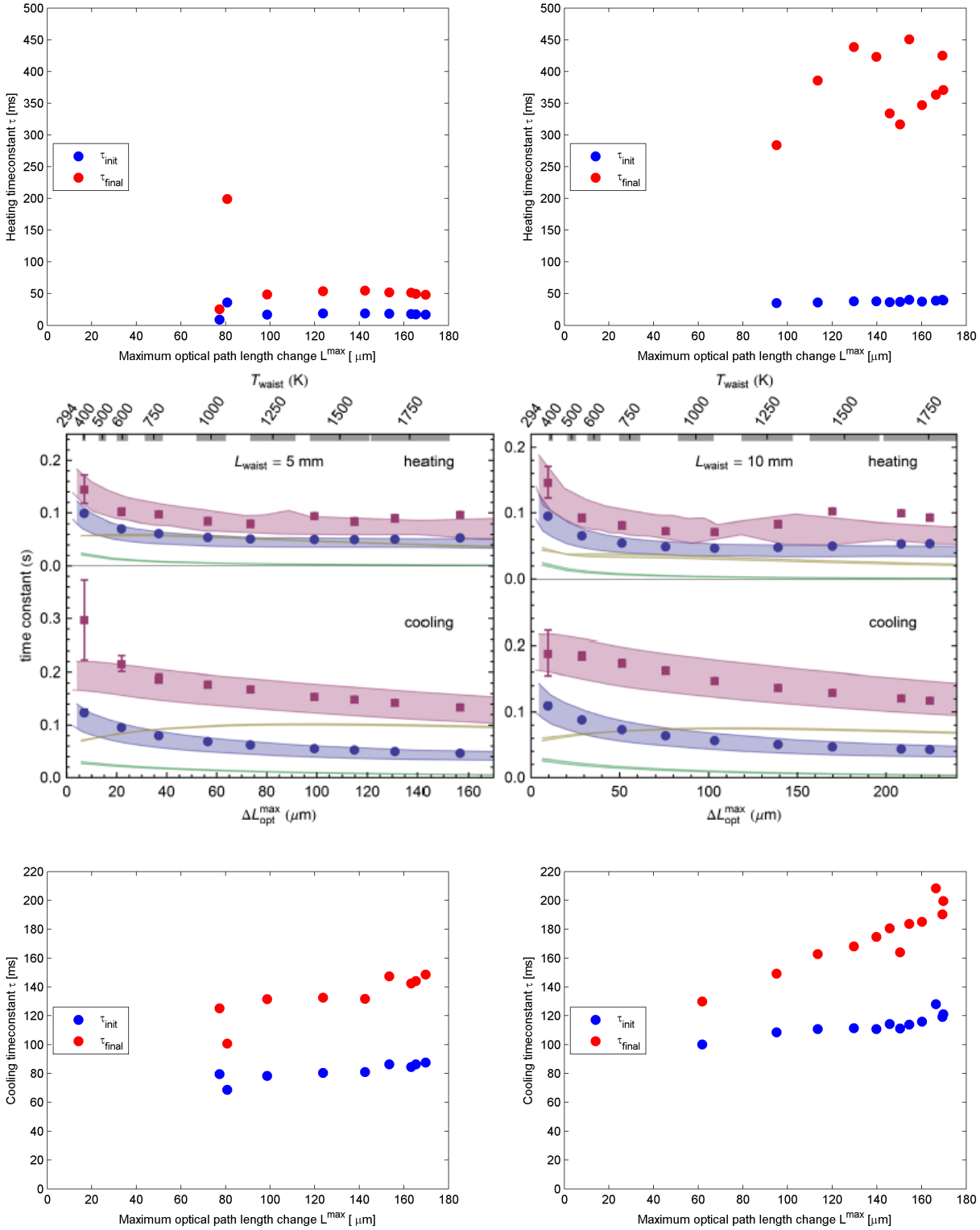

Figure 5.1: The data for the time constants obtained in this experiment together with the data obtained in [3]. Top left: heating time constants for the d = 500 nm (1 mm waist) fiber. Top right: heating time constants for the d = 400 nm (2 mm waist) fiber. Center: cooling and heating time constants as found in [3]. Blue dots are initial and red squares are final time constants. The blue and red bands are initial and final rates for FED theory and the green/yellow line are initial/final rates for Planck theory. Bottom left: cooling time constants for the d = 500 nm (1 mm waist) fiber. Bottom right: cooling time constants for the d = 400 nm (2 mm waist) fiber.

same general rising trend as for the cooling, and even indicated that a maximum had been reached.

We can notice that the fibers in this experiment have a large difference between τ_{init} and τ_{final} for the heating time constants whereas in [3] the fibers have a large difference between τ_{init} and τ_{final} for the cooling time constants.

We have observed that the 500 nm diameter fiber heats and cools faster than the 400 nm diameter fiber. In particular the 500 nm fiber is faster in heating than the 400 nm fiber. The 500 nm fiber also heats faster than the 500 nm fiber in [3], which has a 5 mm long waist, but the cooling rates are more similar. As mentioned, the effective waist section of the 400 nm diameter fiber is expected to be a bit longer than the effective waist section of the 500 nm diameter fiber. That the heating rates of the two fibers differ could be an indication that the length and diameter of the fiber waist influences the fibers heating and cooling rates. This could be explained by the heating energy being easier transported in a fiber with a short effective waist length than in a fiber with a long effective waist length.

It was observed that the optical path length change saturated with power, i.e. that the heating energy added to the fiber was radiated away at the same rate as it was added. The saturation of the optical path length change also indicates (comparing with the data in [3]) that the fibers are described by Plancks law. We also saw that the fact that the cooling rate of the optical path length change dL/dt was observed to depend on the initial heating power might be explained by the fiber radiating the heating energy from its surface which is what is expected from Plancks law. As the time constants was another indication of the fibers following Plancks law, it can therefore be concluded that the radiation of the fibers in this experiment obeys Plancks law.

As we did not see any characteristics in the optical path length change before the fibers broke, we can also conclude that it is not possible to tell in advance from the optical path length change when the fiber is going to break. We also saw that the breaking power seemed to be an individual property of each fiber, but generally the thinner fibers broke at lower powers.

The fibers were tested for memory effects, i.e. if they would behave differently during a 2nd heating. We did not observe any memory effects, since we saw that the fiber heats in approximately the same way the 2.nd time it is heated.

We have seen that preheating the fibers was not an advantage for the fibers in this experiment. The idea behind the preheating was to obtain an initial temperature condition of the fiber, which however already seemed to be reached with the cold fiber in the vacuum chamber.

It was often observed that sudden spikes in optical path length change appeared at the instant the fiber was heated. As these spikes were still observed when the setup was made more stable we assume that they are real and not due to measurement errors. We discussed that the spikes did not appear for all transients and that this could indicate that the spikes appeared when the fiber was heated above a certain temperature T_c for the first time or again after it had cooled. It was also noticed that as the power was increased, the spikes became smaller and even disappearing, which could be an indication of the whole fiber being heated up gradually during the experiment.

5.1 Suggested improvements to the setup

The important issue for making good tapered nanofibers is the fiber cleaning. The flowbox keeps some dust away but I do not think it is enough since the fibers do get dirty when they are produced in the flowbox. I have also noticed that the best fibers were made in the weekends and holidays when there were no other people in the lab. The ideal situation would be to have a clean room for making the fibers and transferring them to the vacuum chamber in here.

It would also be good to find a way to inspect the fiber for dust everywhere before it is transferred to vacuum. The dust could be seen, with the camera, by sending light through the fiber, as the dust can scatter the light. But with the camera the fiber can not be inspected from all positions. Maybe one could inspect UV light on the fiber in order to determine from the fibers fluorescence if there is dust on the fiber. It would also be good to find a way to inspect the fiber for dust again when it is inside the vacuum chamber.

The power of the heating laser is increased by increasing the current of the laser when the heating laser is blocked and the fiber is cooling. This is not the optimal way to do it, because it is not possible to change the current in the same amount of time every time, so the heating and cooling experiments takes different amounts of time and therefore it can be difficult to investigate e.g. preheating. It would be better to have a switch; so that the laser power is the same but the total power is varied by varying the time interval in which the power is applied.

Also a mechanical arm to block and unblock the heating laser when the fiber is heated and cooled could be an improvement as the the blocking and unblocking then would be done in the same way every time.

Chapter 6

Outlook

6.1 Adiabatic fibers

It could be interesting for a future experiment to pull an adiabatic fiber and test its thermal properties in vacuum. This would require writing an algorithm that could do the opposite of the algorithm that we have now, i.e. finding how to pull the fiber with the current fiberpulling setup in order to get the optimal adiabatic shape. One could e.g. be inspired by [17] and their algorithm [36]. Then it could be investigated if the fibers breaking power depends on the fiber shape.

6.2 Nanofiber resonators

Tapered nanofibers are used for achieving an efficient atom light coupling using the evanescent field of light. The light-matter coupling can also be enhanced using the nanofiber as an optical microresonator. The light is enhanced here because it passes the atoms many times and can thus interact with the atoms several times. Tapered nanofibers can e.g. be used as Fabry Perot resonators with implemented fiber bragg gratings in the nanofiber [37], and these nanofiber resonators can show thermally excited mechanical modes [38]. Designing fibers with these properties could also be an outlook.

Another experiment could be to make tapered nanofiber loops [39]. A nanofiber loop creates a resonator for the light, as here the light is enhanced by moving around the nanofiber loop many times. In this way the light can interact with the atoms several times and efficient atom light coupling can be achieved.

We did try to loop the fibers around themself but the fibers broke every time. One could be inspired by the method of first twisting and then looping the fiber used in [40]. However our group has just recently succeeded in creating a nanofiber loop, of which a picture is shown in figure 6.1.

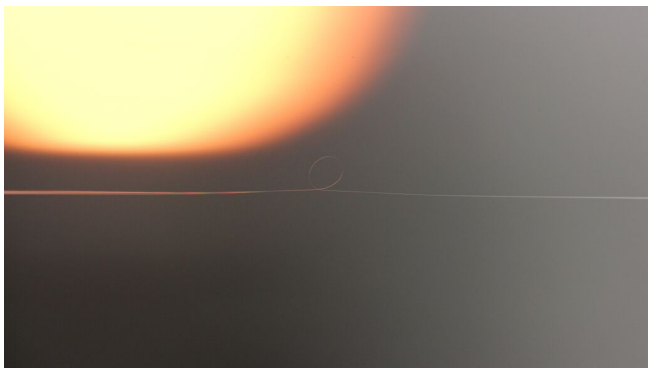

Figure 6.1: A nanofiber loop. The loop and the picture is made by J.B. Béguin and used here with his permission.

The loop was made by driving the stages a bit (approximately 5 mm) closer to each other, and then the flow in the flowbox made the fiber twist and this created loops on the fiber. If the fiber is then pulled slowly apart again (approximately 1-2 mm) then there will only be one loop left on the fiber. It is possible to make loops on the fiber because the tension in the fiber is low. It is most attractive to make small loops (with a small radius, of about 1 mm) because then the FSR and finesse of the loop will be high. A high finesse defines a good cavity with a good coupling. For the use of nanofiber loops it will also be attractive to make adiabatic fibers as high transmission fibers will increase the finesse of the cavity.

Chapter 7

Appendix

7.1 Electronics

A more detailed hand drawing of the electronics described in section 3.3.1 is seen on figure 7.1.

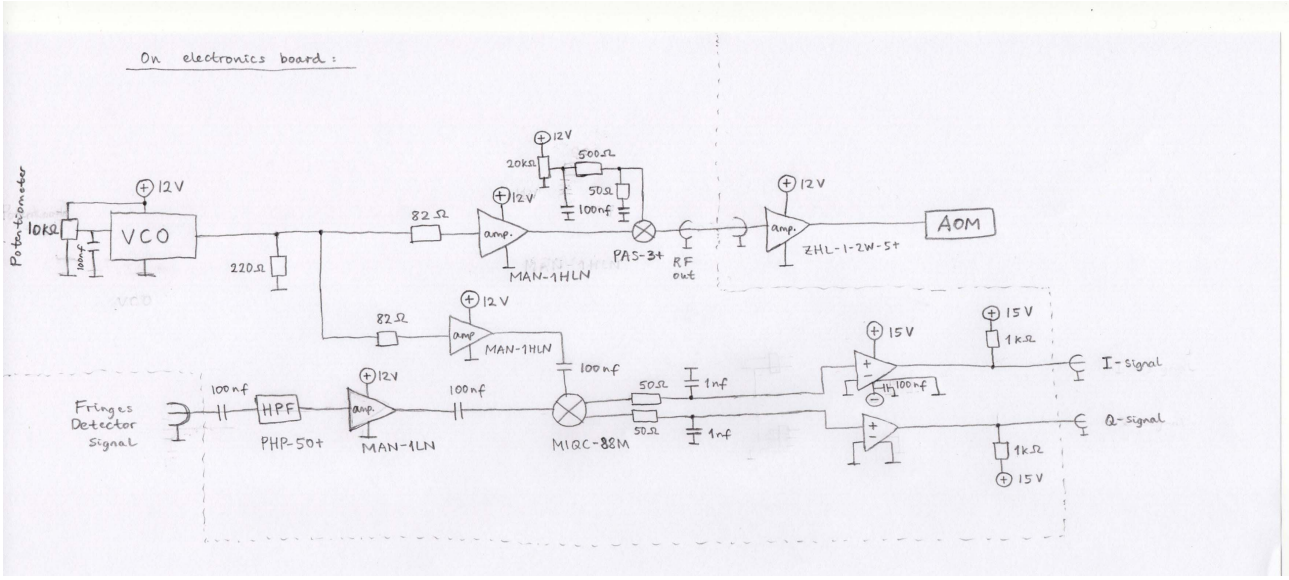

Figure 7.1: Hand drawing of the electronics for data sampling. The dashed line divides the elements on the electronics board, figure 3.24, and outside of it.

Bibliography

[1] E. Vetsch, D. Reitz, G. Sagué, R. Schmidt, S. T. Dawkins, and A. Rauschenbeutel. Optical interface created by laser-cooled atoms trapped in the evanescent field surrounding an optical nanofiber. *Phys. Rev. Lett.*, 104:203603, 2010.

[2] D. Reitz, C. Sayrin, R. Mitsch, P. Schneeweiss, and A. Rauschenbeutel. Coherence properties of nanofiber-trapped cesium atoms. *Phys. Rev. Lett.*, 110:243603, 2013.

[3] C. Wuttke and A. Rauschenbeutel. Thermalization via heat radiation of an individual object thinner than the thermal wavelength. *Phys. Rev. Lett.*, 111:024301, 2013.

[4] http://www.thefoa.org/tech/ref/basic/fiber.html.

[5] http://www.corning.com/opticalfiber/products/smf-28.

[6] Jesper Lægsgaard. Introduction to dielectric waveguides (teacing material from DTU).

[7] http://hypertextbook.com/facts/1997/laurenboyd.shtml.

[8] P.W. Milonni and J.H. Eberly. Laser physics. Wiley, 2010.

[9] http://www.rp-photonics.com/fibers.html.

[10] J. E. Hoffman, F. K. Fatemi, G. Beadie, S. L. Rolston, and L. A. Orozco. Rayleigh scattering in an optical nanofiber as a probe of higher-order mode propagation. *Optica*, 416-423, 2015.

[11] A. Petcu-Colan, M. Frawley, and S. N. Chormaic. Tapered few-mode fibers: mode evolution during fabrication and adiabaticity. *Journal of Nonlinear Optical Physics and Materials*, 20, 293-307, 2011.

[12] J. D. Love, W. M. Henry, W. J. Stewart, R. J. Black, S. Lacroix, F. Gonthier. Tapered single-mode fibres and devices. *Optoelectronics, IEE Proceedings J*, 138, 343-354, 1991.

[13] M. C. Frawley, A. Petcu-Colan, V. G. Truong, and S. Nic Chormaic. Higher order mode propagation in an optical nanofiber. *Optics Communications*, 285, 4648–4654, 2012.

[14] C. Baker and M. Rochette. A generalized heat-brush approach for precise control of the waist profile in fiber tapers. *Opt. Mater. Express*, 1, 1065-1076, 2011.

[15] R. Nagai and T. Aoki. Ultra-low-loss tapered optical fibers with minimal lengths. *Opt. Express*, 22, 28427-28436, 2014.

[16] P. R. Kordell, J. D. Wong-Campos, S. L. Rolston, S. Ravets, J. E. Hoffman and L. A. Orozco. Intermodal energy transfer in a tapered optical fiber: optimizing transmission. *J. Opt. Soc. Am. A* 30, 2361-2371, 2013.

[17] J. E. Hoffman, S. Ravets, J. A. Grover, P. Solano, P. R. Kordell, J. D. Wong-Campos, L. A. Orozco, and S. L. Rolston. Ultrahigh transmission optical nanofibers. *AIP Advances*, 4:067124, 2014.

[18] J. M. Ward, A. Maimaiti, Vu H. Le, S. Nic Chormaic. Optical micro- and nanofiber pulling rig. *The Review of scientific instruments 2014*, 85, 111501, 2014.

[19] S. Ravets, J. E. Hoffman, L. A. Orozco, S. L. Rolston, G. Beadie, and F. K. Fatemi. A low-loss photonic silica nanofiber for higher-order modes. *Optics Express*, 21, 18325-35, 2013.

[20] F. Orucevic, V. Lefèvre-Seguin, and J. Hare. Transmittance and near-field characterization of sub-wavelength tapered optical fibers. *Opt. Express*, 15, 13624-13629, 2007.

[21] T. A. Birks and Y. W. Li. The shape of fiber tapers. *Journal of Lightwave Technology*, 10, 432-438, 1992.

[22] H. L. Sørensen. Controlling the shape of subwavelength-diameter tapered optical fibers. Master Thesis, University of Copenhagen 2013.

[23] H. L. Sørensen, E. S. Polzik, J. Appel. Heater self-calibration technique for shape prediction of fiber tapers. *Journal of Lightwave Technology*, 32, 1886-1891, 2014

[24] Y. Fan, S. B. Singer, R. Bergstrom, and B. C. Regan. Probing planck's law with incandescent light emission from a single carbon nanotube. *Phys. Rev. Lett.*, 102:187402, 2009.

[25] V. A. Golyk, M. Krüger, and M. Kardar. Heat radiation from long cylindrical objects. *Phys. Rev. E*, 85:046603, 2012.

[26] V. P. Carey, G. Chen, C. Grigoropoulos, M. Kaviany and A. Majumdar. A review of heat transfer physics. *Nanoscale and microscale thermophysical engineering*, 12, 1-60, 2008.

[27] S. Holleis, T. Hoinkes, C. Wuttke, P. Schneeweiss, A. Rauschenbeutel. Experimental stress strain analysis of tapered silica optical fibers with nanofiber waist. *Appl. Phys. Lett.* 104, 163109, 2014.

[28] J.-B. Beguin, E. M. Bookjans, S. L. Christensen, H. L. Sørensen, J. H. Müller, E. S. Polzik, and J. Appel. Generation and detection of a sub-poissonian atom number distribution in a one-dimensional optical lattice. *Phys. Rev. Lett.*, 113:263603, 2014.

[29] J. Lee, J. A. Grover, J. E. Hoffman, L. A. Orozco and S. L. Rolston. Inhomogeneous broadening of optical transitions of ^{87}Rb atoms in an optical nanofiber trap. *arXiv preprint*, 1412.6754, 2014.

[30] F. L. Kien, K. Hakuta, D. Reitz, P. Schneeweiss, and A. Rauschenbeutel. Quantum dynamics of an atom orbiting around an optical nanofiber. *Phys. Rev. A*, 87:063607, 2013.

[31] A. Rauschenbeutel. Glasfasern dunner als licht. *Natur & Geist, Forschungsmagazin der Johannes Gutenberg-Universität Mainz*, 19-21, 2009.

[32] L. Russell, R. Kumar, V. B. Tiwari, and S. Nic Chormaic. Measurements on release recapture of cold ^{87}Rb atoms using an optical nanofibre in a magneto-optical trap. *Optics Communications*, 309:313–317, 2013.

[33] J. Bures and R. Ghosh. Power density of the evanescent field in the vicinity of a tapered fiber. *J. Opt. Soc. Am. A*, 16, 1992-1996, 1999.

[34] http://quantop.nbi.ku.dk/research/nanofiber/.

[35] E. R. I. Abraham and E. A. Cornell. Teflon feedthrough for coupling optical fibers into ultrahigh vacuum systems. *Applied Optics Vol.* 37, 10, 1762-1763, 1998

[36] http://drum.lib.umd.edu/handle/1903/15069.

[37] S. Bruckner, M. Rothhardt, C. Wuttke, M. Becker and A. Rauschenbeutel. Nanofiber fabry perot microresonator for nonlinear optics and cavity quantum electrodynamics. *Opt. Lett.* 37, 1949-1951, 2012.

[38] C. Wuttke, G. D. Cole, and A. Rauschenbeutel. Optically active mechanical modes of tapered optical fibers. *Phys. Rev. A*, 88:061801, 2013.

[39] Chen, Y. George, Ding, Ming, Newson, P. Trevor and G. Brambilla. A review of microfiber and nanofiber based optical sensors, *The Open Optics Journal*, 7, 32-57, 2013

[40] L. Ding, C. Belacel, S. Ducci, G. Leo, and I. Favero. Ultralow loss single-mode silica tapers manufactured by a microheater. *Appl. Optics.*, 49:2441, 2010.